2015-09-01

Unconventional Hydrocarbon Potential of a Middle Triassic Source Rock in the West-Central Sverdrup Basin, Canadian Arctic Archipelago

Kondla, Danielle

UNIVERSITY OF CALGARY

Unconventional Hydrocarbon Potential of a Middle Triassic Source Rock in the West-Central Sverdrup Basin, Canadian Arctic Archipelago

by

Danielle Michelle Kondla

A THESIS

SUBMITTED TO THE FACULTY OF GRADUATE STUDIES

IN PARTIAL FULFILMENT OF THE REQUIREMENTS FOR THE

DEGREE OF MASTER OF SCIENCE

GRADUATE PROGRAM IN GEOLOGY AND GEOPHYSICS

CALGARY, ALBERTA

AUGUST, 2015

Abstract

Organic-rich Middle Triassic strata of the Sverdrup Basin have been identified as source rocks; however their potential as a self-sourced, unconventional hydrocarbon reservoir has not been examined. This study uses a combination of organic and inorganic geochemical, petrographic, and petrophysical techniques to provide insights into the hydrocarbon potential and reservoir characterization. Factors influencing organic matter (OM) distribution during deposition are established to develop an understanding of the depositional system. Effects from diagenesis and thermal maturation are investigated to reveal the present reservoir conditions. Suboxic to anoxic bottom waters and minimal clastic dilution conditions associated with the base of regressive systems tracts are favorable for high primary OM preservation. OM in the thermally mature interval of the studied strata is dominated by solid bitumen, which has a negative effect on reservoir quality by occluding porosity. However, this interval does have capacity to generate oil and gas.

Acknowledgements

Thanks to Cathy Hubbell and Faye Nicholson for help with the many administrative tasks throughout my graduate program, Kristine Evans, Micky Horvath, Megan Slotboom, and Sarah Saad for help with sample preparation, and the National Energy Board and Richard Fontaine for supplying the core for this project. I am grateful to Ross Stewart, Dr. Chris DeBuhr, Samuel Aquino, and Dr. Amin Ghanizadeh for their technical expertise. I wish to thank Geoscience for New Energy Sources, GSC, Tight Oil Consortium, U of C, and Canada Graduate Scholarship-Masters, NSERC for generous funding of this project. I am grateful to my co-authors Dr.'s Hamed Sanei, Chris Clarkson, Omid Haeri Ardakani, Ashton Embry, Jiang Chunqing, and Xibo Wang for their guidance during the research, writing and submission of the two manuscripts resulting from this thesis. Thanks to Dr.'s Keith Dewing and Steve Grasby for thoughtful reviews of the two manuscripts. Thanks to Dr. Benoit Beauchamp for teaching me how to use CorelDraw, an indispensable skill. I am thankful to Omid for mentoring me, supporting me, and making me feel like part of our research group. Many thanks to my fellow students and colleagues for sharing this journey with me and making it so enjoyable. Thanks to my friends for never giving up on me. I am grateful, as always, for my incredible family, who supports me in whatever I choose to do, and would do anything to help me achieve my goals. I am grateful to Chris, my supervisor, for his kindness, boundless knowledge, and organization. I am grateful to Hamed, also my supervisor, for his unwavering confidence in my abilities, constant support and availability. I cannot express how thankful I am to both Chris and Hamed for the amazing opportunities they have presented me with; it has truly changed my life.

Table of Contents

List of Tables

List of Figures

Chapter One: **Introduction**

1.1 Purpose and Importance of Study

The primary objective of this research is to identify the unconventional hydrocarbon potential of fine-grained Middle Triassic strata of the Sverdrup Basin in the Canadian Arctic. The secondary objective includes characterization of dispersed organic matter (OM) in relation to fine-grained strata to develop a greater understanding of how OM may affect reservoir quality in mudrocks, should these be exploited for hydrocarbon production. These findings may be applied to other self-sourced reservoirs. Achievement of these objectives developed insight into geologic controls affecting the distribution and quality of potential hydrocarbon reservoirs within Middle Triassic strata of the Sverdrup Basin, primarily focused on dispersed OM and its interactions with the mineral components of the rock.

The Middle Triassic strata of the Sverdrup Basin have been previously studied for source rock potential and are typically grouped together with other Triassic-aged source rocks (i.e., Schei Point Group). However, detailed study of Middle Triassic strata as a possible self-sourced reservoir has not been conducted. Separation of Middle Triassic strata from other Triassic-aged source rocks for detailed study is important due to differences in basin-wide climatic and tectonic conditions during the Triassic Period. Previous studies of Middle Triassic rocks of the Sverdrup Basin have been conducted primarily at a regional scale (e.g., Goodarzi et al., 1989; Dewing and Obermajer, 2011), making the high-resolution sampling and analysis of this study novel. Results have generated new, detailed information about subtle changes in depositional conditions over time in the Middle Triassic.

New research of unconventional hydrocarbon resources, particularly tight and shale oil and gas reservoirs has become a central theme in industry and academia. The challenges of studying fine-grained, organic rich reservoirs include the small-scales of porosity, permeability and lithologic variation as well as the heterogeneity of these properties. Study of these qualities requires different techniques than those used for investigating conventional, coarser-grained reservoirs; this is due to both changes in fluid behavior within the pore networks of fine-grained rocks and simply due to the difficulty of visualization of most properties in mudrocks, even at the resolution of transmitted light microscopy.

The integration of multiple analyses in this study has permitted thorough characterization of the Middle Triassic rocks of interest. Use of individual techniques can provide detailed and useful information about each component of the rock. By synthesizing information from each technique, we can develop an account of how all aspects of the reservoir interact and contribute to the petroleum system. Data supplied from different analyses can also be used to substantiate interpretations and conclusions. For example, when interpreting the depositional environment of each interval in this study, redox-sensitive trace elements, organic petrology, hydrocarbon source characterization, and core examination were each referenced to establish the strongest interpretations. The use of multiple data sources becomes especially important when investigating complex systems, such as using trace element enrichment in marine sediments to determine depositional conditions. Complex systems may be affected by numerous factors, making it difficult to filter the background 'noise' from the overall signal.

The variety of techniques used in this study enabled physical and chemical characterization of the OM components of the rock as well as the interactions of these components with the mineral fraction of the rock. By combining standard Rock-Eval analysis

with a modified extended slow heating cycle (Sanei, et al., 2015), organic petrology, and scanning electron microscopy, links between organic geochemical properties and petrographic observations were made, demonstrating the differences of each fraction of OM, and the effects each has on reservoir quality and hydrocarbon potential. The complex behavior of OM within self-sourced reservoirs necessitates its comprehensive characterization, especially in frontier basins and newly developed areas. The pore network of these rocks was examined using techniques developed specifically for mudrocks (i.e., low pressure nitrogen gas adsorption) as well as more conventional analyses (i.e., He pycnometry-derived porosity). This allowed identification of pores from the micro- (<2 nm) to macropore (>50 nm) size range, all of which are present within these rocks. However, even with the use of multiple techniques, complete characterization of the pore network in these rocks requires further study.

As conventional hydrocarbon targets in accessible basins of the world become depleted, new sources of petroleum may need to be identified. Despite the discovery of 21 substantial conventional petroleum fields in the Sverdrup Basin during exploration between 1969 and 1986 (Chen et al., 2000), these resources have not been developed, mainly because of economic limitations. However, if global energy demands and preferences continue along current trends, development of these conventional resources as well as exploration for unconventional reservoirs can be expected in the future.

1.2 Study Approach

To better understand the objectives of this thesis, research was focused on the interaction of OM with rock mineral matrix. Efforts were made to understand the factors that controlled the distribution of each OM component during deposition as well as the associations of these components under present reservoir conditions. To address the primary controls on OM

distribution in the Sverdrup Basin during the Middle Triassic, the following topics were investigated: how depositional conditions varied over time and in different areas of the basin and; how depositional conditions affected production, accumulation, and preservation of OM within these areas. Organic geochemical parameters, thermal maturity, and porosity were investigated to reveal the effects of burial diagenesis on the OM and rock matrix.

Core samples from three wells intersecting the fine-grained Middle Triassic strata of the Sverdrup Basin were collected (Collingwood K-33, Skybattle Bay M-11, and Pollux G-60; Fig. 1.1). Samples were analysed for a variety of organic (Rock-Eval pyrolysis) and inorganic (inductively coupled plasma-mass spectrometry [ICP-MS] bulk elemental analysis) geochemical parameters, as well as petrophysical values related to porosity (immersion bulk density, He-pycnometry grain density, low pressure adsorption). Visualization of the core was achieved at various scales using macroscopic core examination, reflected light microscopy, and scanning electron microscopy (SEM). Data collected from the various analyses were compiled to interpret the petroleum system. Details of the methods used are included in Chapters 2, 3, 4 and appendices.

1.3 Geological Framework

The Sverdrup Basin is a 1300 km-long rift basin located in the Queen Elizabeth Islands in the Canadian Arctic (Balkwill, 1978) (Fig. 1.1). It comprises rocks ranging in age from Mississippian to Neogene, of marine, non-marine, intrusive, and extrusive origin (Balkwill, 1978). Basin formation began with rifting in the Mississippian, followed by gradual thermal subsidence (Embry and Beauchamp, 2008). A subsequent phase of rifting occurred during the Early to Late Cretaceous, with deposition in the basin ending in the Late Eocene with uplift and deformation due to the Eurekan Orogeny in the east (Embry and Beauchamp, 2008). The tectonic

forces acting on the basin in conjunction with variable sedimentation rates over time resulted in a complex depositional history overprinted on gradual thermal subsidence signatures. Sediments were predominantly derived from Devonian-aged rocks along the southern and eastern margins of the basin (Patchett et al., 2004; Embry and Beauchamp, 2008). During the Carboniferous to the Early Jurassic, minor amounts of sediments were also delivered to the basin from the north from a landmass known as Crockerland (Embry, 1991).

The focus of this thesis is the Middle Triassic succession, which differs from the Early and Late Triassic successions in several respects. Mobilization of mid-Carboniferous evaporite deposits began during the deposition of Middle Triassic sediments, drastically affecting their structure and thicknesses (Embry, 1991 and references therein). Sediment supply to the basin was less during the Middle Triassic compared to both the Early and Late Triassic, influencing the size of the deep basin as well as current energy levels and bottom water oxygenation (Embry, 1991 and references therein). The Middle Triassic strata can be divided into two 3rd order stratigraphic sequences, while the Late Triassic strata is divided into seven 3rd order sequences (Embry, 1991), indicating a much more dynamic environment of deposition in the latter epoch. The transition from Middle Triassic to Late Triassic also marks a change from a subtropical to temperate climate (Embry, 1991 and references therein), impacting the weathering and erosion of rocks surrounding the basin.

Middle Triassic strata of the Sverdrup Basin are assigned to either the Schei Point Group (along the southern basin margin) or the equivalent Blaa Mountain Group (basin centre) (Embry, 1984a, 1984b, 1991, 2011; Embry and Beauchamp, 2008) (Fig. 1.2). The Middle Triassic strata are marine-deposited and consist of two lithostratigraphic formations: the Roche Point (southern basin margin) and Murray Harbour formations (basin centre), and two 3rd order stratigraphic

sequences: Anisian and Ladinian (Embry, 1984a, 1984b, 1991, 2011; Embry and Beauchamp, 2008). Sandstone bodies dominate the southern basin margins and change lithofacies to silt and mudstone towards the north. The Roche Point Formation contains four members (Eldridge Bay, Cape Caledonia, Chads Point, and Gore Point) and the Murray Harbour Formation contains two members (informal "lower member", and Cape Caledonia). Each of the 3rd order sequences consists of a thin transgressive systems tract (TST) overlain by a thicker, coarsening-upwards regressive systems tract (RST).

1.4 Study Area

The samples studied in this thesis were collected from three cores taken from three different oil and gas wells drilled in the Sverdrup Basin. The three wells each have cored intervals that intersect fine-grained rocks of the Middle Triassic succession in the west-central part of the basin. The cored intervals each represent strata deposited in different areas of the basin as well as at different times during the Middle Triassic. The three wells are Collingwood K-33, Skybattle Bay M-11, and Pollux G-60 (Fig. 1.1). Collingwood K-33 is located on Sabine Peninsula of northeast Melville Island. The cored interval is part of the Ladinian-aged Cape Caledonia Member of the Roche Point Formation and was deposited along the southern margin of the basin (Embry, 1984a) (Fig 1.2). Skybattle Bay M-11 is located on the southern point of Lougheed Island. The cored interval is part of the Murray Harbour Formation and contains segments of both the Anisian-aged informal "lower member" and the overlying Ladinian-aged Cape Caledonia Member (Embry, 1984a; Embry and Podruski, 1988) (Fig. 1.2). The Anisian interval was deposited near the southern basin margin and the Ladinian interval was deposited closer to the basin axis, in deeper water. Pollux G-60 is located on the northern end of Ellef Ringnes Island. The cored interval is taken from the Anisian "lower member" of the Murray

Harbour Formation and was deposited near the northern margin of the basin (Embry, 1984a) (Fig. 1.2). Details of each well and core are included in Chapter 3 and appendix A.

1.5 Previous Work

Previous studies of Middle Triassic strata in the Sverdrup Basin have focused on source rock characterization rather than self-sourced reservoir characterization. These studies provide information related to regional thermal maturity, oil migration, and hydrocarbon potential of the units. Dewing and Obermajer (2011) compiled data from previous studies and used quality control methods to confirm basin-wide thermal maturity of Middle Triassic strata; they found an overall decrease in maturity from overmature in the deep basin to immature along the southern margins. Other studies (e.g., Gentzis and Goodarzi, 1991; Gentzis and Goodarzi, 1993; Gentzis et al., 1996; Jones et al., 2007) found local variations in thermal maturity due to increased heat flow associated with salt diapirism and igneous intrusives, as well as differences in subsidence and uplift from variable local and regional tectonic influences. OM has been identified as predominantly Type I and II, with excellent potential to generate oil (e.g., Gentzis and Goodarzi, 1991; Gentzis and Goodarzi, 1993; Gentzis et al., 1996; Mukhopadhyay et al., 1997).

Conventional hydrocarbon reservoirs within the Triassic succession are present in marine sandstones of the Bjorne (Lower Triassic), Roche Point (Middle Triassic), and Pat Bay Formations (Upper Triassic) (Waylett and Embry, 1992). However, these reservoirs are minor compared to other substantial conventional reservoirs in younger Mesozoic units (i.e., Lower Jurassic Heiberg, King Christian and Maclean Strait Formations; Upper Jurassic Awingak Formation) (Waylett and Embry, 1992). The hydrocarbons that fill these conventional reservoirs are mainly gas, with lesser amounts of oil; many of these oils have been correlated with source rocks from the Middle-Upper Triassic Schei Point and Blaa Mountain Groups (Brooks et al.,

1992). All of the discovered petroleum fields in the basin are structurally controlled, occurring in anticlines and domes resulting from Eurekan orogenic-derived deformation or salt tectonism (Brooks et al., 1992). The estimated reserves contained in these fields are 500.3 x 10^9 m^3 natural gas and 294.1 x 10^6 m^3 of crude oil (Chen and Osadetz, 2011), accounting for 23 and 10% of Canada's conventional natural gas and crude oil reserves (Canadian Association of Petroleum Producers, 1999).

1.6 Organization of Thesis

This thesis contains two research chapters in addition to introduction, methods, and conclusion chapters, and appendices. Chapters 3 and 4 were written as separate documents with the intent of publication as peer-reviewed journal articles. As a result, there is some overlap of information between the two, particularly with regards to methods and geological background. Chapter 3 investigates the depositional environment of Middle Triassic strata preserved in each of the three cores, the factors that controlled these conditions, and how they affected OM distribution. Chapter 4 examines the most thermally mature core of the study (Skybattle Bay M-11) in detail to determine the effects of OM and mineral matrix on reservoir quality. The appendices contain bulk data from each analysis as well as results of analyses conducted but not incorporated into the research chapters.

1.7 Contributions of Authors

Each of the two manuscripts comprising Chapters 3 and 4 were created by the student (first author) with contributions by various co-authors. The first author was responsible for all research conducted including preparation of samples, core logging, organic petrology, porosity measurement, and interpretation of data, with valuable guidance and suggestions from H. Sanei, C.R. Clarkson, and O.H. Ardakani. Rock-Eval analysis was conducted by R. Stewart (Geological

Survey of Canada (GSC) Calgary), ICP-MS was conducted at Acme Laboratories, Vancouver, BC, SEM work was conducted by C. DeBuhr (University of Calgary), and low pressure nitrogen gas adsorption was conducted by S. Aquino (University of Calgary). Analysis and interpretation of online thermal desorption/pyrolysis-gas chromatography-mass spectrometry/flame ionization detection (TD/Py-GC-MS/FID) data was completed by J. Chunqing (GSC Calgary), and derivation of mineralogy from bulk elemental composition was conducted by X. Wang (GSC Calgary). The first author wrote all sections of each manuscript, with amendments suggested by H. Sanei, C.R. Clarkson, and O.H. Ardakani. A.F. Embry provided input to some sections pertaining to the stratigraphy contained in Chapter 3. Chapter 3 has also benefitted from critical review by three anonymous reviewers following submission to a peer reviewed journal; it has subsequently been accepted for publication.

Figure Captions

Figure 1.1: Map of the Sverdrup Basin showing the paleooutline of the basin (heavy solid line) and axis (dashed line) as well as the paleogeographic location of Crockerland. Locations of the studied wells are marked with black circles. Large black arrows along the southern margin indicate the predominant sediment source to the basin; small black arrow along the northern margin indicates a minor sediment source to the basin (Crockerland) (after Embry and Beauchamp, 2008). Shaded area indicates extent of Middle Triassic strata both in the subsurface and as outcrop (after Embry, 1991). Line of section for Figure 1.2 is indicated by dotted line.

Figure 1.2: Middle Triassic stratigraphy of the western Sverdrup Basin. Section line is shown in Figure 1.1. 3rd order stratigraphic sequences are represented by lithofacies changes (Embry, 1984a, 2011). Numbered core locations are indicated by black squares: 1) Collingwood K-33; 2) Skybattle Bay M-11; and 3) Pollux G-60.

Figures

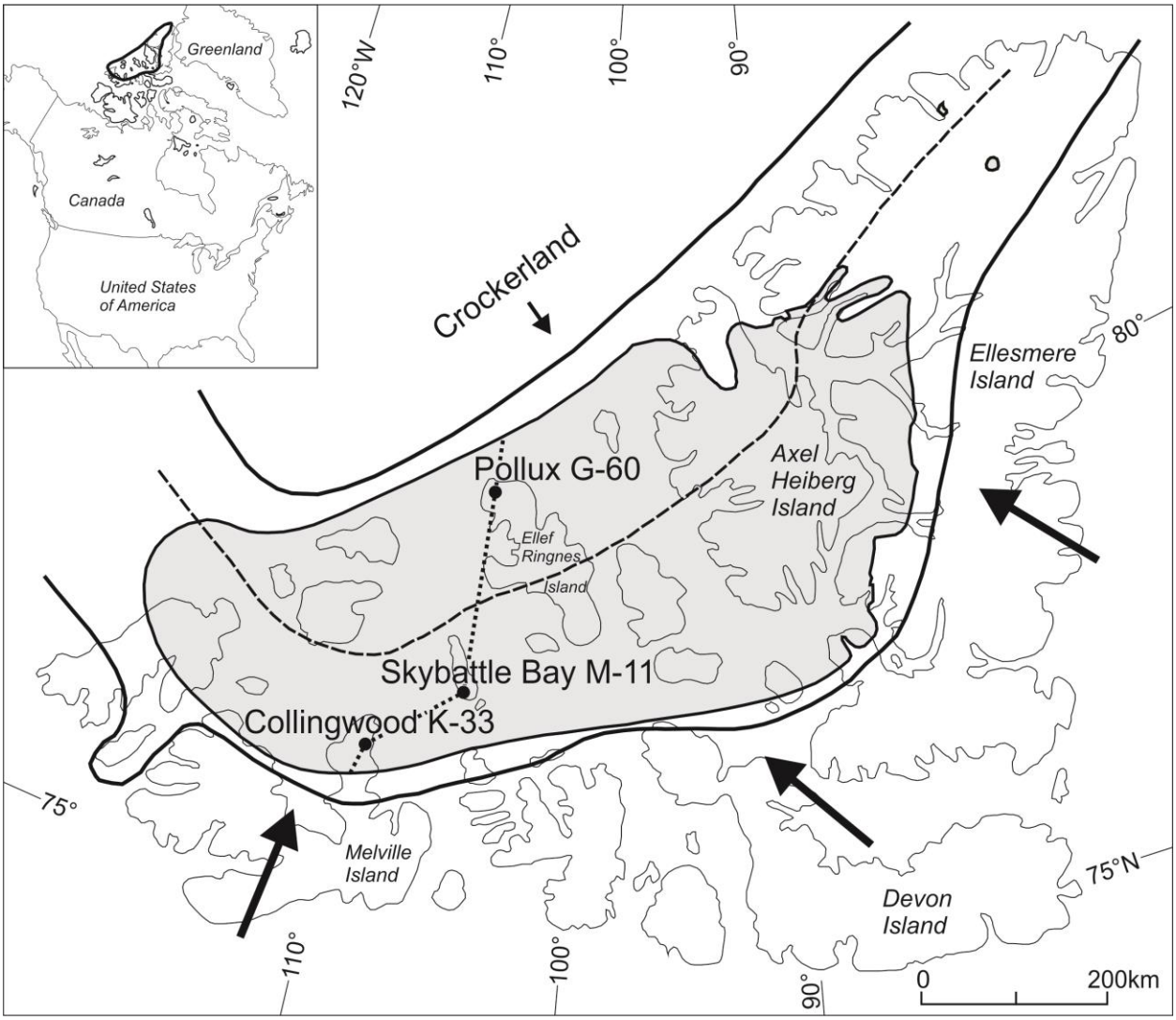

Figure 1.1

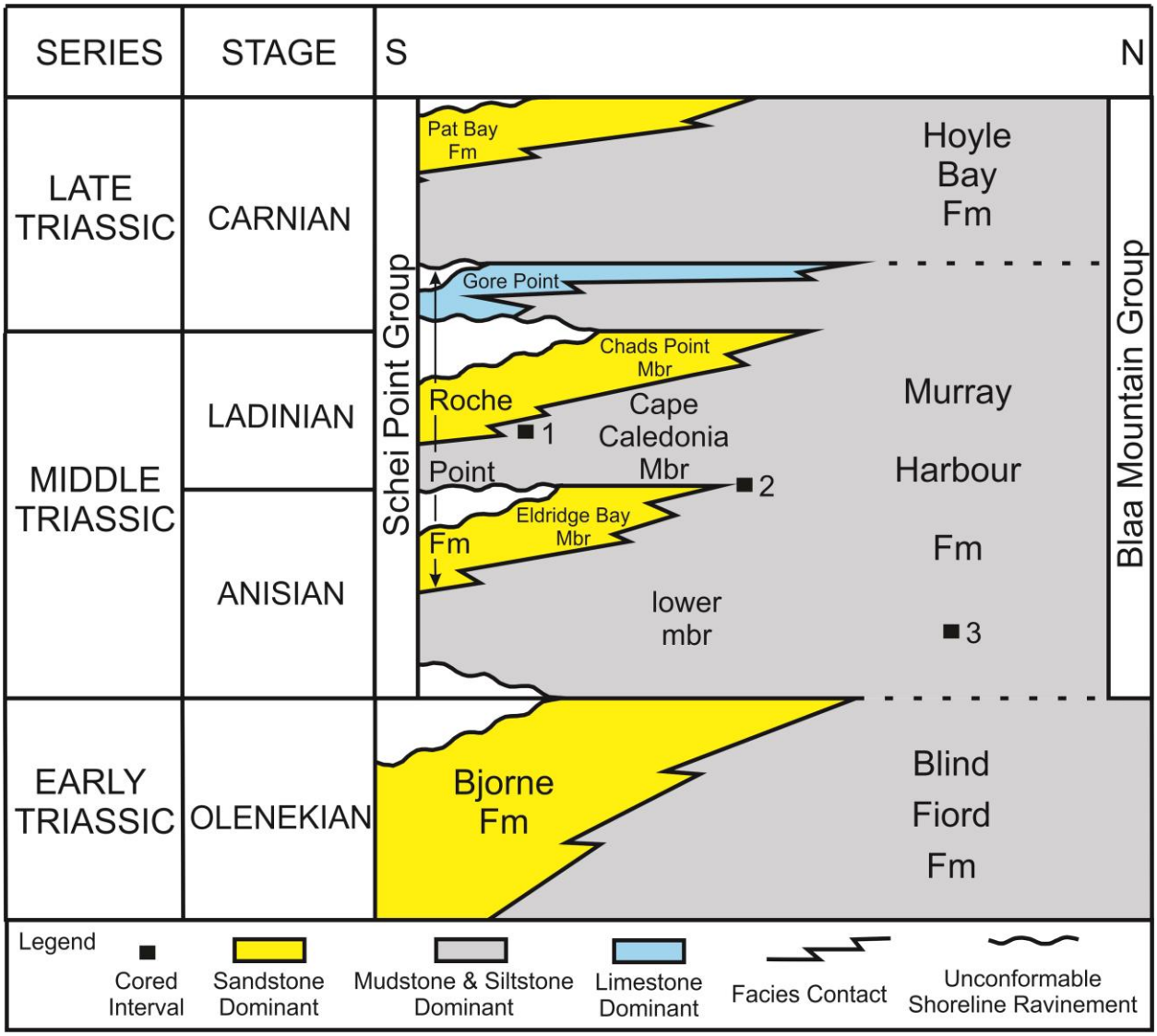
SERIES
STAGE
S
N
LATE TRIASSIC
CARNIAN
MIDDLE TRIASSIC
LADINIAN
ANISIAN
EARLY TRIASSIC
OLENEKIAN
Schei Point Group
Blaa Mountain Group
Pat Bay Fm
Hoyle Bay Fm
Gore Point
Chads Point Mbr
Roche Point Fm
1
Cape Caledonia Mbr
2
Eldridge Bay Mbr
lower mbr
Murray Harbour Fm
3
Bjorne Fm
Blind Fiord Fm
Legend
Cored Interval
Sandstone Dominant
Mudstone & Siltstone Dominant
Limestone Dominant
Facies Contact
Unconformable Shoreline Ravinement
Figure 1.2

Chapter Two: **Materials and Methods**

This chapter lists analytical techniques utilized during completion of the research for this thesis. A variety of complimentary techniques were used to more completely characterize organic matter (OM) within the rock as well as its interactions with the mineral components. Not all data collected was used in the research chapters, but has been included in appendices. Low pressure nitrogen gas adsorption was only conducted on the organic rich portion of the Skybattle Bay M-11 core, as this was determined to be the only interval of the three studied cores that has potential as a self-sourced reservoir.

2.1 Core Sampling and Logging

Three cores were identified as fine-grained Middle Triassic rock from the wells drilled during hydrocarbon exploration in the Sverdrup Basin. Each of the three cores was logged at the centimetre scale and assigned to lithofacies based on rock colour, composition, grain size, physical and biogenic structures, fossils, bedding and mineralogy to provide sedimentological context for the studied samples (Appendix A). At approximately 20 cm intervals, between 3 and 10 g of rock were collected from the core using a Dremel tool. Due to sampling restrictions, sample removal was only permitted along the outer edge of the core and at broken end segments. A total of 150 samples were collected: 28 from Collingwood K-33, 81 from Skybattle Bay M-11, and 41 from Pollux G-60. An allotment of each sample was crushed to powder via porcelain mortar and pestle for use in Rock-Eval analysis, inductively coupled plasma-mass spectrometry (ICP-MS), and online thermal desorption/pyrolysis-gas chromatography-mass spectrometry/flame ionization detection (TD/Py-GC-MS/FID).

2.2 Rock Eval 6 Analysis

2.2.1 Standard Rock-Eval Cycle

Rock Eval 6 analysis (the most recent version of the Rock-Eval apparatus) was completed at the Geological Survey of Canada (GSC), Calgary laboratory to provide basic organic geochemical data for the study (Appendix B). All 150 samples were analyzed following procedures for the standard cycle as outlined in Lafargue et al. (1998). This cycle involved the introduction of 70 mg of powdered rock into an oxygen-free oven at 300°C for 3 min where volatilization of free hydrocarbons occurred resulting in generation of the S1 pyrogram curve (mg HC/g Rock). Pyrolysis of the remaining OM occurred as temperature was increased by 25°C per min up to 650°C, producing hydrocarbons (S2 mg HC/g Rock), organic-sourced CO_2 (S3, mg CO_2/g Rock), and mineral-sourced carbon (S3', mg CO_2/g Rock). The sample was then transferred to an oxidation oven at 300°C and temperature was increased by 20°C per min until 850°C. During this phase, any remaining organic carbon (S4CO_2, mg CO_2/g Rock; S4CO, mg CO/g Rock) and mineral-sourced carbon (S5, mg CO_2/g Rock) was oxidized. A flame ionization detector recorded the release of hydrocarbons during volatilization and pyrolysis of OM and resulted in the generation of pyrogams corresponding to each evolved product.

2.2.2 Extended Slow Heating Rock-Eval Cycle

Twelve samples from the organic rich part of the Skybattle Bay M-11 core were selected for analysis using the extended slow heating temperature (ESH) cycle, a modified Rock-Eval cycle following procedures from Sanei et al. (2015). The ESH cycle allowed better resolution of different fractions of OM within the rock, compared to the standard cycle. Pyrolysis began at 150°C for 10 min allowing volatilization of free hydrocarbons similar to the standard Rock-Eval cycle. This lower initial temperature resulted in volatilization of only the lightest free

hydrocarbons ($S1_{ESH}$, mg HC/g Rock). Next, temperature was increased by 10°C per min up to 650°C, allowing desorption of medium to heavy hydrocarbons ($S2a_{ESH}$, mg HC/g Rock) and generation of hydrocarbons from kerogen and solid bitumen ($S2b_{ESH}$, mg HC/g Rock). The oxidation phase of the ESH cycle followed the same procedures as those used in the standard Rock-Eval cycle.

2.3 Organic Petrology

Organic petrology was conducted on 30 samples, which were selected to represent variations in Rock-Eval values within each interval. A portion of each rock sample was coarsely crushed (~2-5 mm) using mortar and pestle. The crushed material was placed in a mold, set in an epoxy-resin mixture, and subsequently polished to produce a pellet of randomly-oriented rock fragments. The pellets were examined under oil immersion (n=1.518 at 23°C), in both white and ultraviolet (UV) light (G 365 nm excitation, 420 nm filter) using a Zeiss Axio Imager II reflected light microscope at the GSC Calgary. Sample examination included maceral identification and description, reflectance measurements, fluorescence microscopy, and grain size measurements.

2.4 Online Thermal Desorption/Pyrolysis-Gas Chromatography-Mass Spectrometry/Flame Ionization Detection (TD/Py-GC-MS/FID) Analysis

Three samples were selected from the Skybattle Bay M-11 core for online thermal desorption/pyrolysis-gas chromatography-mass spectrometry/flame ionization detection (TD/Py-GC-MS/FID) analysis (Appendix C). Two samples were from the organic rich part of the core, while the third was from the lower, organic lean part of the core. The samples from the organic rich portion of the core were selected based on the shape of their pyrograms from the standard Rock-Eval cycle; one displayed a prominent front shoulder on the S2 peak, which is typical of the majority of samples, while the other had no front shoulder. A Frontier EGA/PY-3030D

pyrolyzer interfaced to an Agilent GC-MSD/FID dual detection system (GSC Calgary) was used for analysis to identify the type and relative abundances of free and generated hydrocarbons in the samples. Approximately 65 mg of powdered rock was heated at 300°C for three min causing desorption of free hydrocarbons. Next, the samples were heated at 350°C for three min causing thermal desorption of heavier hydrocarbons. The organic rich sample with the prominent front shoulder was then pyrolysed for 30 seconds at 650°C to generate hydrocarbons from solid OM within the sample. Evolved hydrocarbons from both the thermal desorption and pyrolysis stages were cryo-trapped at -186°C and analysed in a PONA 50 m x 0.20 mm x 0.5 μm GC column using helium carrier gas at a flow rate of 1 mL/min. Hydrocarbons were separated in the GC column based on boiling points; temperature was held at 33°C for 10 min, increased by 3°C per min up to 63°C, then increased by 6°C per min up to 325°C and held for 35 min. Mass spectrometer detectors identified the type of compounds and flame ionization detectors quantified them, based on mass spectra and GC retention times, respectively, from literature.

2.5 Inductively Coupled Plasma-Mass Spectrometry

ICP-MS was conducted on all samples at Acme Labs in Vancouver, Canada to determine bulk elemental concentration for use as redox and clastic input proxies and for derivation of mineralogy (Appendix D). Samples were prepared by digesting approximately 500 mg of powdered rock in an open system. Powder was heated in a solution of H_2O, -HF, -$HClO_4$, and HNO_3, (2:2:1:1) to complete dryness and subsequently heated and dissolved in a 50% HCl solution. Aerosolized samples were then introduced into the ICP-MS where the high-temperature ICP source converted atoms of each element into ions via argon plasma. These ions were then guided into the mass spectrometer through skimmer cones, which allowed passage of only the central portion of the generated ion beam. The ions were then separated based on their mass-to-

charge ratio with a quadrupole mass filter that used rapidly alternating AC and DC voltages to allow ions of a certain mass-to-charge ratio to pass through for detection. The rapid variation of voltages allowed analysis of multiple elements. Concentrations of 59 major, minor, trace and rare earth elements in each sample were determined with this analysis.

2.6 Scanning Electron Microscopy

Five samples were selected from the 30 organic petrology pellets for field emission scanning electron microscope (FESEM) imaging and energy-dispersive X-ray spectroscopy (EDXS). One representative sample was chosen from each of the Collingwood K-33 and Pollux G-60 wells, and three samples were chosen from the Skybattle Bay M-11 well: one from each of the three sequence stratigraphic systems tracts. SEM imaging and EDXS mapping were conducted to identify the composition and texture of the mineral fraction of the rock. Imaging was completed at the Instrumentation Facility for Analytical Electron Microscopy (University of Calgary) using the FEI Quanta 250 Field Emission Gun scanning electron microscope. Organic petrology pellets were re-polished using diamond to avoid contamination from aluminium, and carbon coated for improved conductivity. Samples were placed in a high vacuum chamber, bombarded with electrons and imaged using backscattered and secondary electrons. EDXS mapping of areas of interest resulted in elemental compositions of the mineral fraction.

2.7 Porosity

Effective porosity was calculated using grain and bulk density values for 33 uncleaned samples from all three cores (Appendix E). Porosity values were studied to reveal the potential capacity for hydrocarbon storage within the rock. Bulk density values were calculated following weighing of each sample (rock fragments) in both air and n-hexane. Grain density was determined based on the principles of Boyle's Law using a He gas pycnometer in the Tight Oil

Consortium laboratory at the University of Calgary. The He pycnometer consists of two chambers; one vacant and the other containing the sample. Inert He gas flowed into the sample chamber that was subsequently sealed. The gas then penetrated open and connected pores as small as one angstrom. Once equilibrium pressure between the sample and the chamber was reached, He was allowed to flow into the vacant chamber and after equilibrium was achieved between the two chambers, the volume of the sample was determined.

2.8 Low-Pressure N_2 Gas Adsorption

Of the samples used for porosity calculation, 14 were crushed to 20-35 US mesh size and analysed using low-pressure N_2 gas adsorption following the procedures of Gregg and Sing (1982) (Appendix F). This analysis was also conducted in the Tight Oil Consortium laboratory at the University of Calgary. This analysis was conducted to determine the pore-size distribution of pores measuring less than 200 nm in diameter and to identify the predominant pore geometry. Samples were prepared for analysis by outgassing in a vacuum overnight at 60°C to remove any adsorbed contaminants. A 3Flex Surface Characterization Analyzer was used in conjunction with N_2 gas to determine the surface area of samples. Nitrogen gas was injected into the sample chamber incrementally, with pressure equilibrium reached between each addition of gas. After each stage of gas injection, the quantity of N_2 molecules adsorbed to the sample was calculated. The N_2 molecules adsorbed to the sample surface first to form a single layer (monolayer), then a layer of multiple N_2 molecules (multilayer), and with subsequent gas additions, eventually filled the pores via condensation, beginning with the smallest in diameter. From this process, adsorption and desorption isotherms were generated and interpreted to determine sample surface area using the Langmuir (based on the creation of a monolayer of N_2 molecules on the sample) and Brunauer-Emmett-Teller (BET) analyses (based on multilayer adsorption of N_2 molecules).

Using the Barrett-Joyner-Halenda (BJH) method, the adsorption branch of each isotherm was inverted to determine pore-size distribution.

2.9 Mineralogy Derivation

Mineralogy of 51 samples from the organic rich portion of the Skybattle Bay M-11 core was derived using bulk elemental values determined from ICP-MS. This method began by converting each major element (i.e., Si, Fe, Na, K, Ca, P, Mg, Ti, Al, and Mn) to their oxides using a conversion factor. Sulphur was also determined to be a major element but was not converted to its oxide because it was interpreted to mainly be associated with sulfide minerals (i.e., pyrite). Mineral carbon values from Rock-Eval analysis were used to convert carbon to its oxide. Organic carbon concentration was determined from TOC values. Correlation coefficients (Pearson's r, $p<0.05$, Microsoft Excel Analysis ToolPak™) were calculated from all oxides and TOC concentrations to determine associations and, in conjunction with petrographic observations, were used to infer the most probable minerals or mineral groups present. Based on these inferences, quartz, anatase, clay mineral (mixed layer illite-smectite), carbonate (calcite, dolomite and siderite), sulphide (pyrite), and phosphate (apatite) percentages were calculated. These values were used for characterizing the mineral fraction of the rock.

Chapter Three: **Depositional Environment and Hydrocarbon Potential of the Middle Triassic Strata of the Sverdrup Basin, Canada**

Danielle Kondla[a,b], Hamed Sanei[a,b], Ashton Embry[a], Omid H. Ardakani[a], and Christopher R. Clarkson[b]

[a]Geological Survey of Canada, Calgary

[b]Department of Geoscience, University of Calgary

Accepted for publication in International Journal of Coal Geology, June 23, 2015[1]

3.1 Abstract

This study summarizes the results of petrographic and geochemical analysis of Middle Triassic strata from the Sverdrup Basin in the Canadian Arctic. In this work, we investigate the distribution and depositional conditions of dispersed organic matter (OM) as a preliminary step towards understanding the potential of this stratigraphic interval as an unconventional reservoir. Closely-spaced samples from three Middle Triassic cores (southern margin, basin centre, northern margin) are analyzed using Rock-Eval analysis, inductively coupled plasma-mass spectrometry (ICP-MS), and organic petrology. Total organic carbon (TOC) ranges between 0 and 4.8 wt. %, with the most organic rich interval having a median TOC value of 3.2 wt. %.

---

[1] Reprinted from International Journal of Coal Geology, vol. 147-148, D. Kondla, H. Sanei, A. Embry, O.H. Ardakani, C.R.Clarkson, Depositional environment and hydrocarbon potential of the Middle Triassic strata of the Sverdrup Basin, Canada, p. 71-84, Copyright 2015, with permission from Elsevier.

Kerogen type varies from Type II to Type III throughout the sampled intervals. Samples from near the top of the regressive systems tract of the Anisian 3rd order sequence (basin centre) and near the middle of the Ladinian 3rd order sequence (southern margin) contain predominantly reworked, highly oxidized macerals and abundant coarser clastic material. Results are interpreted to support oxic to suboxic depositional conditions for these intervals. By contrast, samples from near the base of regressive systems tracts of both sequences (basin centre and northern margin) have the highest amounts of TOC (i.e., median = 3.2 wt.% and 1.4 wt.%), containing retained migrabitumen and abundant labile primary kerogen, respectively. The base of the Ladinian regressive systems tract near the basin axis was deposited under anoxic conditions and can be considered a prospective shale oil interval. Small-scale cyclic clastic influx episodes along the northern margin of the basin show changes from oxic to suboxic bottom waters. These cycles may be considered evidence for northerly-derived sediment from Crockerland during the Middle Triassic. The results and interpretations of this study can be applied to analogous fine-grained successions in other basins to better understand their unconventional reservoir potential.

3.2 Introduction

Many Canadian basins have been evaluated for unconventional hydrocarbon potential, with the exception of the frontier basins including those in the Canadian Arctic. As global energy demands continue to increase, hydrocarbon exploration and development will be driven towards these remote basins. Improvements to technology have made exploitation of shale-hosted and tight reservoirs economical, unlocking new resources and generating new interest in units formerly viewed only as source rocks. Middle Triassic, organic rich mudstone and siltstone units are present in the Sverdrup Basin in the Canadian Arctic Archipelago (Fig. 1.1) and are included in the Murray Harbour Formation. Between 1969 and 1986, 119 drilled wells, mainly in the

western part of the Sverdrup Basin, led to the discovery of 8 oil and 25 gas pools (Chen et al., 2000). The Murray Harbour Formation has already been identified as one of the major source rocks for many of these hydrocarbon pools (Brooks et al., 1992).

Previous studies of Triassic-aged dispersed organic matter (OM) classify Middle and Upper Triassic strata as a single source rock unit (e.g., Gentzis and Goodarzi, 1991; Gentzis and Goodarzi, 1993; Mukhopadhyay et al., 1997). Rock-Eval analysis, vitrinite reflectance, and biomarkers have been used to establish the regional thermal maturity of the Schei Point and Blaa Mountain groups (e.g., Goodarzi et al., 1989; Dewing and Obermajer, 2011). These studies found increasing thermal maturity from the edges of the Sverdrup Basin to the axis, likely the result of increasing burial depth. More localized studies (e.g., Gentzis and Goodarzi, 1991; Gentzis and Goodarzi, 1993; Gentzis et al., 1996) reveal variations in thermal maturity at a smaller scale within the Schei Point Group. These variations are attributed to differential uplift and subsidence rates, as well as increased heat flow from igneous intrusions and salt diapirs. Characterization of Schei Point Group OM in these studies as well as by Mukhopadhyay et al. (1997) show mainly Type I and Type II marine kerogen with oil generation potential and thermal maturities ranging from immature to mature. Hydrocarbons within the Schei Point Group show excellent association with discovered oils in the basin, indicating the Schei Point Group rocks are one of the main sources of hydrocarbons for these pools (Brooks et al., 1992).

This study investigates the distribution and type of dispersed OM in these Middle Triassic strata, as well as the associated depositional conditions. Results provide insight into how prospective these strata may be for unconventional hydrocarbon exploration and identify the most prospective areas. These insights can be applied to analogous fine-grained self-sourced reservoirs to better understand their heterogeneous nature.

3.3 Geological Setting and Study Area

The Sverdrup Basin is a southwest-northeast trending rift basin located in the Canadian Arctic Archipelago (Balkwill, 1978). It is approximately 1300 km long and 350 km wide, covering a total area of 300 000 km² (Embry and Beauchamp, 2008). The formation of the basin began with rifting associated with the Ellesmerian Orogen during the Early Carboniferous (Balkwill, 1978). Slow, passive subsidence of the newly formed basin was punctuated by periods of regional and local uplift resulting from changes to tectonically induced stresses acting on the basin (Embry and Beauchamp, 2008). Those authors note that periods of uplift combined with highly variable rates of sediment input, changed the extent and depth of the basin dramatically, from more than 2 km of water depth in the Early Triassic to nearly complete subaerial exposure at the end of the Late Triassic. Renewed rifting of the basin commenced in the Early Cretaceous and ended by the Late Cretaceous. Deposition in the Sverdrup Basin ended with deformation of the eastern part of the basin and regional uplift of the western portion as a result of compression during the Late Eocene Eurekan Orogeny. Throughout the evolution of the Sverdrup Basin, the major sediment source was siliciclastic Devonian strata along the southern and southeastern margins of the basin (Patchett et al., 2004; Embry and Beauchamp, 2008) (Fig. 1.1). A minor sediment source area (Crockerland) existed to the north of the basin from the Carboniferous to the Early Jurassic (Embry, 1993) (Fig. 1.1).

The focus of this study is the Middle Triassic succession (Fig. 1.2), dated through ammonite and pelecypod fossils located in coarse-grained lithofacies and correlated throughout the basin (Tozer 1961a, 1961b, 1963, 1967, 1970). Regional stratigraphic studies have resulted in a lithostratigraphic and sequence stratigraphic framework for Middle Triassic strata throughout the Sverdrup Basin (Fig. 1.2) (Embry, 1984a, 1984b, 1991, 2011; Embry and Beauchamp, 2008).

Two formations comprise the Middle Triassic strata, the sandstone-dominant Roche Point Formation and the mud-siltstone-dominant Murray Harbour Formation. Both of these formations are part of the Middle-Upper Triassic Schei Point Group, along the southern margins of the basin (Embry, 1984a). The Murray Harbour Formation is also included in the Middle-Upper Triassic Blaa Mountain Group, which consists of equivalent deep-water strata within the central portion of the basin (Embry, 1984a). The Roche Point Formation is subdivided into four members, listed in ascending order: sandstone-dominant Eldridge Bay Member, mud-siltstone-dominant Cape Caledonia Member, sandstone-dominant Chads Point Member, and limestone-dominant Gore Point Member. The Murray Harbour Formation can be divided into two members; an informal "lower member" and the overlying Cape Caledonia Member (Fig. 1.2) (Embry, 1984b).

The Middle Triassic interval comprises one second order sequence and consists of two 3rd order sequences of Anisian and Ladinian age (Fig. 1.2) (Embry, 1991). Each of these sequences is subdivided into a transgressive systems tract (TST) and overlying regressive systems tract (RST). The two 3rd order sequences of the Middle Triassic each contain a thin TST, which is sandstone-dominant on the basin margins and becomes mudstone and siltstone dominant further basinward. Each sequence consists mainly of a RST, which records a coarsening-upward (shallowing-upward) succession capped by an unconformity on the basin margins and by a conformable maximum regressive surface in the central portion of the basin. Used in conjunction with geochemical and organic geochemical methods, this sequence framework can be used to begin to establish the unconventional reservoir potential of the unit. This paper identifies how OM accumulation and preservation relates to the paleogeographic location, depositional environment, and sequence stratigraphic position within the Middle Triassic succession.

Along the southern and eastern basin margins the Murray Harbour Formation was deposited in mid-outer shelf environments with the overlying Roche Point Formation strata representing shallow shelf to delta plain deposits. Basinward, the sandstones of the Roche Point Formation change lithofacies to offshore shelf mudstone and siltstone, which are part of the Murray Harbour Formation (Fig. 1.2) (Embry, 1984a). The Murray Harbour Formation represents outer shelf and slope deposits and has an estimated maximum thickness of 300 m (Embry and Beauchamp, 2008).

3.4 Sampling and Methods

The cores chosen for this study are taken from three oil and gas wells located along an approximately S-N transect across the west-central part of the Sverdrup Basin (Fig. 1.1). The Collingwood K-33 well is located on Melville Island, along the southern margin of the basin. The core is taken from the mud-siltstone-dominant Cape Caledonia Member of the Roche Point Formation and the strata are interpreted as mid-shelf deposits (Embry, 1984a). The cored interval is in the middle portion of the Ladinian RST, just below the facies change between the Cape Caledonia Member and the sandstone-dominant Chads Point Member (Fig. 1.2) (Embry, 1984a). Six metres and 90 centimetres of core was recovered from the depth interval of 1898.9 – 1917.2 m.

The Skybattle Bay M-11 well is located on Lougheed Island and is further basinward than the Collingwood K-33 well, just south of the basin axis (Fig. 1.1). The cored interval is from the middle of the Murray Harbour Formation and includes the boundary between the Anisian sequence below and the Ladinian sequence above (Fig. 1.2). Consequently it contains the uppermost portion of the Anisian RST, a thin Ladinian TST, and the basal portion of the

Ladinian RST. Eighteen metres and twenty centimetres of core was recovered from the depth interval of 2520.0 – 2538.2 m.

Pollux G-60 is located on northern Ellef Ringnes Island close to the northern margin of the basin. The well is furthest away from the southern sediment source, but is closest to Crockerland, a low lying land area to the north of the basin present from the Carboniferous to the Jurassic (Embry, 1993) (Fig. 1.1). The core is intersects the base of the Murray Harbour Formation of Anisian age (Tozer 1961a, 1961b, 1963, 1967, 1970). From a sequence stratigraphic perspective, the core captures the base of the RST of the Anisian sequence (Fig. 1.2); the base of the core is 35 m above the Anisian maximum flooding surface (MFS). Nine metres and 10 centimetres of core was recovered from the depth interval of 1371.6 – 1380.7 m.

Each of the three cores were logged and divided into lithofacies prior to sample collection. Between 3 and 10 g of rock was collected at approximately 20 cm intervals for a total of 150 samples. A portion of each sample was crushed using a porcelain mortar and pestle for Rock-Eval 6 analysis and inductively coupled plasma-mass spectrometry (ICP-MS). Rock-Eval 6 analysis was completed on all samples at the Geological Survey of Canada (GSC), Calgary following programmed temperature heating for the default cycle. Seventy milligrams of powdered bulk rock sample was introduced into a pyrolysis oven, under N_2 conditions, and held at 300°C for 3 min resulting in desorption of free hydrocarbons (S1, mg HC/g Rock). Temperature was then increased at a rate of 25°C per min up to 650°C leading to the thermal cracking of kerogen and subsequent release of hydrocarbons (S2, mg HC/g Rock), organic-sourced CO_2 (S3, mg CO_2/g Rock), and a portion of mineral-sourced carbon (S3', mg CO_2/g Rock). Following completion of pyrolysis, samples were moved to an oxidation oven where temperature was increased from 300°C to 850°C at a rate of 20°C per min. This phase oxidized

any residual organic carbon (S4CO_2, mg CO_2/g Rock; S4CO, mg CO/g Rock) and the remainder of mineral-sourced carbon (S5, mg CO_2/g Rock). Relevant calculated parameters include total organic carbon (TOC) [pyrolysable organic carbon (PC%) + residual organic carbon (RC%)], hydrogen index (HI = S2 x 100/TOC, mg HC/g TOC), and oxygen index (OI = S3 x 100/TOC, mg CO_2/g TOC). For a more detailed account of Rock-Eval procedures and calculations, readers are referred to Lafargue et. al. (1998). Accuracy and precision of Rock-Eval pyrolysis parameters were determined through use of the reference standard, 9107, prepared from the Colorado Shale. This standard was analyzed prior to each new batch of samples and at least once every 15 samples to ensure consistency of measurements. Anomalous samples were re-analysed to determine their validity. Measured parameters have an accuracy and precision that deviate by less than 5% from the reference standard, with the exception of accuracy values of S3 for Pollux G-60 that deviate by less than 15% from the reference standard.

ICP-MS was conducted on all samples at Acme Labs in Vancouver, Canada. Rock samples were heated in HNO_3, -$HClO_4$, and -HF, dried, and dissolved in HCl. Concentrations of Mo, Cu, Ni, Co, U, V, Cr, Zn, Zr, Ti, and Al were then determined via mass spectrometry. Accuracy and precision of ICP-MS values were determined by use of the reference standard OREAS 45e, prepared from a lateritic soil from Western Australia, as well as duplicate analysis of random samples. ICP-MS parameters have an accuracy and precision that deviate by less than 5% from the reference standard values, with the exception of accuracy values for Ni, Cr, U, and Ti, which deviate by less than 8%. Duplicate sample precision values show less than 5% error for most samples, less than 10% error for two Co duplicates, less than 8% error for one Zn duplicate, and less than 7% error for two Zr duplicates.

Based on the results of Rock-Eval 6 analysis, 30 samples were chosen for organic petrologic examination to visualize areas of each lithofacies containing high, low and moderate levels of TOC, S2 and HI. Samples were coarsely crushed and used to make polished pellets of randomly-oriented rock fragments using a cold-setting epoxy-resin mixture. Pellets of each sample were examined using a Zeiss Axio Imager II reflected light microscope, under oil immersion (n=1.518 at 23°C) using both white and ultraviolet (UV) light and 50x and 100x objectives. Fluorescence microscopy was conducted using ultraviolet G 365 nm excitation with a 420 nm filter. The Diskus-Fossil software paired with the microscope facilitates the rapid and precise measurement of reflectance on numerous particles, allowing collection of a statistically significant amount of data, a minimum of 50 reflectance measurements in dispersed organic matter samples (Barker and Pawlewicz, 1993).

Polished pellets were also used to measure grain sizes in each sample using UV light and the Diskus-Fossil software measuring tool. A minimum of 100 randomly oriented grain diameter measurements were collected on each sample for use in grain size analysis. High numbers of measurements were collected from randomly oriented rock fragments throughout the polished pellet samples, since large numbers of random measurements will usually show a normal distribution; this accounts for measuring diameter only in a two-dimensional section. Descriptive studies such as this are recommended to use a minimum number of 100 measurements to achieve normal distribution and statistical significance (Fraenkel et al., 1993). Efforts were made to measure only detrital mineral grains. Bioclasts were not included in grain size measurements. One disadvantage to our method is that it does not completely reflect the total proportion of clay sized material, since the majority of these grains are below the resolution of the microscope.

3.5 Results & Discussion

Results and interpretations are discussed by well along a transect from south to north across the Sverdrup Basin. The collective data are used to interpret depositional environment. Emphasis is placed on the main factors that control the distribution of organic carbon in sediment. These include: autochthonous biomass productivity, preservation of OM, and dilution effects caused by clastic material and allochthonous OM.

A suite of redox sensitive elements are used to interpret depositional conditions of material preserved in each of the cores. The elements were chosen for analysis based on their potential usefulness as both paleo-redox (Mo, Cu, Ni, Co, U, V, Cr, Zn) and detrital influx (Zr, Ti) proxies. Al was analysed for normalization purposes. Enrichment factors (EF) were calculated for each of the elements using $EF = [(X/Al)_{sample}/(X/Al)_{PAAS}]$ where X and Al represent the weight concentrations of the redox element of interest and Al, respectively, and PAAS is the post-Archean Australian Shale (Taylor and McLennan, 1985), chosen for normalization. EF values >3 and >10 are considered to indicate detectable and substantial levels of authigenic enrichment of an element, respectively (Algeo and Tribovillard, 2009). Covariation of Mo-U can be used distinguish between oxic, suboxic, and anoxic bottom water conditions, following the methods of Algeo and Tribovillard (2009). Additionally, correlations between redox elements (Mo, Cu, Ni, Co, U, V, Cr, Zn) and TOC can be used to highlight relationships between the elements and OM as wells as infer syndepositional redox conditions. Statistical analysis of EF and TOC values was completed with Pearson's r correlation using Microsoft Excel Analysis ToolPak™ and significance of $p<0.05$.

3.5.1 Collingwood K-33

Core from the Collingwood K-33 well consists predominantly of calcareous, argillaceous, grey to light grey siltstone, most of which is moderately to well bioturbated (Appendix A). The proportion of argillaceous material varies with depth. Dispersed pelecypod fragments and framboidal pyrite clusters are common to rare. Grain size analysis of the samples reveals grain sizes ranging from clay (<4 μm) to very fine-grained sand (62-125 μm). Average grain size for all samples is medium silt (16-31 μm) (Fig. 3.1a). The clasts are poorly sorted ranging from subangular to subrounded.

The core is organic lean with TOC ranging from 0.09 to 0.83 wt.% (Table 3.1). Rock-Eval analysis indicates that kerogen type is predominantly Type II (autochthonous, marine) based on the slope-derived HI value (360 mg HC/g TOC) from the data points (Fig. 3.2) (Langford and Blanc-Valleron, 1990; Cornford et al., 1998). The S2 versus TOC plot is generally a more reliable designator for kerogen type compared to the pseudo Van Krevelen plot, since the former is based on measured values and the latter based on ratios of measured values (HI = S2 x 100/TOC, OI = S3 x 100/TOC) (Lafargue et al., 1998). The ratios can become skewed when TOC values are very low, as is the case in this core, due to hydrocarbon retention from the mineral matrix effect (Langford and Blanc-Valleron, 1990). Rock-Eval software may not accurately pick the values for S2 and S3, and in conjunction with very low TOC values, can cause exaggerated ratio values. Organic petrology indicates a mixture of autochthonous and allochthonous macerals including high-reflecting reworked vitrinite, inertinite, (semifusinite and inertodetrinite), and dark-brown, amorphous bituminite (Fig. 3.3a). Bituminite, in this study, is defined as bacterially degraded or oxidized liptinitic matter (e.g., geolipids and fragments of algae or plankton with substantial amounts of bacterial biomass present) (Teichmüller, 1989).

Fluorescence microscopy reveals low to moderate abundance of yellow-green fluorescing liptodetrinite (e.g., algal fragments) and occasional well-preserved acritarchs (Fig. 3.3b). Bituminite is visible as dark red-brown fluorescing macerals.

Reflectance measurements were collected on all maceral types within the petrographic samples; however, not all measurements can be considered valid or accurate representations of thermal maturity of the rock. Based on these reflectance values, the majority of measured macerals appear to be allochthonous, reworked, or oxidized and therefore do not reveal the thermal history of the unit. The autochthonous OM in these samples is represented by bituminite and liptinitic macerals, neither of which has been sufficiently thermally matured to generate bitumen for reflectance measurements. Bitumen generated from these autochthonous macerals would, if present, likely reflect the thermal maturity of the samples. Bituminite macerals are not reliable for reflectance measurements due to degradation by microbial activity. Additionally, there is no formula presently available by which to convert bituminite reflectance measurements to other recognized indices of thermal maturity. Therefore, none of the reflectance values from OM in these rocks represent the true thermal maturity of the interval. The median T_{max} value for the samples is 434°C (Table 3.1), indicating that they are immature and just outside the oil generation window. Reflectance values measured on vitrinitic macerals (the only macerals present that can supply valid measurements), represent thermal maturity that is much higher than that determined by Rock-Eval's T_{max}. This further supports the inference that most of the macerals are allochthonous, with variable degrees of oxidation, which is reflected in the wide range of reflectance values. However, T_{max} values may be unreliable in samples with very low TOC, S1, or S2 values (Espitalie et al., 1985), such as the Collingwood K-33 samples. In this case, the bright yellow-green fluorescence of autochthonous OM (e.g., Fig. 3.3b) may add

qualitative support to the thermal immaturity of the samples, even if T_{max} cannot be considered reliable. Thermal immaturity at this location in the basin is consistent with regional studies and is attributed to insufficient burial depth owing to thinner overlying strata deposited along the basin margin (Goodarzi et al., 1989).

All samples from Collingwood K-33 show variable enrichment in Mo (Mo_{EF} = 1.7-42.4) and less enrichment in U (U_{EF} = 1.1-2.7) (Table 3.2). Most of these samples have Mo_{EF}/ U_{EF} values greater than the seawater Mo/U molar concentration (Fig. 3.4). Based on the classification methods of Algeo and Tribovillard (2009), these samples plot along the particulate shuttle pathway, with greater enrichment in Mo than U. The particulate shuttle is the process by which molybdate ions (and other metal ions) adsorb to manganese and iron oxyhydroxides in an oxic marine water column. These complexes subsequently settle and, under anoxic bottom water conditions, are reduced and release the adsorbed Mo delivering it to the sediments (Algeo and Tribovillard, 2009). U has not been shown to be affected by this particulate shuttle, which may provide a mechanism for greater enrichment of Mo compared to U in the Collingwood K-33 samples. However, low EF (EF < 3) for all redox elements examined (Cu, Ni, Co, U, V, Cr, Zn) except for Mo (Table 3.2), are strongly suggestive of either oxic conditions during deposition of the Collingwood K-33 sediments, or remobilization of redox elements due to later oxidation of sediments (i.e., bioturbation). Bioturbation evidence observed in core led to the interpretation of oxic bottom water conditions; therefore, Mo enrichment is likely the result of other factors, in addition to bottom water redox conditions in these samples.

Mo content in marine sediments can be provided by three main sources: 1) lithogenic Mo, delivered to the basin by erosion of continental landmass; 2) biogenic Mo, associated with OM either through adsorption or inclusion; and 3) authigenic Mo, precipitation of Mo or

adsorption to other mineral phases under oxic or anoxic conditions (Poulson Brucker et al., 2009). Ni and Cr show positive correlations with TOC but the other redox elements (Mo, Cu, Co, U, V, Zn) show no covariance with TOC (Table 3.3), which suggests that redox elements are associated mainly with the detrital fraction of the rock rather than the organic fraction. This may indicate that Mo was simply more abundant in the water column due to lithogenic sources compared to other redox elements. There is a positive correlation between Mo and Zr, Ti, supporting detrital delivery of Mo (Table 3.3). Mo_{EF} values are not so high that substantial sediment sequestration mechanisms need to be established for these samples. It appears that oxygenation of bottom waters at the time of sediment deposition both inhibited preservation and contributed to in situ oxidation of OM in these sediments.

Temporal variations of conservative lithophilic elements such as Zr and Ti in the core can be used as proxies for detrital clastic input into the system (Sageman and Lyons, 2004 and references therein). Both Zr_{EF} and Ti_{EF} are low (EF < 3) for the entire cored interval of Collingwood K-33 with the majority of values for both elements between 1.0 and 1.5 (Fig. 3.5a). Compared to the more organic rich cored intervals, this core shows a coarser grain size (predominantly medium silt) (Fig. 3.1a, 3.1b, 3.1c), which indicates higher energy conditions and dilution with clastic mineral material. This is not reflected in the detrital proxy EF, but is visually evident both macro and microscopically. These sediments were deposited in a mid- to inner shelf environment in the middle portion of the Ladinian RST, near the facies change to prograding shelf sands of Chads Point Member (Embry, 1984a). The southern sediment source supplied influx of both Devonian clastic material as well as reworked macerals derived from the eroded rocks (Patchett et al., 2004), resulting in dilution of primary OM in the sediments. The

proximity to the southern basin margin also facilitated the transport of terrestrial OM to the basin, but not without substantial oxidation en route.

3.5.2 Skybattle Bay M-11

The Skybattle Bay M-11 core was extracted near the middle of the Murray Harbour Formation and preserves sediments deposited in both shallower and deeper water environments. The lower portion of the core contains the uppermost portion of the Anisian RST, capped by an unconformable shoreline ravinement (Embry and Podruski, 1988). The overlying TST of the Ladinian sequence is 11 cm thick and capped by a maximum flooding surface. The remainder of the core represents the basal portion of the Ladinian RST. For the purpose of this study, the core is divided into an upper and lower portion along the maximum flooding surface at the boundary between the Ladinian TST and RST (Fig. 3.6). This surface, which coincides with the lithostratigraphic boundary between the "lower member" and the Cape Caledonia Member, is chosen as a divider because the lithology and OM characteristics change across this boundary. For a detailed description and interpretation of the sequence stratigraphy of the Skybattle Bay M-11 core, readers are referred to Embry and Podruski (1988).

The lower portion of the core (Anisian RST and Ladinian TST) consists of three main lithologies: The lower 7.5 m consists of calcareous dark grey mudstone, very thinly interbedded with calcareous grey to light grey siltstone. It is moderately to well bioturbated with moderate to abundant dispersed pyrite framboids (<1 mm in diameter). The abundance of siltstone interbeds is variable and some show cross laminations. Grain size analysis reveals a range of grain sizes from clay (<4 μm) to very fine-grained sand (62-125 μm) and an average grain size of medium silt (16-31 μm) (Fig. 3.1b). Clasts are poorly sorted and subangular. This lithology sharply

transitions upwards into calcareous, silty, very fine-grained sandstone (62-125 μm), which is heavily bioturbated.

The top 11 cm of the lower portion of the core (Ladinian TST) consists of clast-supported conglomerate with grey siltstone and fine- to medium-grained sandstone (125-500 μm) matrix. The conglomerate clasts are up to 10 cm in length and are composed of fossil fragments, pyrite, mudstone and phosphate. The sorting is poor and the clasts are angular to rounded. This conglomerate unconformably overlies the lower silty sandstone, marking a submarine unconformity (unconformable shoreline ravinement) and the sequence boundary between the Anisian RST and the Ladinian TST.

The upper portion of the core (Ladinian RST, Cape Caledonia Member) is calcareous black mudstone that is very thinly interlaminated with calcareous grey-brown siltstone. There are occasional beds containing phosphate nodules and phosphate intraclasts. Pelecypod fragments, micaceous grains and organic fragments are all common. Pelecypod fragments typically align along bedding planes. Grain size analysis shows grain size ranging between clay (<4 μm) and very fine-grained sand (62-125 μm). Average grain size is fine to medium silt (8-31 μm) (Fig. 3.1b). The clasts are poorly sorted ranging from subangular to angular.

The samples from the lower portion of the Skybattle Bay M-11 core are organic lean with TOC ranging from 0.22 to 0.93 wt.% (Table 3.1). This contrasts sharply with the upper portion of the core, which is organic rich; TOC for the upper portion ranges from 1.48 to 4.82 wt.% (Table 3.1). Samples from the lower portion of the core contain predominantly terrestrial Type III kerogen (Fig. 3.2). The S2 versus TOC plot is used for kerogen typing in this portion of the core due to the very low TOC values, for reasons discussed in section 4.1. Organic petrologic examination of these samples reveals a variety of macerals that include high-reflecting, reworked

vitrinite, inertinite, and occasional presence of bituminite and pore-filling bitumen (Fig. 3.3c). The maceral assemblage is quite similar to that of the Collingwood K-33 samples; however no fluorescence of macerals is observed. In contrast, samples from the upper portion of the core contain mainly marine Type II kerogen. Organic petrology reveals that these samples contain mainly matrix bitumen (i.e., solid migrabitumen disseminated throughout clay-sized grains) but also show the same variety of macerals as the lower portion albeit in much smaller abundances (Fig. 3.3d). Much of the solid bitumen filling larger pores is associated with framboidal pyrite and diagenetic carbonate crystals (Fig. 3.3e). Exuded oil and bitumen saturate smaller pores within the clay-rich matrix and fill larger pores along the boundaries of mineral grains and bioclasts (Fig. 3.3f). Aside from the dull orange-brown fluorescence exhibited by some accumulations of matrix bitumen, the samples from the upper portion of the core show little to no fluorescing liptinitic material.

Figure 3.2 indicates a mixture of Type II and III kerogen for samples from the upper portion of the core, and mainly Type III kerogen for samples from the lower portion of the core. These classifications are consistent with organic petrographic observations (Fig. 3.3c, 3.3d). Two samples from the upper portion of Skybattle Bay M-11 show anomalously high S2 values; the values of these samples were confirmed by duplicate analysis and by the overall accuracy and precision of the dataset. Organic petrographic observations of these samples show abundant phosphatic nodules, which rapidly exude free hydrocarbons under the influence of UV light. These nodules seem to supply porosity for accumulation of heavy and light oils, which results in anomalously high S1 and S2 values. Median T_{max} values of 438°C and 443°C for the lower and upper portions of the core, respectively, indicate that both intervals are within the peak oil generation window for Type II kerogen (Tissot et al., 1987).

Populations of OM can be identified on the reflectograms of measured reflectance values (e.g., Fig. 3.7a). Only the lowest-reflecting population of bitumen (i.e., matrix bitumen) is representative of the thermal maturity of the unit. Using VRo% = (BRo% + 0.03)/0.96 (Bertrand and Malo, 2001) where VRo% is the equivalent vitrinite reflectance value, and BRo% is the bitumen reflectance value, VRo% = 0.83, for the matrix bitumen population in Figure 3.7a. This VRo% places the unit within the peak oil generation window, in agreement with T_{max} values for the interval. Measurements of this population of bitumen were difficult to obtain, despite the pervasive nature of it, due to poor surface quality. The higher-reflecting population of bitumen is generally found filling larger pore spaces and is typically associated with framboidal pyrite and diagenetic carbonate crystals, both of which can be products of bacterial sulphate reduction (BSR) of OM (Machel, 2001) (Fig. 3.3e). BSR requires adequate water circulation to provide the necessary dissolved SO_4^{2-} for the reaction to progress effectively (Machel, 2001); therefore, OM within larger pores is expected to facilitate this process better than OM within very small pores such as those within the clay-rich matrix. This population of solid bitumen shows higher reflectance values than the unaffected matrix bitumen due to pseudo-maturation effects by bacteria, in addition to subsequent thermal maturation. The higher-reflecting bitumen population also has a wider range of reflectance values due to variable degrees of degradation. The reworked vitrinite and inertinite populations represent allochthonous OM, which also do not represent the thermal maturity of the unit.

As in Collingwood K-33, vitrinite from the lower portion of the Skybattle Bay M-11 core shows a wide range of reflectance values, higher than the T_{max}-equivalent for the core, indicating their reworked and oxidized nature. The lower abundance of these macerals in the upper portion of the core compared to the lower portion of the core is suggestive of dilution by autochthonous

OM produced in the water column. This is consistent with the interpretation that the upper portion of the core was deposited at the beginning of the Ladinian RST, when basin waters extended inland, after maximum transgression (Embry and Podruski, 1988). Associated conditions such as increased water depth, decreased current energy, and increased distance to the basin margin and sediment source due to transgression facilitated production and accumulation of marine biomass.

High productivity in the organic rich upper portion of the core is evident not only by high TOC values but also by the low proportion of initial RC deposited in the system. A linear regression line for these samples on a plot of S2 versus TOC can be used to derive the initial RC in the system prior to production of primary kerogen (i.e., when S2 was equal to zero) (Cornford et al., 1998) (Fig. 3.2). The regression line x-intercept has a value of -0.76 wt.%, which is unusual; typically samples show positive x-intercept values. We interpret this as an indication of production and local migration of bitumen. This may also be the result of degradation of free light hydrocarbons initially present in the rock, to heavier hydrocarbons since the time of core extraction, therefore influencing the relationship between TOC and S2 in the samples. Additionally, the initial RC value for this interval must have been quite low to become overwhelmed by S2 currently present in the samples. Present median RC for the interval is 2.62 wt.% (Table 3.1) or 82 % of the present median TOC value. The increase in RC since deposition is the result of thermal degradation of OM, since the well is within the oil generation window. The slope of the regression line (Fig. 3.2), when multiplied by 100, represents the HI value of the interval overall, without the effects of inert OM (Cornford et al., 1998). The regression line slope-derived HI value for the upper portion of the core is 159 mg HC/g TOC. This is similar to the measured median HI value of 192 mg HC/g TOC, further supporting minimal inertinite

influence on the system. This HI value is lower than the HI values derived from the other wells, and reflects the higher thermal maturity of the Skybattle Bay M-11 samples; as hydrocarbons were generated and expelled from the rock, the hydrogen-rich components of the kerogen were as well. This illustrates the importance of knowing the thermal maturity of samples when interpreting results from Rock-Eval, especially when comparing values from samples sets of different maturities.

Most of the samples from the lower portion of the core are depleted in Mo (Mo_{EF} = 0.5-5.2) and similar to PAAS values in U (U_{EF} = 1.1-1.2) (Table 3.2). Most samples also show Mo_{EF}/ U_{EF} values less than the Mo/U molar concentration for seawater (Fig. 3.4). Based on classification methods from Algeo and Tribovillard (2009), these values are indicative either of oxic bottom water conditions during deposition or remobilization of both elements as a result of oxidation of sediments. Nearly all of the studied redox elements have EF values < 3, again indicating deposition of sediments under oxic bottom water conditions or loss of redox elements due to sediment oxidation (i.e., bioturbation) (Table 3.2). The lower portion of the Skybattle Bay M-11 core contains evidence of bioturbation, which is consistent with these redox proxy interpretations. Cu and Ni show positive correlation with TOC, Zn shows negative correlation, but the other redox elements in the lower portion of the core do not show covariance with TOC (Table 3.3). This indicates that redox elements are likely primarily supplied by the detrital fraction of the rock, similar to redox elements of Collingwood K-33.

The two samples collected from the TST of the core show markedly different EF for some redox elements compared to the rest of the lower portion of the core (i.e., the Anisian RST). Mo and U both have EF >10, while Cr has EF >3. Samples show substantial enrichment in Mo and U as well as Mo_{EF}/ U_{EF} ratios less than seawater Mo/U molar concentrations, a pattern

similar to modern sediments in the Black Sea (Algeo and Tribovillard, 2009) (Fig. 3.4). These authors interpreted this pattern in Black Sea sediments as depletion of Mo in the water column due to limited Mo replenishment, resulting in enrichment of U relative to Mo in sediments, a common situation in restricted, anoxic basins. However, low EF for most of the other redox elements in the TST samples suggests oxic depositional conditions (or remobilization due to oxidation). The TST represents a period of rapid base level rise, resulting in basinal sediment starvation, submarine erosion, and winnowing of sediments deposited at the end of the Anisian RST (Embry, 1984a). This environment is complex, with many factors affecting the geochemistry of the sediments; therefore the use of redox elements as redox proxies for this interval may not be reliable.

Samples from the upper portion of the core have different redox element geochemistry compared to the lower portion of the core. Mo is enriched in most of these samples (Mo_{EF} = 5.4-439.9) but U enrichment remains low (U_{EF} = 1.1-3.8) (Table 3.2), with all samples plotting above the seawater Mo/U molar concentration line (Fig. 3.4). These samples are within the particulate shuttle pathway defined by Algeo and Tribovillard (2009), similar to the Collingwood K-33 samples. However, unlike Collingwood K-33 samples, upper Skybattle Bay M-11 samples show positive correlation with TOC for Cu, Ni, V, and Cr, suggesting that redox element sequestration in the sediments is likely associated with the organic fraction (Table 3.3). It should be noted that this core is thermally mature and that the effects of diagenesis and catagenesis on redox element remobilization are still poorly understood (e.g., Abanda and Hannigan, 2006). None of the redox elements (with the exception of Mo) show substantial enrichment compared to PAAS values, which implies anoxic bottom water conditions as opposed to euxinic, since the

later setting tends to greatly enhance accumulation of redox elements (Algeo and Maynard, 2004 and references therein).

Zr_{EF} and Ti_{EF} for most of the samples from the upper and lower portion of the Skybattle Bay M-11 core are close to and just below PAAS values (Fig. 3.5b). These proxies do not show considerable difference in detrital influx between the upper and lower portions of the core, despite macro- and microscopic observations indicating otherwise. The lower portion of the core has a higher proportion of coarser-grained material (predominantly medium silt) compared to the upper portion of the core (predominantly fine to medium silt) (Fig. 3.1b). This indicates slightly higher energy depositional conditions for the lower portion of the core, both delivering coarser clastic material to dilute OM and limiting deposition of lower density organic particles. It is unclear why the chosen detrital proxies do not reflect grain size differences in the two portions of the core, as typically these elements are associated with coarser fractions of rock (Sageman and Lyons, 2004 and references therein). Zr_{EF} values for the two TST samples, are highly depleted compared to PAAS values (Fig. 3.5b), which is consistent with the sediment-starved state of the basin at that time. However, as Ti_{EF} values do not show this same trend, these proxies may be affected by other, presently unknown factors.

3.5.3 Pollux G-60

The Pollux G-60 core was extracted near the base of the Murray Harbour Formation on the northern basin margin and is located near the base of the Anisian RST. Three lithofacies and one sublithofacies are recognized in the cored strata. Lithofacies 1 is calcareous dark grey mudstone, very thinly interlaminated with grey-brown siltstone, and is moderately to well bioturbated. Lithofacies 2 is calcareous mudstone and siltstone as described in lithofacies 1, but with very thin plane parallel laminations and no macroscopically visible bioturbation. 1-2 mm

fragments of OM and pelecypod impressions are present rarely. Sublithofacies 2a is similar to lithofacies 2, but mudstone interlaminae dominate. Lithofacies 3 is similar to lithofacies 2a, but includes dispersed white chert nodules, 1-15 mm in diameter, rounded to elongate in shape and often with euhedral pyrite crystals in the centre. Pelecypod impressions and OM fragments are present rarely to occasionally. The contacts between the lithofacies are gradual.

Figure 3.1c illustrates the variation in grain size between high TOC (>2 wt.% TOC) and low TOC (<1wt.% TOC) intervals for the Pollux G-60 core; low TOC intervals have a greater proportion of larger grain sizes compared to high TOC intervals. Grain size analysis of all pellet samples in the core reveals that grain size ranges from clay (<4 μm) to very fine-grained sand (62-125 μm) and the average grain size is fine silt (8-16 μm). The clasts are poorly sorted ranging from subrounded to subangular. The standard deviation of grain size measurements is also larger for the low TOC intervals, indicating poorer sorting compared to the higher TOC intervals ($Stdev_{Low\ TOC}$ = 15.7 versus $Stdev_{High\ TOC}$ = 6.3). Framboidal pyrite varies in abundance from low to high, generally increasing with TOC.

The samples from this core show well-defined, gradual cyclostratigraphic variations of increasing and decreasing TOC with depth (Fig. 3.5c). Organic content ranges from organic lean to organic rich, with TOC values between 0.24 and 3.56 wt.% (Table 3.1). Organic petrology reveals a variety of macerals including inertinite, liptinite, bituminite, and high-reflecting, reworked vitrinite (Fig. 3.3g). As in the other cores, the vitrinite displays a wide range of reflectance values, suggesting reworked and oxidized sources. Figure 3.7b shows an example reflectogram with three populations of measured macerals. Bituminite reflectance cannot be used as a thermal maturity index due to the reasons outlined in section 4.1, and the populations of reworked vitrinite and inertinite are allochthonous. Compared to the upper Skybattle Bay M-11

population (Fig. 3.7a), the reworked vitrinite population in this core shows a wider range of reflectance values, suggesting a greater variety of detrital OM supplied to the Pollux G-60 core. Under ultraviolet light, the samples from this well show abundant brightly-fluorescing yellow-green liptodetrinite (algal fragments) and acritarchs as well as reddish-brown fluorescing bituminite (Fig. 3.3h). Kerogen is predominantly Type II with some Type III (Fig. 3.2)

High abundance of strongly yellow-green fluorescing liptinitic OM clearly indicates the samples have not been substantially thermally degraded. As thermal degradation progresses the chemical reactivity of the liptinite group is decreased, reducing the intensity and changing the wavelength of the fluorescence from green to red spectra (Taylor et al., 1998). The median T_{max} value for this interval is 441°C. The onset of oil generation is approximately between T_{max} values of 430°C and 435°C for Type II and Type III kerogen (Tissot et al., 1987). T_{max}-based oil generation thresholds place these rocks within the early oil generation window; however organic petrographic observations suggest thermal immaturity (i.e., abundant fluorescing liptinitic material, absence of bitumen). The kinetics of conversion of kerogen to hydrocarbons are complex and not fully understood and the use of T_{max} as a thermal index is further complicated by mixtures of kerogen types (Tissot et al., 1987). Thus it is important to consider oil and gas generation thresholds as approximate only. In reality, these rocks have likely just commenced oil generation, as S1 values (Table 3.1) show small amounts of free hydrocarbons present. This dataset illustrates the importance of combining organic petrology with Rock-Eval analysis to make correct interpretations. Each technique interpreted alone could result in inaccurate conclusions about the thermal history of the rocks.

The slope of the regression line for these samples (Fig. 3.2) yields an HI value of 503 mg HC/g TOC, leading to the interpretation of mainly Type II kerogen. The initial RC for the system

(x-intercept of regression line in Fig. 3.2) was 0.22 wt.% or 16 % of the present TOC. This is suggestive of relatively limited influx of inert OM to the system.

The lowest TOC intervals are typically associated with lithofacies 1, the bioturbated mudstone and siltstone, while the higher TOC intervals generally coincide with the non-bioturbated lithofacies (i.e., lithofacies 2, 2a, 3) (Fig. 3.5c). The major exception is the interval at the very base of the core (depth 1379.88 – 1380.70 m) where there is no observed evidence of bioturbation but TOC values are <1 wt.%. Bioturbation of these low TOC intervals suggests that bottom waters must have been oxic, containing at least 75 μM of dissolved oxygen at the time of deposition for benthic organisms to survive (Yakushev, 2013). However, interpretation of the elemental redox proxies for this interval is complex. Pollux G-60 samples have detectible to substantial Mo enrichment for most samples (Mo_{EF} = 1.8-16.6) but minimal U enrichment (U_{EF} = 1.4-8.9) (Table 3.2), with Mo_{EF}/ U_{EF} values less than seawater Mo/U molar concentrations (Fig. 3.4). This pattern of Mo-U covariation is interpreted by Algeo and Tribovillard (2009) as suboxic bottom water conditions, reflecting preferential sediment sequestration of U under less reducing conditions (and in the absence of H_2S) compared to Mo. Low TOC samples (TOC <1 wt.%) show both a wider range of Mo and U EF as well as greater enrichment in both elements compared to higher TOC samples (TOC > 1 wt.%) (Table 3.2, Fig. 3.4).

Table 3.4 summarizes correlations between TOC and redox elements for different intervals of the Pollux G-60 core. The higher TOC intervals (>1 wt.%), show positive correlation between TOC and Mo, Cu, Ni, V, Cr (Table 3.3). This suggests that sediment enrichment in Mo, Cu, Ni, V, and Cr in the higher TOC intervals is associated with the organic fraction. All these redox elements have EF that are < 3 (detectable) except for Mo, which has some EF up to 10 (substantial) (Table 3.2); therefore the higher TOC intervals, are likely to represent either oxic or

suboxic bottom water conditions, rather than anoxic or euxinic conditions, which would tend to cause greater enrichment of redox elements. Based on the lack of bioturbation evidence observed in these intervals, as well as the high preservation of labile OM, a suboxic environment is interpreted.

The low TOC intervals (<1 wt.%), show positive correlation between TOC and Cu, and negative correlation between TOC and Mo and U (Table 3.3). Mo shows detectible to substantial enrichment for all low TOC intervals and U shows detectible enrichment for some portions of the low TOC intervals relative to PAAS (Table 3.2). This suggests that Mo and U are not associated with the OM fraction in the low TOC intervals, and are more likely enriched due to other processes. Since both Mo and U and not highly enriched compared to PAAS, delivery of these two elements via detrital influx to the basin is not unreasonable. There are positive correlations between Mo, U and Zr, Ti (Table 3.3), which indicates a detrital mechanism of sediment enrichment in Mo and U. Furthermore, the wide range of Mo and U EF (Table 3.2, Fig. 3.4) suggests a variable supply of these elements, typical of pulses of detrital influx, for example from variable fluvial discharge or deltaic lobe switching. Bioturbation and low TOC content for these intervals in conjunction with minimal enrichment of all other redox elements suggests oxic bottom water conditions at the time of deposition.

Zr_{EF} and Ti_{EF} are both near 1.0 for most of the interval, indicating little enrichment from PAAS values. Zr_{EF} does show some variation with depth (Fig. 3.5c), with slight enrichment in Zr corresponding to the low TOC intervals. Macro and microscopic observation and measurement of grain size and distribution (Fig. 3.1c) reveal that the low TOC intervals show a higher proportion of larger silt-sized clasts compared to the high TOC intervals (> 2 wt.%). A higher TOC cut-off value was chosen for grain size display, to more clearly exemplify the differences

between the two end-members of the cycles. A higher proportion of larger silt-sized sediment is suggestive of higher energy water conditions limiting deposition of clay and low density particles (i.e., OM). It appears that relatively constant high primary productivity in the water column at this location was punctuated by periodic increases in clastic input, resulting in dilution of OM and lowering of TOC. The intervals of high TOC are interpreted as deposition of these rocks near the beginning of the Anisian RST, when the basin was near maximum transgression, creating low energy conditions suitable for OM accumulation. The gradual character of the TOC cycles in this core is suggestive of gradual changes to the energy conditions at this location in the basin (i.e., increase and decrease in water depth, accommodation space, or detrital input), resulting in variable grain size delivery. The low and high TOC intervals are end-members of a continuum of maximum and minimum influx of detrital material, respectively, with moderate TOC intervals reflecting a combination of influx levels during transition. If energy conditions were the result of more rapid events (i.e., turbidite flows, storm deposits), we would expect to see much sharper transitions in TOC content, sharp contacts between lithofacies, and sedimentary structures typically associated with those events such as fining upwards successions.

Evidence for sedimentation derived from the northerly-located Crockerland is present in the form of marine sandstone facies that grade into siltstone and mudstone towards the south (Embry, 1993, 2009). Presently, these marine sandstones have been identified in both Lower and Upper Triassic strata, but not within Middle Triassic strata (Embry, 2009). The siltstone intervals identified in the Pollux G-60 core could be evidence supporting pulses of clastic input from Crockerland during the Middle Triassic, albeit in a more distal setting than the marine sandstone of the Early and Late Triassic. If these intervals could be traced laterally to other locations along

the northern margin of the Sverdrup Basin, the source area could be identified with greater certainty.

3.5.4 Basinal Overview

Organic richness in Middle Triassic strata of the Sverdrup basin relates to the transgressive and regressive cycles present within the 3rd order sequences. Observed changes in detrital input are the result of increasing and decreasing distance of a specific locality from sediment source, changes in water depth, or current energy levels. The water depth at the locality and the associated changes in depositional conditions affect all other factors controlling OM production, accumulation, and preservation. These effects are particularly evident at Collingwood K-33 and Skybattle Bay M-11, where relative water depth variations caused major changes to depositional conditions. At the location of Pollux G-60, smaller scale fluctuations in TOC are predominantly the result of pulses of clastic dilution. These pulses may represent smaller-scale, high frequency changes of sediment delivery superimposed on the larger scale transgressive-regressive variations reflected in the 3rd order sequences.

3.6 Conclusions

The cores from the Middle Triassic succession of the Sverdrup Basin examined in this study reveal a range of OM types and abundances. These OM variations are primarily dependent on the location within the basin as well as the stratigraphic position in the two 3rd order sequences of the Middle Triassic strata. The position in the sequences relates to the level of preservation of OM, the production of marine biomass, and the degree of dilution of accumulated OM by clastic and allochthonous organic material. The results and conclusions of this study contribute to the organic and inorganic geochemical understanding of heterogeneous fine-grained successions; these findings can be applied to other potential unconventional reservoirs to

facilitate better characterization and prediction of prolific zones. The conclusions from this study are as follows:

1) Samples from the Collingwood K-33 well are organic lean, with a mixture of autochthonous Type II and allochthonous Type III kerogen. Low total organic carbon (TOC) values for this core can be attributed to predominantly oxic depositional conditions. Dilution of OM by coarser clastic material also contributes to the low TOC values.

2) The Anisian part of the Skybattle Bay M-11 core is organic lean, containing allochthonous Type III kerogen, contrasting with the organic rich, mainly autochthonous Type II kerogen of the Ladinian part of the core. Oxic depositional conditions dominated the Anisian interval along with higher clastic input to the basin compared to the Ladinian interval. The Ladinian interval was deposited in anoxic bottom water conditions. The organic rich, thermally mature base of the Ladinian RST in this part of the basin is the most prospective in terms of hydrocarbon potential and could be considered for shale oil exploration.

3) The samples from the Pollux G-60 core show a range of TOC values, varying with depth, in cycles of increasing and decreasing geochemical parameters. Kerogen is predominantly autochthonous Type II, with the highest abundance of it deposited under suboxic conditions. The intervals of lowest TOC are mainly the result of dilution of OM by pulses of coarser clastic influx and oxic bottom water conditions.

4) The intervals of coarser siltstone in the Pollux G-60 core may be indicative of sedimentation derived from the Crockerland source area, located north of the basin from the Carboniferous to the Jurassic. Conclusive evidence for northerly-derived clastic input during the Middle Triassic has not been identified presently. Recognition of similar periodic siltstone

intervals in other locations along the northern margin of the Sverdrup Basin could serve to support northerly-derived sedimentation.

Table Captions

Table 3.1: Summary statistics of Rock-Eval analysis for Middle Triassic samples.

Table 3.2: Summary statistics of enrichment factors (EF) relative to PAAS values (Taylor and McLennan, 1985) for redox elements studied in Middle Triassic samples as well as Al wt.% values used to calculate EF. *Skybattle Bay M-11 Lower statistics do not include the two samples from the Ladinian transgressive systems tract due to the difference in geochemical environment compared to the Anisian regressive systems tract.

Table 3.3: Correlation coefficients for total organic carbon (TOC) and enrichment factors (EF) relative to PAAS values (Taylor and McLennan, 1985) of all studied trace elements. Correlation coefficients for EF of detrital proxy elements (Zr, Ti) and EF of all studied elements. Bolded values indicate statistically significant positive correlation. Bolded, italicized values indicate statistically significant negative correlation. (Pearson's r correlation; $p<0.05$; Microsoft Excel Analysis ToolPak™).

Table 3.4: Summary of statistically significant correlations between total organic carbon (TOC) and redox-sensitive trace elements in Pollux G-60 for the low TOC (<1 wt.%) and high TOC (>1 wt.%) intervals. (Pearson's r correlation; $p<0.05$; Microsoft Excel Analysis ToolPak™, see Table 3.3 for values).

Tables

Table 3.1

Well Name	S1	S2	S3	T_{max}	HI	OI	TOC	PC	RC	PC/TOC	RC/TOC
	mg HC/g rock	mg HC/g rock	mg CO_2/g rock	°C	mg HC/g TOC	mg CO_2/g TOC	wt.%	wt.%	wt.%	%	%
Collingwood K-33											
Median	0.07	1.07	0.25	434	238	56	0.47	0.11	0.36	24	76
Minimum	0.01	0.08	0.20	428	89	35	0.09	0.01	0.07	11	70
Maximum	0.17	2.69	0.38	436	324	256	0.83	0.25	0.58	3	89
n = 28											
Skybattle Bay M-11 (Upper)											
Median	0.80	6.28	0.37	443	192	12	3.20	0.60	2.62	19	81
Minimum	0.38	2.37	0.26	425	151	8	1.48	0.26	0.96	15	42
Maximum	3.50	13.73	0.61	449	542	26	4.82	1.39	4.05	58	85
n = 51											
Skybattle Bay M-11 (Lower)											
Median	0.12	0.46	0.37	438	76	60	0.63	0.06	0.57	10	90
Minimum	0.05	0.20	0.25	434	51	37	0.22	0.03	0.19	8	86
Maximum	0.23	0.94	0.44	445	110	159	0.93	0.11	0.82	14	92
n = 30											
Pollux G-60											
Median	0.52	5.76	0.27	441	411	22	1.37	0.53	0.84	39	61
Minimum	0.06	0.47	0.19	437	196	8	0.24	0.06	0.18	25	55
Maximum	1.17	17.51	0.43	443	492	125	3.56	1.54	2.02	45	75
n = 41											

Table 3.2

Table 2

Well Name	Mo EF	U EF	V EF	Zn EF	Cu EF	Ni EF	Cr EF	Co EF	Al
									wt.%
Collingwood K-33									
Median	6.76	1.46	1.42	1.46	0.86	1.43	1.63	0.82	3.59
Minimum	1.69	1.13	1.30	0.88	0.51	0.83	1.25	0.50	1.05
Maximum	42.40	2.70	1.66	5.00	2.31	2.28	2.44	1.14	4.81
n = 28									
Skybattle Bay M-11 (Upper)									
Median	11.46	1.23	1.84	2.81	1.87	2.71	2.74	0.79	4.76
Minimum	5.43	1.08	1.21	1.03	1.21	1.64	1.64	0.63	1.93
Maximum	439.88	3.83	4.45	9.53	3.34	16.69	4.23	3.79	5.82
n = 51									
Skybattle Bay M-11 (Lower)*									
Median	0.90	1.20	1.05	1.06	0.54	1.01	1.22	0.73	5.75
Minimum	0.46	1.06	0.98	0.91	0.44	0.85	0.99	0.59	4.41
Maximum	5.18	1.54	1.21	1.52	0.63	1.29	1.57	0.84	7.01
n = 30									
Pollux G-60 <1 wt.% TOC									
Median	6.00	2.91	1.85	2.31	1.20	1.51	2.11	0.80	3.07
Minimum	2.02	1.76	1.72	1.43	1.07	1.14	1.72	0.57	1.35
Maximum	16.60	8.86	2.09	4.50	1.55	1.94	2.49	1.16	3.91
n = 16									
Pollux G-60 >1 wt.% TOC									
Median	3.44	2.08	2.08	2.33	1.68	2.01	2.22	0.81	4.80
Minimum	1.81	1.42	1.68	1.55	1.34	1.64	1.79	0.67	3.78
Maximum	9.18	3.16	3.80	6.61	2.47	3.34	4.03	0.99	5.47
n = 25									

Table 3.3

Well Name											
Collingwood K-33		Mo EF	Cu EF	Ni EF	Co EF	U EF	V EF	Cr EF	Ti EF	Zr EF	Zn EF
n=28	TOC	0.13	0.23	**0.48**	0.27	0.13	-0.01	**0.45**	-0.14	***-0.40***	-0.10
	Ti EF	**0.60**	0.28	0.24	-0.15	0.34	0.29	**0.57**	1.00	**0.81**	0.34
	Zr EF	**0.48**	0.21	0.03	-0.32	0.21	0.14	**0.39**	**0.81**	1.00	0.48
Skybattle Bay M-11 Upper		Mo EF	Cu EF	Ni EF	Co EF	U EF	V EF	Cr EF	Ti EF	Zr EF	Zn EF
n=51	TOC	0.19	**0.70**	**0.35**	0.17	-0.21	**0.68**	**0.59**	0.00	0.05	0.21
	Ti EF	-0.06	-0.09	-0.13	-0.05	-0.13	0.04	-0.14	1.00	**0.86**	***-0.64***
	Zr EF	0.08	0.01	0.02	0.08	-0.01	0.06	0.00	**0.86**	1.00	***-0.50***
Skybattle Bay M-11 Lower		Mo EF	Cu EF	Ni EF	Co EF	U EF	V EF	Cr EF	Ti EF	Zr EF	Zn EF
n=28	TOC	0.06	**0.40**	**0.43**	-0.15	0.12	0.36	0.23	0.13	0.05	***-0.45***
	Ti EF	0.07	0.01	0.19	-0.15	**0.64**	**0.73**	**0.53**	1.00	**0.69**	***-0.52***
	Zr EF	-0.23	-0.01	0.15	-0.29	**0.93**	**0.72**	**0.76**	**0.69**	1.00	-0.32
Pollux G-60 <1 wt.% TOC		Mo EF	Cu EF	Ni EF	Co EF	U EF	V EF	Cr EF	Ti EF	Zr EF	Zn EF
n=16	TOC	***-0.68***	**0.54**	0.28	0.09	***-0.55***	0.10	0.31	***-0.61***	***-0.74***	0.48
	Ti EF	**0.51**	-0.26	0.09	0.27	**0.56**	0.04	-0.37	1.00	**0.79**	0.00
	Zr EF	**0.68**	-0.39	0.02	0.16	**0.70**	-0.06	-0.28	**0.79**	1.00	-0.18
Pollux G-60 >1 wt.% TOC		Mo EF	Cu EF	Ni EF	Co EF	U EF	V EF	Cr EF	Ti EF	Zr EF	Zn EF
n=25	TOC	**0.49**	**0.77**	**0.81**	0.10	0.21	**0.89**	**0.87**	-0.14	***-0.41***	0.27
	Ti EF	-0.07	-0.06	0.09	0.18	***-0.53***	-0.05	-0.24	1.00	0.16	-0.24
	Zr EF	-0.02	-0.17	-0.16	0.13	0.18	-0.29	-0.11	0.16	1.00	-0.02

Table 3.4

Interval	Elements with Positive Correlation to TOC	Elements with Negative Correlation to TOC
Low TOC (<1 wt.%)	Cu	Mo, U
High TOC (>1 wt.%)	Mo, Cu, Ni, V, Cr	

Figure Captions

Figure 3.1: Grain size variation histograms resulting from measured random grain diameters for the studied wells, showing grain size distribution: a) Collingwood K-33; b) Skybattle Bay M-11 (lower portion of core) n=729. Microscopic grain size distribution for the Ladinian transgressive systems tract was not included due to the predominance of large (macroscopic) clast sizes; Skybattle Bay M-11 (upper portion of core) n=1376; c) Pollux G-60: Only samples with <1 wt.% total organic carbon (TOC) and >2 wt.% TOC are included in this histogram, to best illustrate grain size variation between lithological end-members; See text for further explanation. VF: very fine; F: fine; M: medium; C: coarse for silt and sand sized grains.

Figure 3.2: a) S2 versus TOC (total organic carbon) plot from all core samples (n=150) showing kerogen type classifications. Data points from organic rich intervals (Skybattle Bay M-11 upper, and Pollux G-60) are fitted with linear regression lines to interpret effects from inert kerogen in the system. See text for explanation.

Figure 3.3: Photomicrographs of organic matter types in each of the Middle Triassic cores. All images are taken under oil immersion and in reflected white light unless specified otherwise. a) Collingwood K-33: bituminite (Bt), inertinite (I), reworked vitrinite (RV), and degraded algae (DA) in a siltstone matrix with framboidal pyrite; b) Collingwood K-33 (UV light): brightly fluorescing acritarchs, indicating thermal immaturity of samples; c) Skybattle Bay M-11 lower: reworked vitrinite (RV) and inertinite (I) in a siltstone matrix with framboidal pyrite; d) Skybattle Bay M-11 upper: matrix bitumen (MB) filling small pores within the clay matrix; reworked vitrinite (RV); e) Skybattle Bay M-11 upper: higher-reflecting bitumen (B) filling a larger pore with abundant framboidal pyrite in a clay matrix; f) Skybattle Bay M-11 upper (UV

light): Blue-green fluorescence of free hydrocarbons (HC) accumulating along planar bioclasts or detrital mica grains; g) Pollux G-60: bituminite (Bt), inertinite (I), and possible reworked vitrinite (RV?) in a clay and siltstone matrix with minimal framboidal pyrite; h) Pollux G-60 (UV light): yellow-green fluorescing prasinophytes and acritarchs indicating thermal immaturity of samples.

Figure 3.4: Log-log plot of Mo_{EF} versus U_{EF} for all core samples. Solid horizontal line shows the PAAS value for Mo, since some samples show Mo depletion. Dashed lines show seawater (SW) molar ratio and fractions of Mo/U (Algeo and Tribovillard, 2009 and references therein). The two outlying Skybattle Bay M-11 Lower data points represent samples from the Ladinian transgressive systems tract. EF: enrichment factor relative to PAAS values (Taylor and McLennan, 1985).

Figure 3.5: Plots of TOC, Zr_{EF}, and Ti_{EF} versus depth. Dashed vertical lines on Zr_{EF}, and Ti_{EF} represent the PAAS values for each element. a) Collingwood K-33; b) Skybattle Bay M-11; c) Pollux G-60: A simplified lithofacies column is shown along the right side of the TOC versus depth plot. Lithofacies 1 (LF1) is moderately to well bioturbated mudstone and siltstone; Lithofacies 2, 2a, and 3 are laminated, non-bioturbated mudstone and siltstone. See text for full lithofacies descriptions. EF: enrichment factor relative to PAAS values (Taylor and McLennan, 1985).

Figure 3.6: Core photo of Skybattle Bay M-11 showing important surfaces. The maximum flooding surface (MFS), which marks the base of the Ladinian regressive systems tract (RST), divides the core into an upper and lower portion for the purpose of the study. The unconformable shoreline ravinement (SR-U) marks the sequence boundary between the Anisian and Ladinian

sequences. RST: Regressive systems tract; TST: Transgressive systems tract. Black and white scale blocks are each 10 cm in length.

Figure 3.7: Representative reflectograms from organic rich intervals showing semi-quantitative distribution of organic matter. a) Skybattle Bay M-11 Upper: The total reflectogram can be divided into four populations; matrix bitumen, bitumen, reworked vitrinite, and inertinite. The bitumen population can be used to determine the thermal maturity of the sample, while the other populations have all been affected by other processes causing increased reflectance values. See text for discussion; b) Pollux G-60: The total reflectogram can be divided into three populations; bituminite, reworked vitrinite, and inertinite. The bituminite population is the only autochthonous organic material in these samples, but measurements cannot be used as thermal indices. See text for discussion.

Figures

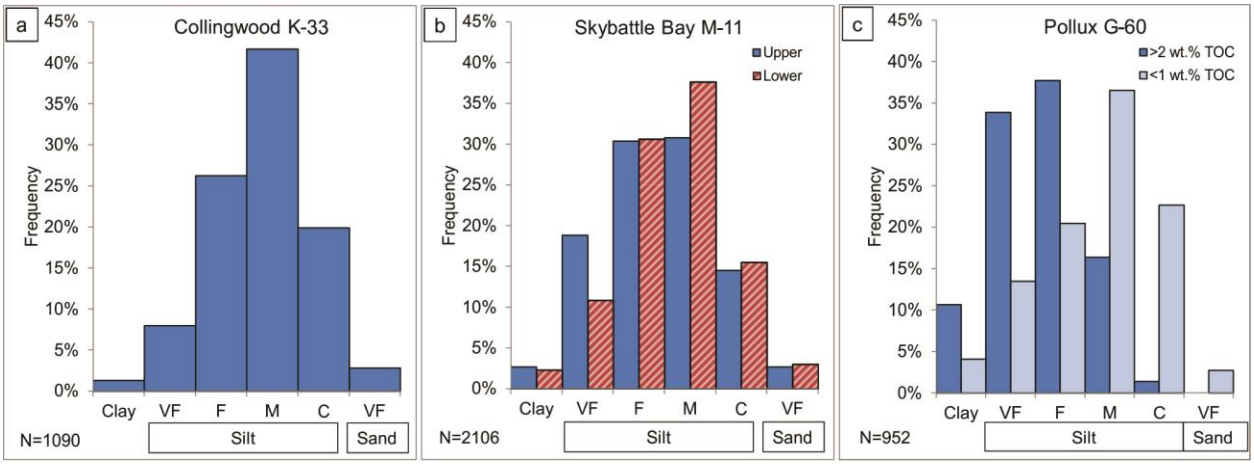

Figure 3.1

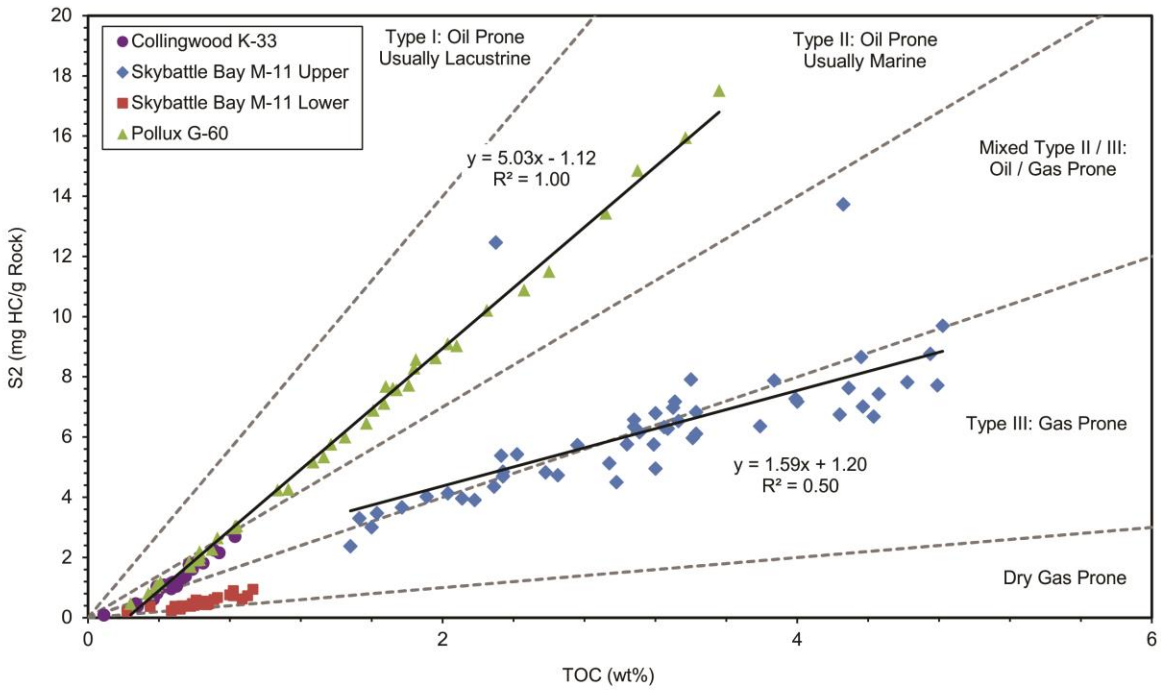
Collingwood K-33
Skybattle Bay M-11 Upper
Skybattle Bay M-11 Lower
Pollux G-60
Type I: Oil Prone
Usually Lacustrine
Type II: Oil Prone
Usually Marine
Mixed Type II / III:
Oil / Gas Prone
Type III: Gas Prone
Dry Gas Prone
y = 5.03x - 1.12
R² = 1.00
y = 1.59x + 1.20
R² = 0.50
S2 (mg HC/g Rock)
TOC (wt%)
0
2
4
6
8
10
12
14
16
18
20

Figure 3.2

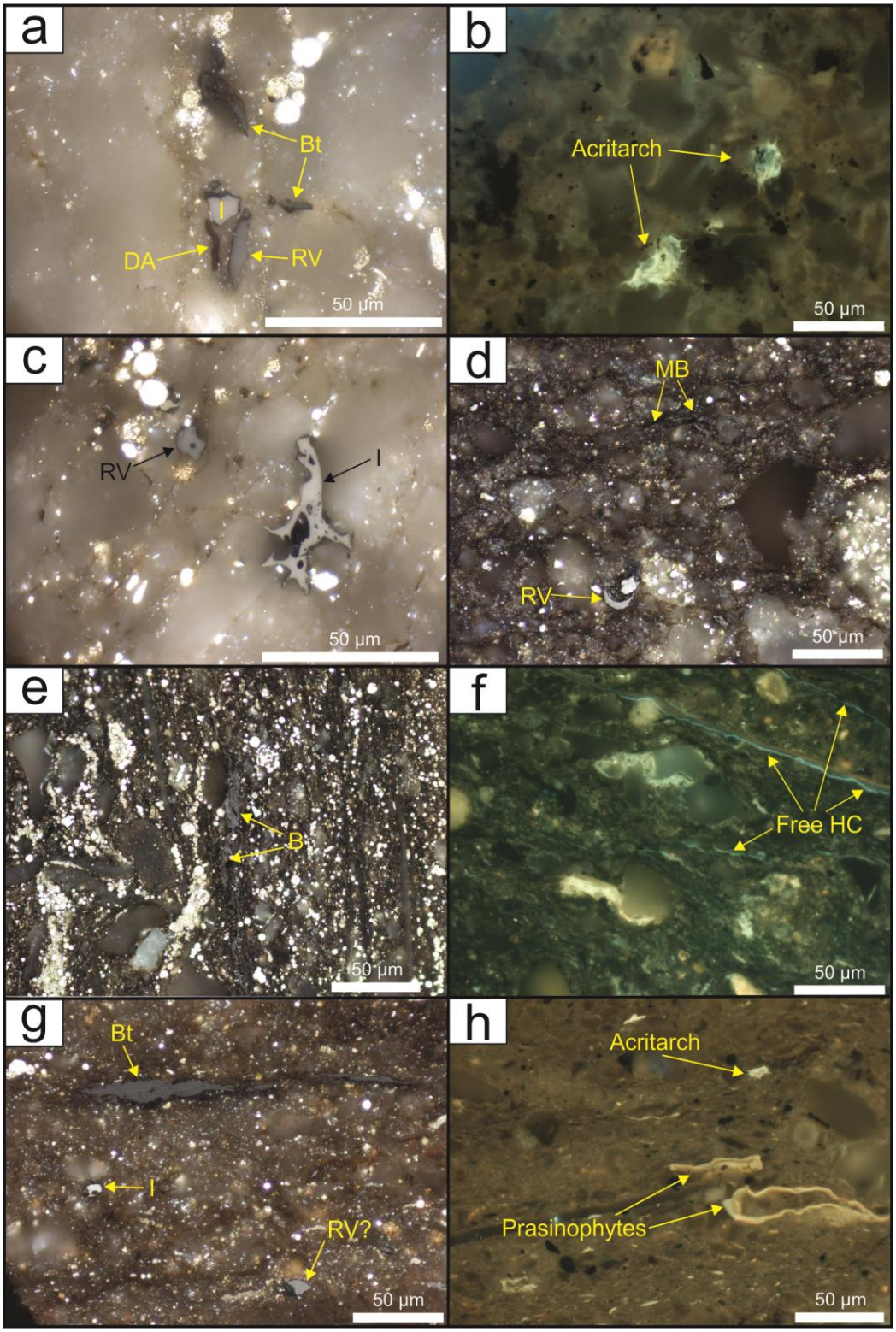
a
Bt
I
DA
RV
50 µm
b
Acritarch
50 µm
c
RV
I
50 µm
d
MB
RV
50 µm
e
B
50 µm
f
Free HC
50 µm
g
Bt
I
RV?
50 µm
h
Acritarch
Prasinophytes
50 µm

Figure 3.3

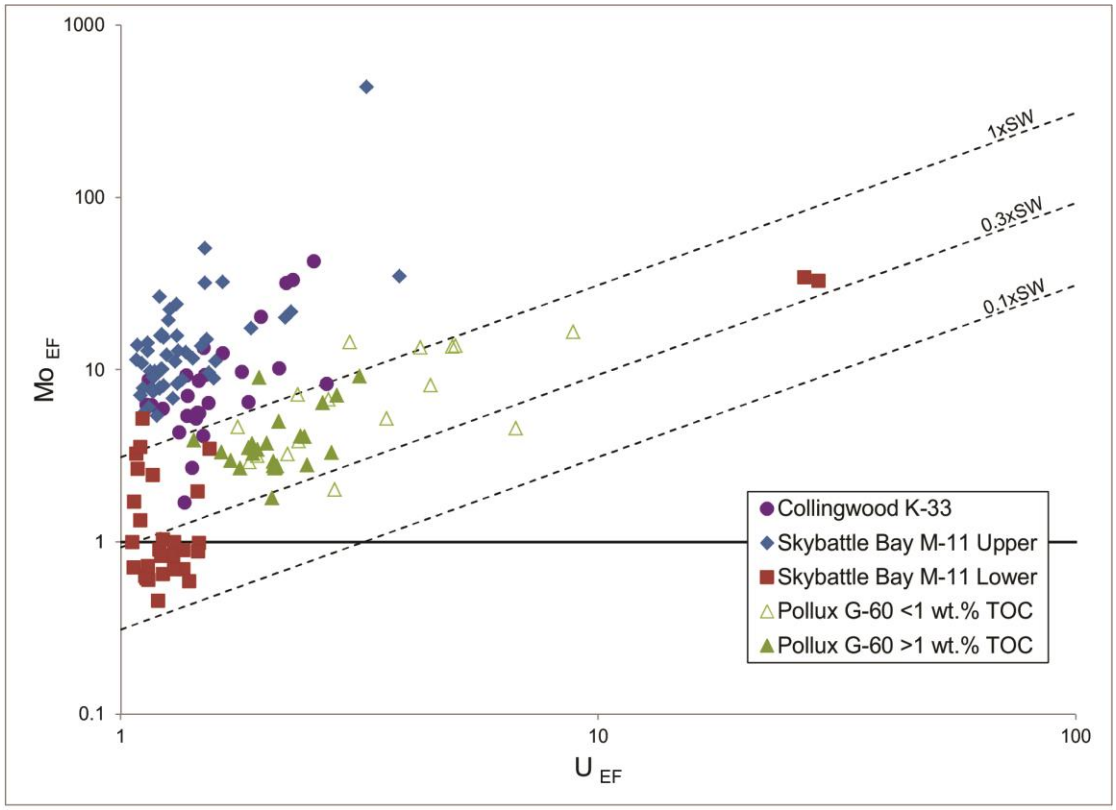
1000
100
10
1
0.1
Mo EF
1
10
100
U EF
1xSW
0.3xSW
0.1xSW
Collingwood K-33
Skybattle Bay M-11 Upper
Skybattle Bay M-11 Lower
Pollux G-60 <1 wt.% TOC
Pollux G-60 >1 wt.% TOC

Figure 3.4

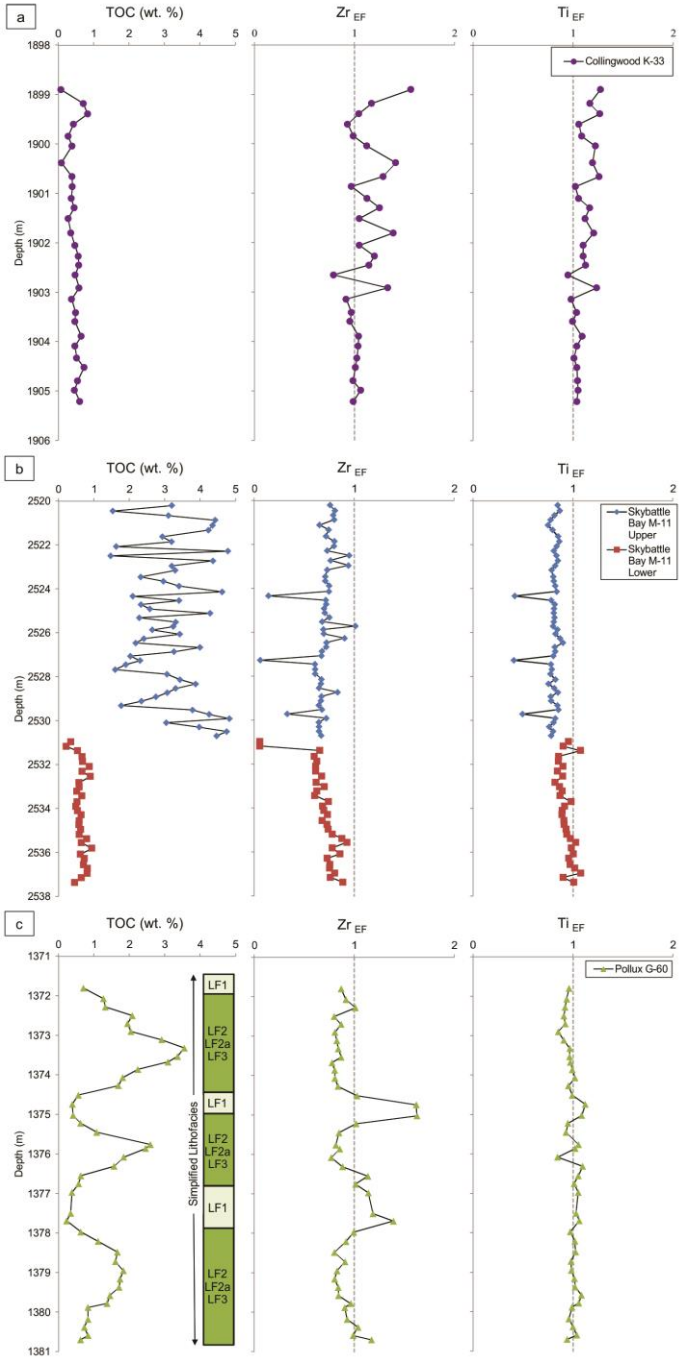
a
TOC (wt. %)
Zr EF
Ti EF
Collingwood K-33
Depth (m)
b
Skybattle Bay M-11 Upper
Skybattle Bay M-11 Lower
c
Pollux G-60
Simplified Lithofacies
LF1
LF2
LF2a
LF3

Figure 3.5

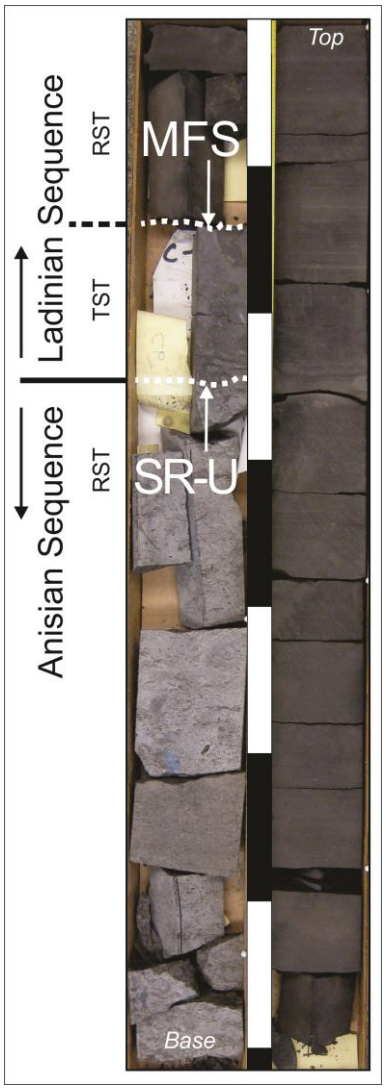
Top
Ladinian Sequence
RST
MFS
TST
Anisian Sequence
RST
SR-U
Base

Figure 3.6

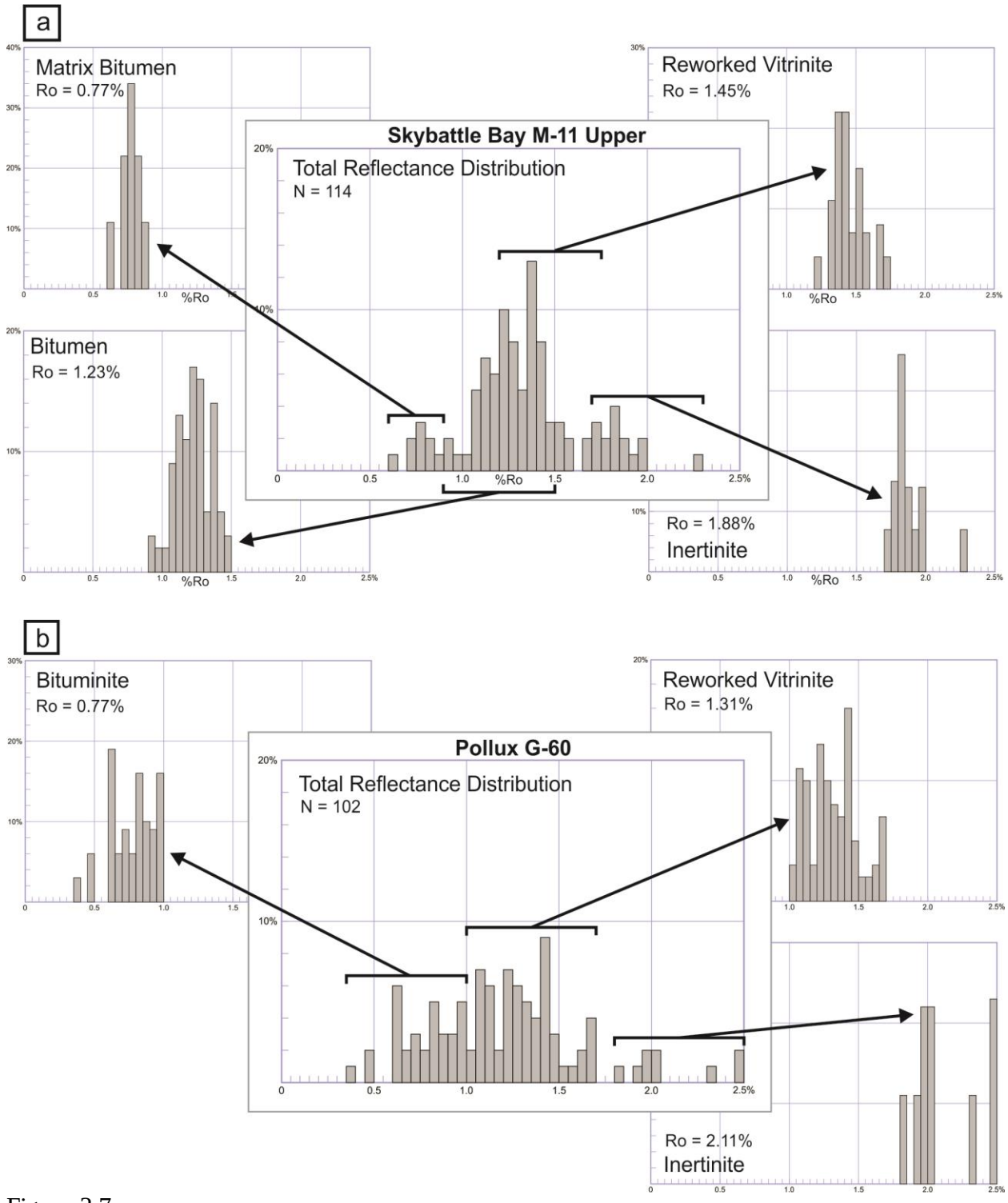
a
Matrix Bitumen
Ro = 0.77%
Reworked Vitrinite
Ro = 1.45%
Skybattle Bay M-11 Upper
Total Reflectance Distribution
N = 114
Bitumen
Ro = 1.23%
Ro = 1.88%
Inertinite
%Ro
b
Bituminite
Ro = 0.77%
Reworked Vitrinite
Ro = 1.31%
Pollux G-60
Total Reflectance Distribution
N = 102
Ro = 2.11%
Inertinite

Figure 3.7

Chapter Four: **Effects of Organic and Mineral Matter on Reservoir Quality in a Middle Triassic Mudstone in the Canadian Arctic**

Danielle Kondla[a,b], Hamed Sanei[a,b], Christopher R. Clarkson[b], Omid H. Ardakani[a], Xibo Wang[a,c], and Chunqing Jiang[a]

[a]Geological Survey of Canada, Calgary

[b]Department of Geoscience, University of Calgary

[c]State Key Laboratory of Coal Resources and Safe Mining, China University of Mining and Technology (Beijing)

Submitted to International Journal of Coal Geology, July 2015

4.1 Abstract

This study examines the hydrocarbon potential of the Middle Triassic Murray Harbour Formation (Sverdrup Basin, Arctic Canada) as a self-sourced reservoir. The Murray Harbour Formation consists of organic-rich mudstone and siltstone that has contributed oil and gas to the majority of known hydrocarbon fields in the basin. Organic matter (OM) and mineral fractions of the interval are investigated to characterize the effect that each fraction has on reservoir quality. The interval of interest is within the oil generation window, with a T_{max} of 443°C and total

organic carbon (TOC) value of 3.20 wt.% (median, n=51). A modified method of Rock-Eval analysis, referred to as the extended slow heating (ESH) cycle, where heating occurs at a slower rate of 10°C per minute up to 650°C, was utilized to better resolve different fractions of OM. In conjunction with organic petrology, this allowed correct identification of the components of TOC and the effects each has on reservoir quality and hydrocarbon potential for the unit.

Three main OM fractions are identified: i) light free hydrocarbons, ii) medium to heavy fluid-like hydrocarbon residue (FHR), and iii) kerogen and solid bitumen. The kerogen and solid bitumen fraction comprises allo- and autochthonous kerogen as well as solid bitumen. This fraction is dominated by solid bitumen, which is present in two petrographically observable forms: matrix and lump solid bitumen. Matrix bitumen is primarily disseminated within the clay-rich matrix and fills smaller pores, whereas lump solid bitumen fills larger pores. TOC has a negative correlation with porosity (Pearson's r correlation coefficient = -0.65; $p<0.05$, n = 12, Microsoft Excel Analysis ToolPak™), indicating that it occupies pore space, with a detrimental effect on hydrocarbon storage and flow at the present level of thermal maturity. However, thermally overmature areas of the Murray Harbour Formation may have increased microporosity within the solid bitumen network that could provide additional adsorption sites for generated gas within the reservoir. Macro- and microscopic phosphate nodules (likely high-density apatite) appear throughout the interval, and under fluorescence microscopy, are observed to retain light free hydrocarbons and FHR. A strong positive correlation between porosity and grain density (Pearson's r correlation coefficient = 0.95; $p<0.05$, n = 12, Microsoft Excel Analysis ToolPak™) suggests that these nodules contribute to porosity and provide capacity for hydrocarbon storage within the rock. This important observation can be applied to other phosphate-rich mudrock

plays, including the coeval Doig Formation Phosphate Zone in the established Alberta Basin, to identify and exploit prolific zones.

4.2 Introduction

Mudrocks are typically homogeneous at the macroscopic scale, but are notoriously heterogeneous at the microscopic scale. Previously, limitations in technology have made these rocks difficult to study and even with current advances, their analysis remains challenging. However, depletion of many conventional hydrocarbon reservoirs in accessible locations is necessitating greater understanding of these fine-grained rocks to efficiently develop them as unconventional resources. Small-scale variations in mineralogy (both allo- and authigenic) and organic matter (OM) can have large impacts on the quality of self-sourced hydrocarbon reservoirs. Therefore, it is important to identify the causes of these variations and the effects they can have in to predict the best targets for hydrocarbon production. Because OM fractions can affect porosity both negatively (e.g., Sanei et al., 2015) and positively (e.g., Jarvie et al., 2007), each self-sourced reservoir must be studied individually with regards to the role OM plays in their quality.

The Sverdrup Basin is the location of many conventional hydrocarbon fields not yet exploited due to economic and infrastructure constraints (Chen et al., 2000). Due to these limitations, as well as others including the remote location, harsh climate, and fragile ecosystems of the Canadian Arctic, the tight and shale oil and gas potential of the basin has yet to be investigated in detail.

This study integrates a variety of techniques to analyze core samples from the Middle Triassic Murray Harbour Formation to determine the effect that various fractions of organic and mineral matter have on reservoir quality. This study of the unconventional hydrocarbon potential

of the Murray Harbour Formation is important for the future development of Canada's northern resources, as well as the advancement of understanding self-sourced reservoirs in other well-developed basins.

4.3 Study Area

The organic-rich mudstone and siltstone of the Murray Harbour Formation was deposited during the Middle Triassic in the Sverdrup Basin, located in the Canadian Arctic Archipelago. The Sverdrup Basin is a 1300 km-long rift basin containing strata from Mississippian to Neogene in age (Balkwill, 1978). During the Middle Triassic, the basin experienced two major transgressive-regressive cycles (Embry, 1991). The first of these transgressions occurred at the beginning of the Anisian, and the second, at the beginning of the Ladinian. During the regressive phases, overall sedimentation to the basin remained low resulting in minimal progradation of shelf sands from the southwest (Embry, 1991). Basinward, abundant organic carbon was deposited in marine shelf and deep basin settings as the mud and silt of the Murray Harbour Formation (Embry, 2011). The Murray Harbour Formation extends over most of the Sverdrup Basin, with the exception of northeastern Ellesmere Island and along the southern basin margins, where the equivalent sandstone-dominated Roche Point Formation replaces it (Embry, 1984a, 1991). It consists of the Anisian informally named "lower member" and the Ladinian Cape Caledonia Member (Embry, 1984) and has an estimated maximum thickness of 300 m (Embry and Beauchamp, 2008). Previous studies of the Murray Harbour Formation have focused on source-rock potential and regional thermal maturity rather than localized self-sourced reservoir potential (e.g., Gentzis and Goodarzi, 1991; Brooks et al., 1992; Gentzis and Goodarzi, 1993; Gentzis et al., 1996; Mukhopadhyay et al., 1997; Dewing and Obermajer, 2011).

Samples for this study were collected from core extracted from the well Skybattle Bay M-11 (Fig. 4.1). The well is located on the southern tip of Lougheed Island in the west-central part of the Sverdrup Basin. The samples are from the Cape Caledonia Member of the Murray Harbour Formation, in an interval that corresponds to the base of the Ladinian 3rd-order stratigraphic sequence, deposited at the beginning of the second regressive phase in the Middle Triassic (Embry and Podruski, 1988). The studied interval preserves sediments deposited in a mid to outer marine shelf setting (Embry and Podruski, 1988) and redox-sensitive trace elements suggest anoxic bottom water conditions (Kondla et al., 2015). The core consists of calcareous, black mudstone interlaminated with grey-brown siltstone (Fig. 4.2). Beige, subround to round phosphatic nodules (up to several centimetres in diameter) are present at various intervals, along with pelecypod fragments aligned parallel to bedding. Grain size ranges from clay (8-13 μm) to very fine-grained sand (62-125 μm), with phosphate and mudstone intraclasts up to very large pebble (32-64 mm). 51 samples were taken at approximately 20 cm intervals between the depths of 2520.0 and 2530.69 m.

4.4 Methods

4.4.1 Organic Petrology

Ten samples were selected for organic petrology based on parameters from standard Rock-Eval analysis. Samples were chosen to reveal the complete spectrum of variation in TOC, S2 and HI values for the interval. Whole-rock samples were coarsely crushed and made into polished pellets of randomly-oriented rock set in an epoxy-resin mixture. Each pellet was studied under oil immersion (n=1.518 at 23°C), in both incident and ultraviolet (UV) light (G 365 nm excitation, 420 nm filter) using a Zeiss Axio Imager II microscope located at GSC Calgary. 50x

and 100x objectives were used. A mineral standard of yttrium-aluminum-garnet (YAG) with known reflectance of 0.906% was used for calibration for reflectance measurements.

4.4.2 Rock-Eval Analysis

Seventy mg of each of the 51 samples was powdered and used for standard Rock-Eval analysis (Lafargue et al., 1998) at the Geological Survey of Canada (GSC), Calgary laboratory. For standard programmed temperature heating, bulk powdered rock was heated in an N2 atmosphere pyrolysis oven. Initially, temperature remained at 300°C for 3 minutes, facilitating thermal desorption of free hydrocarbons within the rock (S1, mg HC/g Rock). Following this initial iso-temperature stage, temperature was increased by 25°C per minute until the final temperature of 650°C was reached. During this stage, kerogen was thermally cracked, generating hydrocarbons (S2, mg HC/g Rock) and organic-sourced CO_2 (S3, mg CO_2/g Rock). Powdered rock was then oxidized with temperature increasing by 20°C per minute from 300 to 850°C evolving any remaining organic carbon (S4CO_2, mg CO_2/g Rock; S4CO, mg CO/g Rock). Total organic carbon [TOC = pyrolysable organic carbon (PC%) + residual organic carbon (RC%)], hydrogen index (HI = S2 x 100/TOC, mg HC/g TOC), and oxygen index (OI = S3 x 100/TOC, mg CO_2/g TOC) were then calculated using the measured parameters of both pyrolysis and oxidation.

Twelve of the 51 samples were selected for analysis using a modified Rock-Eval cycle referred to as the extended slow heating temperature (ESH) cycle (Sanei et al., 2015). The ESH cycle began pyrolysis with an initial temperature of 150°C where sample material was held for 10 minutes. This facilitated desorption of free hydrocarbons in the sample, in the same manner as the standard Rock-Eval cycle, however the lower iso-temperature of the ESH cycle ensured that only the lightest fraction of free hydrocarbons were volatilized ($S1_{ESH}$, mg HC/g Rock).

Temperature was then increased at the rate of 10°C per minute up to 650°C, much slower than the standard Rock-Eval cycle heating rate. This longer pyrolysis process resulted in the evolution of hydrocarbon peaks corresponding to $S2a_{ESH}$, from desorption of medium to heavy hydrocarbons, and $S2b_{ESH}$, from thermal cracking of kerogen and solid bitumen (both in mg HC/g Rock). The $S2a_{ESH}$ peak formed between 150 and 350°C and the $S2b_{ESH}$ peak formed between pyrolysis temperatures of 350 and 650°C. The oxidation cycle followed the same procedures as the standard Rock-Eval cycle.

Precision and accuracy of Rock-Eval parameters were determined using the GSC reference standard, 9107, prepared from the Colorado Shale. This standard was analyzed prior to analysis of each sample set and at least once every 15 samples. Anomalous samples were re-analysed to determine their validity. Measured parameters have an accuracy and precision within 5% of the reference standard values.

4.4.3 Online thermal desorption/pyrolysis-gas chromatography-mass spectrometry/flame ionization detection (TD/Py-GC-MS/FID) analysis

One sample was selected for online thermal desorption/pyrolysis-gas chromatography-mass spectrometry/flame ionization detection (TD/Py-GC-MS/FID) analysis at GSC Calgary. The sample was selected based on the shape of the standard Rock-Eval pyrogram. This sample displays a prominent front shoulder on the S2 peak. TD-GC-MS/FID analysis was used to identify free hydrocarbons within the sample and Py-GC-MS/FID was used to characterize the hydrocarbons generated from solid OM. Analysis was performed using a Frontier EGA/PY-3030D pyrolyzer interfaced to an Agilent GC-MSD/FID dual detection system, where approximately 65 mg of powdered rock was tested in two phases of heating. The first phase held the sample at 300°C for three minutes, facilitating desorption of free hydrocarbons under the

same conditions as the S1 peak of the standard Rock-Eval cycle. The second phase held the sample at 350°C for a further three minutes, emulating conditions associated with release of hydrocarbons in the initial part of the S2 peak from the standard Rock-Eval cycle (i.e., front shoulder). Following thermal desorption, the sample was flash-pyrolysed for 30 seconds at 650°C (Py-GC-MS/FID). Desorbed and generated hydrocarbons were cryo-trapped at -186°C, and following completion of pyrolysis, were analysed in a PONA 50 m x 0.20 mm x 0.5 μm GC column using helium carrier gas at a flow rate of 1 mL/min. The GC oven temperature was programmed from a constant temperature of 33°C for 10 minutes, followed an increase in temperature at 3°C per minute up to 63°C, and finally increased by 6°C per minute up to 325°C and maintained for 35 minutes. The hydrocarbons were thus separated within the GC column based on their boiling points. Mass spectrometer and flame ionization detectors were then used to identify and quantify the compounds, respectively, based on published GC retention times and mass spectra.

4.4.4 Scanning Electron Microscopy

One sample was selected amongst the 10 organic petrology pellets for field emission scanning electron microscope (FESEM) imaging and energy-dispersive X-ray spectroscopy (EDXS) to characterize the distribution and composition of the inorganic fraction of the rock. This work was conducted at the University of Calgary's Instrumentation Facility for Analytical Electron Microscopy using the FEI Quanta 250 Field Emission Gun scanning electron microscope. The samples were introduced into a high vacuum chamber and bombarded with electrons. Backscatter electron (BSE) images identify the average atomic number of the elements in the samples giving relative compositions of minerals. EDXS used backscattered electrons to

map the spatial distribution of specific elements within the samples. Mineralogy was then assumed based on associations of elements distributed in grains.

4.4.5 Total Bulk Elemental Concentration and Mineralogy Derivation

All 51 samples were analysed for bulk elemental concentration using inductively coupled plasma-mass spectrometry (ICP-MS) at Acme Labs in Vancouver, Canada. Approximately 500 mg of powdered rock was digested in an open system to complete dryness in an acid solution of H_2O-HF-$HClO_4$-HNO_3 in a 2:2:1:1 ratio. The residue was then re-heated with 50% HCl, cooled, and brought up to required analysis volume with dilute HCl. Each sample was split in half, for duplicate analysis at random intervals. Each sample was then analysed using mass spectrometry to determine the concentrations of 59 elements. This suite of elements was primarily used for deriving mineralogical concentrations of the samples.

Precision and accuracy of elemental concentrations were determined using the reference standard OREAS 45e, prepared from a lateritic soil from Western Australia, as well as random duplicate analysis of sample splits. Most values have less than 5% error in precision for random splits, and less than 10% error for accuracy and precision compared to the reference standard.

Mineral concentration of the samples was derived from elemental concentrations determined from ICP-MS. This technique has been used on other sub-sets of samples that have mineral concentrations determined via X-ray diffraction (XRD) analysis and results were comparable. Use of this method is beneficial for sample sets that already have bulk elemental data but would benefit from mineralogical data as well; mineralogical data can be accurately estimated without devoting additional sample material and cost to XRD. The method began with identification of major elements comprising the sample (generally >1 wt.%) and subsequent conversion of each to oxide concentration using the appropriate factor. Sulphur was not

converted to oxide concentration because sulphur is inferred to primarily be associated with sulfide minerals (i.e., pyrite) rather than associated with other minerals in oxide form. Carbon was converted to oxide using mineral carbon values from Rock-Eval analysis and TOC was used to account for the contribution from organic carbon to the bulk composition. Silicon was not among the elements measured in ICP-MS, therefore SiO_2 concentration was calculated using the following formula (concentration values in wt.%):

$[SiO_2]$ = 100 - [sum of major oxides/elements] - [oxides of mineral carbon] - [sum of trace elements] - [TOC]

Next, a correlation matrix was created of all the oxide and TOC concentrations to visualize associations between each. Correlation coefficients were determined using Pearson's r correlation with the Microsoft Excel Analysis ToolPak™ with significance $p<0.05$. These associations, along with available petrographic observations, were used to guide inferences about the most likely minerals or mineral groups present in the sample. The concentrations for quartz, anatase, clay minerals (likely mixed layer illite-smectite), carbonates (likely a combination of calcite, dolomite and siderite), sulphides (likely pyrite), and phosphate (likely apatite) were calculated for the studied samples. Percent error, using 100 as total rock composition, ranges between 0.2 and 0.4% (Table 1), indicating that this method gives an acceptable estimate of mineralogy for each sample.

4.4.6 Porosity, Pore Geometry, and Pore-Size Distribution

All 10 of the samples chosen for organic petrology plus two additional samples were used to calculate porosity values. Grain and bulk density measurements were determined on 'as-received' rock fragments using helium pycnometry and immersion in n-hexane, respectively. Porosity error values for this method are within 0.05% based on repeated analysis of samples.

Eleven of the above samples were analysed using low-pressure N_2 adsorption to characterize the pore geometry and pore-size distribution of pores measuring < 200 nm in diameter. Rock samples were crushed to 20-35 US mesh size and subsequently outgassed in a vacuum, at a constant temperature of 60°C, overnight. N_2 adsorption isotherms were generated using a 3Flex Surface Characterization Analyzer and interpreted using the Brunauer-Emmett-Teller (BET) and Langmuir analysis to determine surface area. The adsorption branch of isotherms was inverted using the Barrett-Joyner-Halenda (BJH) method to determine pore-size distribution. Readers are referred to Gregg and Sing (1982) for details of these methods.

4.5 Results

4.5.1 Organic Petrology

Examination of samples using reflected light microscopy shows that dispersed organic matter (i.e., the kerogen and solid bitumen fraction) is dominated by solid bitumen. Occasional inertinitic and reworked or detrital vitrinitic fragments are visible as well. Solid bitumen is visible in two forms: matrix bitumen and lump solid bitumen, which can be petrographically discerned from each other based on reflectance values and morphology. Matrix bitumen is structureless and disseminated throughout small pores provided by the clay-rich matrix, whereas lump solid bitumen fills mainly larger pores associated with mineral grains and bioclasts; it can sometimes be observed to retain the external shape of primary algal material (Fig. 4.6a). Matrix bitumen has lower reflectance values (typically 0.6-0.9%), which corresponds to the thermal maturity derived from T_{max} values, and represents the actual thermal maximum of the unit. Lump solid bitumen typically has higher reflectance values (0.9-1.5%) with a much broader range of values compared to matrix bitumen. Matrix bitumen mainly fills smaller pores of the clay-rich matrix and occasionally accumulates in larger shelter porosity created by mineral grains,

bioclasts, and detrital OM (Fig. 4.6b). The matrix bitumen is soft, making it difficult to find high quality polished surfaces for reflectance measurements; however valid reflectance measurements can be obtained with persistence. Lump solid bitumen predominantly accumulates within larger pores, and often contains carbonate minerals and framboidal pyrite within the accumulations. Lump solid bitumen is harder than matrix bitumen, as evidenced by the abundance of polished, good quality surfaces available for reflectance measurement, and overall higher reflectance values. Matrix bitumen shows dull brown fluorescence under ultraviolet (UV) light, while lump solid bitumen does not fluoresce, demonstrating the difference in the amount of remaining pyrolysable material contained by each.

Light free hydrocarbons are visible in many of the samples when viewed under UV light. They appear as bright blue-fluorescing fluid collecting along the boundaries of planar mineral grains and bioclasts, as well as within some pyrite framboids. Free hydrocarbons are also observed exuding from what appear to be well-defined, fine-grained zones in some samples (Fig. 4.6c). These zones show dull orange fluorescence under UV light and some appear saturated with heavier residual hydrocarbons when viewed under white light (Fig. 4.6d).

4.5.2 Standard Rock-Eval Cycle

Results from the standard cycle of Rock-Eval analysis reveal TOC values ranging from 1.5 to 4.8 wt.% (median = 3.2 wt.%) (Fig. 4.3a) and S2 values between 2.4 and 13.7 mg HC/g Rock (median = 6.3 mg HC/g Rock, n=51) (Fig. 4.3b) (Kondla et al., 2015). These values indicate the interval is organic-rich and has good hydrocarbon generation potential. T_{max} for the interval is 443°C (median, n=51) which is coincident with the peak oil generation window (Fig. 4.3c) and also corresponds to organic petrology evidence of oil generation.

FID pyrograms generated from standard cycle Rock-Eval analysis of samples tend to have poorly-defined bimodal S2 peaks (Fig. 4.4a). A less dominant sub-peak (shoulder) develops prior to the main S2 peak. These shoulders vary in magnitude between samples, comprising negligible to substantial proportions of the total S2 peak.

4.5.3 Extended Slow Heating Temperature Rock-Eval Cycle

While the magnitude of the $S1_{ESH}$, $S2a_{ESH}$, and $S2b_{ESH}$ peaks for each sample is variable, the relative differences between each are the same (e.g., Fig. 4.4b). The $S1_{ESH}$ peak, representing light free hydrocarbons, is consistently negligible which is to be expected for these samples; the core was drilled in 1985, leaving ample time for much of the lighter components to volatilize. The $S2a_{ESH}$ peak characterizes medium to heavy molecular weight fluid-like hydrocarbon residue (FHR) that was not desorbed during the initial iso-temperature stage of heating and corresponds to the shoulder portion of the S2 peak from the standard Rock-Eval cycle (Sanei et al., 2015). The $S2a_{ESH}$ peak is always larger than the $S1_{ESH}$ peak and smaller than the $S2b_{ESH}$ peak, indicating a more substantial fraction of medium to heavy molecular weight FHR compared to light free hydrocarbons in the samples. The $S2a_{ESH}$ peak comprises a combination of the heavier fraction of hydrocarbons from the S1 peak and the shoulder of the S2 peak of the standard Rock-Eval cycle. The $S2b_{ESH}$ peak is always the largest of the three. It is important to note that the $S2b_{ESH}$ peak represents only the labile portion of solid OM contained in the rock (i.e., the kerogen and solid bitumen fraction); the labile portion is the part that was thermally converted to hydrocarbons.

Volume percentages of each OM fraction quantify the distribution of the ESH peaks (Table 2). These volume percentages were calculated using bulk rock density values from each sample and a standard estimated heavy oil density of 0.90 g/cm^3. Light free hydrocarbons and

medium to heavy molecular weight FHR compose less than 1% of the rock volume, whereas the kerogen and solid bitumen fraction composes 6.3% of the rock volume. These values support petrographic observations of predominance of solid bitumen within the samples. The kerogen and solid bitumen volume percentage includes both the hydrocarbons generated from pyrolysis as well as the residual organic carbon (RC) components of primary kerogen, solid bitumen, and detrital and refractory OM.

4.5.4 Online Thermal Desorption/Pyrolysis-Gas Chromatography-Mass Spectrometry/Flame Ionization Detection (TD/Py-GC-MS/FID) Analysis

TD/Py-GC-MS/FID analysis results corroborate the findings from ESH Rock-Eval analysis. There are three fractions of hydrocarbons that were evolved from the sample during TD-GC-MS/FID analysis; the first fraction, free light hydrocarbons, is identifiable from the predominance of C_{12}, C_{14}, C_{16}, and C_{18} normal alkanes (n-alkanes) (Fig. 4.5a) and corresponds to the $S1_{ESH}$ peak. This signature is characteristic of low thermal maturity hydrocarbons derived from marine plankton. It can also be evidence of contamination of samples by hydrocarbon-based drilling muds; however, the well report indicates that water-based mud was used. The second fraction, which corresponds to the $S2a_{ESH}$ peak, is characterized by n-alkanes of higher molecular weight (i.e., > C_{20}) superimposed on an unresolved complex mixture (UCM) hump (Fig. 4.5a). The UCM indicates the presence of a group of hydrocarbons that can be characteristic of crude oil and certain other refined oils and are unresolvable by chromatography due to similarities in chemical properties (Gough and Rowland, 1990, and references therein). The UCM becomes more prominent in biodegraded oils. This signature indicates the presence of medium-weight hydrocarbons, which are a mixture of fresh (based on the superimposed n-alkanes) and degraded hydrocarbons (based on the UCM hump). The third fraction also

corresponds to the $S2a_{ESH}$ peak, and represents heavy hydrocarbons thermally desorbed at temperatures up to 350°C (Fig. 4.5b). These last two fractions of medium and heavy hydrocarbons most likely correspond to the FHR observed microscopically.

Py-GC-MS/FID analysis of the sample reveals the types of hydrocarbons that could be generated from the kerogen and solid bitumen fraction of the rock, if it were allowed to thermally mature further. Gaseous hydrocarbons (C_1-C_4) comprise approximately 35% of generated hydrocarbons, while liquid hydrocarbons comprise the rest. The signature shows a predominance of n-alkanes and alkenes, identifiable as doublets, and ranging in carbon-number between C_5 and C_{35} (Fig. 4.5c).

4.5.5 Scanning Electron Microscopy

EDXS mapping reveals that the well-defined, fine-grained zones recognized during organic petrographic examination, are composed predominantly of calcium and phosphorus (Fig. 4.7a). Based on these elemental associations as well as commonly present minerals in mudrocks, these zones are most likely formed from apatite mineral [$Ca_5(PO_4)_3(OH,F,Cl)$]. Additionally, the hexagonal crystal form of the microcrystals that compose these zones is characteristic of apatite (Fig. 4.7b). Macroscopically observable phosphate nodules (up to several centimetres in diameter) are present at various intervals throughout the core, further supporting the presence of microscopic-scale phosphate minerals (Fig. 4.2). BSE imaging shows abundant porosity within the microcrystalline structure of the phosphate nodules (Fig. 4.7b). The pores are mainly in the macropore size range (> 50 nm), however, smaller mesopores (2 – 50 nm) may exist but visualization is limited by the scale of resolution in FESEM.

4.5.6 Inferred Mineralogy Using Total Bulk Elements and TOC

Table 1 shows results of derived mineralogy of the interval, as well as TOC values that account for the organic fraction of the rock. Two of the samples (2524.33 m and 2527.26 m) show elemental P values that exceed the maximum detectible limit of the analysis (i.e., 5.00 %); both of these samples were examined petrographically, and were found to contain abundant phosphate zones, likely resulting in the high concentrations. Apatite mineral concentrations (median=3.2 %) show agreement with bulk P values, and are based on the assumption that the majority of P is associated with apatite. The interval contains approximately equal proportions of quartz, clay minerals, and carbonate minerals. Pyrite composes a substantial proportion of the rock, with a median value of 2.3 %.

4.5.7 Porosity

Porosity ranges from 1.7 to 10.9 % (median = 3.8 %) (Table 2) and grain density varies between 2.53 and 2.86 g/cm^3. Porosity shows a strong positive correlation with grain density that is suggestive of an association of porosity with mineral grains of high density, such as apatite or pyrite (Fig. 4.8a). Porosity shows a negative correlation with TOC (Fig. 4.8b); the bubble size represents the relative volume percentage of the kerogen and solid bitumen fraction of OM derived from the ESH Rock-Eval cycle, which is predominantly solid bitumen based on petrographic observations. There is a negative correlation between porosity and clay mineral concentration (Fig. 4.8c), and bubble size indicates the kerogen and solid bitumen fraction volume percentage is higher in samples with high clay content and low porosity.

4.5.8 Pore Geometry and Size Distribution

Low pressure nitrogen gas adsorption reveals information about both pore-size distribution and dominant pore geometry of pores that are < 200 nm in diameter. The interval of

interest produces type IV, subtype H3 isotherms for all samples (Fig. 4.9a), which are characteristic of mesoporous solids with slot-shaped pores resulting from aggregates of plate-like particles (Sing et al., 1985). The hysteresis loop characteristic of type IV isotherms results from capillary condensation of N2 within pores causing the desorption branch to deviate from the pathway of the adsorption branch (Sing et al., 1985). BET surface area ranges from 0.62 to 3.88 m^2/g, and shows no relationship with studied geochemical parameters. Pore-size distribution plots derived from the isotherms for each sample shows one of three distributions: bimodal (3 samples), unimodal (2 samples) or multimodal (6 samples) (Fig. 4.9b, 4.9c, 4.9d). The bimodal distribution samples show peaks at both 2 and 3.5 nm, while unimodal samples have a single broader peak that spans the pore width of range of 2 to 4 nm. The multimodal samples show irregular peaks at 3-4 nm, approximately 2 nm, and 1.5 nm. Pore-size distribution indicates that samples have a predominant pore size of 2 to 4 nm (mesopores are classified as 2-50 nm (Rouquérol et al., 1994)). These pore-size ranges may be overestimated due to the measurement of samples in unconfined conditions.

4.6 Discussion

4.6.1 Organic Matter Fractions

Petrographic observations and quantitative data from Rock-Eval and TD-GC-MS/FID corroborate the presence of three main fractions of OM within the Skybattle Bay M-11 interval: light free hydrocarbons, FHR (medium to heavy molecular weight hydrocarbons), and kerogen and solid bitumen (Fig. 4.4, 4.5, 4.6). The light free hydrocarbons fraction ($S1_{ESH}$, < C_{20} n-alkanes) is likely underestimated in the samples due to volatilization over time since extraction of the core. As a result, a portion of the light hydrocarbons are degraded to heavier residues (i.e., FHR). It is therefore probable that FHR is overestimated in core samples. The FHR ($S2a_{ESH}$, >

C_{20} n-alkanes) fraction is the result of degradation of light free hydrocarbons after extraction of the core, as well as in-situ heavier hydrocarbons generated from thermal maturation of OM. The degradation of light free hydrocarbons to heavier residual oils in the core could partially explain the UCM hump observed in the TD-GC-MS/FID curve for the S2aESH peak.

The S2bESH peak plus RC is referred to as the kerogen and solid bitumen fraction, and is represented petrographically by three maceral groups: (i) solid migrabitumen disseminated within clay matrix and small pores as matrix bitumen (Fig. 6a), (ii) larger pore-filling lump solid bitumen (Fig. 4.6b), and (iii) degraded kerogen (e.g., remnant liptinite, vitrinite, inertinite). Matrix and lump solid bitumen appear to constitute the majority of the kerogen and solid bitumen fraction. Matrix bitumen represents consolidated hydrocarbons remaining after the initial thermal cracking of primary kerogen to oil and gas. Most of the lighter hydrocarbons evolved and migrated out of the rock to source adjacent conventional reservoirs or migrated locally and are presently observed as the light free hydrocarbon and FHR fractions. Petrographic observations show dull orange fluorescence of matrix bitumen as well as measured reflectance values indicating oil window thermal maturity. Additional exposure to heat energy and time is required to generate any remaining hydrocarbons from kerogen and solid bitumen. Based on the Py-GC-MS/FID trace signature (Fig. 4.5c) (pyrolysis of the kerogen and solid bitumen fraction), the interval can be interpreted as a low-maturity oil-prone source rock.

The lump solid bitumen and degraded kerogen groups consist mostly of RC and contain less pyrolysable material than the matrix bitumen based on non-fluorescence and high reflectance values. Lump solid bitumen typically fills larger pores within the rock. Most of the lump solid bitumen observed microscopically in the samples shows co-location with framboidal pyrite or carbonate minerals, both of which can be products of bacterial sulphate reduction

(BSR) (Machel, 2001). Furthermore, the morphology of lump solid bitumen commonly resembles algal forms, suggesting degradation of marine–sourced primary OM during early burial. The wide range of reflectance values for this population implies variable degrees of degradation resulting in variable levels of chemical alteration of kerogen. These variable levels of degradation caused different degrees of gelification of primary OM (Taylor et al., 1998 and references therein), resulting in a range of plastic deformation intensity (i.e., some forms of lump solid bitumen closely resemble the shape of algae while others are more amorphous and dispersed between mineral grains). Following early degradation, this primary OM was then thermally matured during deeper burial, resulting in additive effects to reflectance values. Consequently, lump solid bitumen does not represent the thermal history of the unit. Detrital OM are also included in the kerogen and solid bitumen fraction as inertinite and reworked vitrinite; however, measured reflectance values indicate they have mostly exceeded the expected hydrocarbon generation windows due to oxidation (Kondla et al., 2015).

Integration of organic petrology with the ESH Rock-Eval cycle serves as a powerful tool in identification of OM fractions within the samples. It allows both chemical and physical classification of TOC, which is important in unconventional hydrocarbon systems. Each fraction of OM can potentially have different effects on reservoir quality and hydrocarbon potential, and characterization of these fractions and effects can influence exploration methods. If only the standard Rock-Eval cycle had been used for this interval, FHR and solid bitumen may have been misidentified as kerogen, resulting in an entirely different interpretation of the system.

4.6.2 Contributions to Porosity

Relationships between porosity and both organic and mineral fractions of the studied interval are evident. While controls on porosity in mudrocks are highly complex (e.g., Chalmers

et al., 2012; Kuila and Prasad, 2013; Ghanizadeh et al., 2014; Wood et al., 2015), signals that give clues to contributors can be discerned in these samples. TOC shows a negative correlation with porosity (Fig. 4.8b). High TOC samples also contain a higher volume percentage of the kerogen and solid bitumen fraction (Fig. 4.8b). The correlation coefficient for porosity and kerogen vol. % (Peasron's r correlation coefficient = -0.66, $p<0.05$, n=12, Microsoft Excel Analysis ToolPak™) is only slightly improved compared to the correlation coefficient for porosity and TOC wt.% (Pearson's r correlation coefficient= -0.65, $p<0.05$, n=12, Microsoft Excel Analysis ToolPak™), supporting the inference that the kerogen and solid bitumen fraction, specifically solid bitumen, is the predominant fraction of TOC in the studied samples. Therefore, it is expected that these two parameters should exhibit the same trends. As observed petrographically, solid bitumen fills paleo-pores, removing them from available present day porosity for fluid accumulation. Higher saturation of rock intervals with solid bitumen results in lower available porosity. This relationship is similar to trends observed in the Montney Formation in the Alberta Basin, Canada (Sanei et al., 2015; Wood et al., 2015), and has a negative effect on reservoir quality for hydrocarbon storage and flow. This is an important finding, since OM affects reservoir quality in different ways depending on multiple factors including thermal maturity, kerogen type, and mode of occurrence of OM within the rock. Identification of how the OM fraction contributes or detracts from fluid flow and storage is critical to understanding unconventional hydrocarbon systems.

The strong inverse correlation between porosity and clay mineral concentration as well as the relative increase in kerogen and solid bitumen volume percentage with increasing clay minerals (Fig. 4.8c) indicates occupation of pores by solid bitumen. Petrographically, solid bitumen tends to be disseminated in finer-grained areas of the rock (i.e. clay-rich zones) (Fig.

4.6a, 4.6b). Therefore, higher clay mineral concentrations equate to higher saturation with solid bitumen derived from primary kerogen. Clay minerals and OM tend to deposit under similar conditions (e.g., Li and Bennett, 1991), so it is expected that clay-rich intervals should contain a higher abundance of primary OM deposited and subsequently bacterially or thermally degraded.

Porosity and grain density show the strongest correlation of all studied parameters, with increasing grain density associated with increasing porosity (Fig. 4.8a). Apatite and pyrite both have higher densities as compared to other common mudrock-forming minerals (e.g., average density: apatite = 3.19 g/cm^3; pyrite = 5.01 g/cm^3; quartz = 2.65 g/cm^3; calcite = 2.71 g/cm^3). Microscopic phosphate nodules (likely composed of apatite mineral) present in some samples are observed to contain abundant macroporosity (Fig. 4.7b). The bubble size in figure 4.8a illustrates the relative concentration of apatite in each sample; there is an overall increase in concentration with both porosity and grain density. These associations suggest that the porosity provided by phosphate nodules is a substantial contributor to porosity within the interval. Intracrystalline porosity within pyrite framboids may exist; however, there is limited petrographic evidence to show this in these samples. Furthermore, there is no correlation between pyrite mineral concentration and porosity (Pearson's r correlation coefficient = -0.03, $p<0.05$, n=12, Microsoft Excel Analysis ToolPak™) therefore the positive correlation between porosity and grain density (Fig. 4.8a) is likely more strongly associated with apatite rather than pyrite. Petrographic observations reveal that at least a portion of the porosity within phosphatic nodules is presently occupied by light free hydrocarbons and FHR. With thermal maturation of the rock, light hydrocarbons locally migrated to fill the porosity provided by the phosphate nodules. Following extraction of the core from the reservoir, the majority of these light hydrocarbons subsequently condensed to FHR, filling or coating the phosphate nodule pores. Light hydrocarbons can

sometimes be observed exuding from pyrite framboids, however many framboids are contained within lump solid bitumen, which likely occludes any available intracrystalline porosity. The contribution to porosity from both phosphate nodules and pyrite framboids is complex; some of the porosity within each mineral form may be filled with light hydrocarbons, FHR, or solid bitumen As porosity was measured on 'as-received' samples, re-analysis on cleaned samples may result in stronger correlations between porosity, grain density, and apatite and pyrite concentration.

Specific surface areas of typical conventional reservoirs are generally less than 1 m^2/g and mudstone reservoir specific surface areas have been shown to range from 1.0 to 35.4 m^2/g (Kuila and Prasad, 2013; Ghanizadeh et al., 2015). The samples in this interval show specific surface area values that extend through this range of values, with some samples reporting even lower values (i.e., 0.62 m^2/g, 0.88 m^2/g, 0.89 m^2/g, 0.90 m^2/g,). The majority of surface area in mudstones is typically associated with the clay fraction. This wide range of specific surface area values observed in the Murray Harbour Formation samples may be attributable to variations in the saturation of clay mineral associated pores by various fractions of OM, rather than strictly lithology. Some pores may be obstructed or filled by solid bitumen, FHR or light hydrocarbons. Other pores may be open due to volatilization of previously adsorbed gas or light oil. The variation in pore-size distributions observed in the samples may also be due to these same factors (Fig. 4.9b, 4.9c, 4.9d).

Interpretation of pore geometry as slot-shaped and resulting from aggregates of plate-like particles could apply to porosity provided by clay minerals in these samples (Fig. 4.9a). However, caution is advised when interpreting isotherms derived from mudrocks, as pore geometries are much more complex and variable in mudrocks, compared to the geometries

determined from the engineered materials upon which these classifications were based. Realistically, the pore geometries present in these samples as well as other fine-grained rocks, are likely composed of a combination of different pore shapes, from different organic and mineral fractions. Furthermore, pore geometry derived from low pressure nitrogen gas adsorption is only applicable to pores < 200 nm in diameter, which means only smaller scale pore sizes within the rock are characterized. The mesopores in these rocks are likely associated with the clay fraction, typical of meso- and micropores (micropores <2 nm, [Rouquérol et al., 1994]) in mudstones (Kuila and Prasad, 2013) but based on the data generated in this study, specific sources cannot be identified. Further study of the microporosity within these samples using ion-milling preparation in conjunction with FESEM, or higher resolution focused ion beam SEM, or transmission electron microscopy (e.g., Chalmers et al., 2012; Loucks et al., 2012) may provide information regarding nature of this fraction of porosity.

4.6.3 Implications for Areas of Higher Thermal Maturity

Many studies of the effects of OM on reservoir quality in shale and tight hydrocarbon reservoirs have shown a positive relationship between kerogen and microporosity (e.g., Chalmers and Bustin, 2007; Jarvie et al., 2007). The Murray Harbour Formation, at this location and level of thermal maturity shows the opposite trend. However, there is evidence that microporosity increases within all types of kerogen as thermal maturity increases (e.g., Chalmers and Bustin, 2008; Jarvie et al., 2007; Chalmers et al., 2012). If this holds true for solid bitumen in the Murray Harbour Formation, then the correlation between porosity and solid bitumen may reverse in areas that are more thermally mature. A substantial portion of the Murray Harbour Formation is located within the deeper, east-central part of the basin where, regionally, Middle Triassic strata are thermally overmature (Fig. 4.1). Solid bitumen in these overmature areas, which has been

further thermally degraded, will have cracked to produce any remaining hydrocarbons, likely gaseous in form. The resulting pyrobitumen may have developed extensive interconnected microporosity, potentially creating increased adsorption sites for generated gas.

4.6.4 Implications for Analogous Reservoirs

Organic-rich rocks commonly contain phosphate minerals (Parrish, 1995 and references therein), however the exact mechanisms for sediment enrichment of phosphorous in marine settings are incompletely understood. Concentration of dissolved phosphate in marine sediments and pore waters can occur via microbial degradation of organic matter, desorption of phosphate from iron and manganese oxyhydroxides under reducing conditions, or direct precipitation of phosphate from the water column at or below the sediment-water boundary (Föllmi, 1996 and references therein). Phosphorite formation in modern marine settings tends to occur in zones of low sediment accumulation, high primary productivity, and high current activity (Föllmi, 1996 and references therein). These zones are often associated with upwelling currents of deeper, nutrient-rich water that accelerates marine biomass production. The phosphate nodules of the studied interval of the Murray Harbour Formation most likely formed due to sediment and interstitial water enrichment in phosphorus derived from the abundant organic material deposited with the sediments.

While the relationship between phosphate nodules and porosity requires further investigation, findings from this study can be applied to other phosphorous-rich mudstone reservoirs to potentially identify areas of higher porosity. All Murray Harbour Formation samples are enriched in elemental phosphorus compared to the post-Archean Australian Shale (PAAS), and most of them show substantial enrichment (i.e., EF >10). However, phosphorites are defined in literature as sedimentary deposits containing greater than 18 % P_2O_5 (Jarvis et al.,

1994) and all of the studied samples have concentrations below this threshold. Considering this, other 'true' phosphorites, may have even greater porosity contributed by microcrystalline phosphate nodules. Additionally, phosphorites that contain laminae of phosphate minerals may be even more desirable in unconventional reservoirs, as porosity within them is more likely to be connected, facilitating not only storage, but also transmission of hydrocarbons. The interval in this study appears to contain only isolated nodules of phosphate, limiting potential connectivity of porosity in the Murray Harbour Formation.

The Middle Triassic Doig Formation of the Alberta Basin, Canada, is analogous to the Murray Harbour Formation. Specifically, the lower portion of the Doig Formation known as the Phosphate Zone (Edwards et al., 1994) is similar to the interval of the Murray Harbour Formation in this study. The Phosphate Zone of the Doig Formation is organic-rich, with TOC values typically exceeding 2 wt.%, reaching as high as 11 wt.%, and consisting predominantly of marine Type II kerogen (Riediger et al., 1990). The Phosphate Zone is interpreted to have been deposited following a marine transgression of a passive margin (Gibson and Barclay, 1989), similar to the studied interval of the Murray Harbour Formation. Riediger et al. (1990) found that oils sourced from the Phosphate Zone correlate with oils found in reservoirs within the upper parts of the Doig Formation as well as the equivalent Halfway Formation and Late Triassic Charlie Lake Formation. The upper parts of the Doig Formation are established shale gas reservoirs (Golding et al., 2014). The lower part of the Doig Formation, the Phosphate Zone, could potentially benefit from exploration targeting phosphate nodule-rich zones, if the nodules contribute to porosity in the same way they do in the Murray Harbour Formation.

4.7 Conclusions

This research provides important preliminary information regarding reservoir quality and hydrocarbon potential of the Middle Triassic Murray Harbour Formation in the west-central Sverdrup Basin, Arctic Canada. Findings can be applied to analogous shale and tight hydrocarbon reservoirs such as the coeval Doig Formation Phosphate Zone, to potentially improve exploration and development success. The major conclusions from this study are as follows:

1) OM consists of three main fractions: i) light free hydrocarbons, ii) medium and heavy molecular-weight fluid-like hydrocarbon residue (FHR), and iii) kerogen and solid bitumen.

2) The kerogen and solid bitumen fraction is dominated by solid bitumen, which can be present in two distinct forms: matrix bitumen and lump solid bitumen. Matrix bitumen saturates the clay-rich matrix and accumulates mainly in smaller pores throughout the rock. Lump solid bitumen contains less pyrolysable material than matrix bitumen, and consists of OM degraded during the early stages of diagenesis. Both forms of bitumen have a negative effect on reservoir quality by occupying porosity at the present thermal maturity.

3) Phosphatic nodules dispersed throughout the interval contain porosity that contributes to the total porosity of the rock. At least a portion of the porosity provided by these nodules is observed to contain free light hydrocarbons and FHR, making them important hydrocarbon storage features.

4) Solid bitumen may provide microporosity for gas adsorption at higher levels of thermal maturity. Therefore, thermally overmature areas of the Murray Harbour Formation located in the deeper, east-central part of the Sverdrup Basin, may be more prospective for hydrocarbon exploration.

Table Captions

Table 4.1: List of elements for which concentration was determined using Inductively Coupled Plasma-Mass Spectrometry in Murray Harbour Formation samples.

Table 4.2: Derived mineralogy for Murray Harbour Formation samples with percent-error relative to total rock composition of 100%. Summary statistics are listed at bottom of table.

Table 4.3: Quantitative fractions of organic matter derived from Rock-Eval analysis extended slow heating cycle, grain and bulk density, and porosity measurements in Murray Harbour Formation samples. Summary statistics are listed at bottom of table. HC = hydrocarbons; FHR = fluid-like hydrocarbon residue.

Tables

Table 4.1

Major	Minor/Trace				Rare Earth	
Na	Li	Se	Sb	Bi	Sc	Dy
Mg	Be	Rb	Te	Th	Y	Ho
Al	V	Sr	Cs	U	La	Er
P	Cr	Zr	Ba		Ce	Tm
S	Co	Nb	Hf		Pr	Yb
K	Ni	Mo	Ta		Nd	Lu
Ca	Cu	Ag	W		Sm	
Ti	Zn	Cd	Re		Eu	
Mn	Ga	In	Tl		Gd	
Fe	As	Sn	Pb		Tb	

Table 4.2

Sample	Quartz %	Anatase %	Clay minerals %	Carbonates %	Pyrite %	Apatite %	TOC wt.%	Bulk Composition Error %
2520.20	28.7	0.4	35.1	28.3	2.3	1.8	3.20	0.2
2520.45	20.0	0.3	22.0	53.9	1.3	0.8	1.53	0.2
2520.66	24.9	0.3	30.6	36.3	3.0	1.6	3.10	0.2
2520.87	29.3	0.4	35.5	19.8	9.7	0.7	4.42	0.3
2521.11	22.4	0.4	32.6	22.3	2.5	15.2	4.35	0.3
2521.32	25.0	0.4	36.5	24.6	3.0	6.0	4.23	0.2
2521.62	28.4	0.4	35.1	26.5	3.3	3.2	2.93	0.2
2521.85	25.4	0.4	32.3	31.5	2.4	4.6	3.19	0.2
2522.07	28.4	0.3	24.7	32.7	4.3	7.8	1.63	0.2
2522.28	27.1	0.4	33.8	28.6	2.4	2.8	4.78	0.2
2522.49	22.7	0.2	21.1	44.6	3.3	6.4	1.47	0.2
2522.72	27.7	0.4	32.7	28.1	2.5	4.0	4.36	0.2
2522.95	24.0	0.4	31.3	34.7	3.0	3.3	3.20	0.2
2523.15	28.3	0.4	33.0	29.4	2.1	3.4	3.29	0.2
2523.45	27.5	0.3	30.7	30.4	2.8	5.7	2.32	0.2
2523.65	29.4	0.4	33.2	30.4	2.2	1.3	2.96	0.2
2523.87	29.4	0.4	34.1	27.4	2.1	2.9	3.40	0.2
2524.13	30.6	0.4	34.8	23.4	2.1	3.9	4.62	0.2
2524.33	22.3	0.1	16.6	30.0	2.0	26.5	2.10	0.4
2524.53	26.6	0.4	33.0	29.0	2.4	5.0	3.40	0.2
2524.71	25.1	0.4	34.0	33.0	3.1	2.0	2.33	0.2
2524.91	27.5	0.3	29.8	25.5	9.2	4.9	2.58	0.2
2525.11	27.6	0.4	37.8	26.2	2.1	1.4	4.28	0.2
2525.31	32.5	0.4	32.4	27.9	2.5	1.8	2.28	0.2
2525.51	31.3	0.4	36.2	24.9	2.1	1.5	3.31	0.2
2525.71	31.5	0.4	33.4	27.0	2.2	1.9	3.24	0.2
2525.86	29.6	0.4	32.6	29.6	2.2	2.8	2.65	0.2
2526.06	26.9	0.4	36.9	27.9	2.5	1.7	3.42	0.2
2526.26	29.8	0.4	31.9	25.5	3.0	6.8	2.41	0.2
2526.46	33.2	0.4	32.9	27.7	2.2	1.3	2.18	0.2
2526.66	27.0	0.4	35.6	28.7	2.5	1.7	3.99	0.2
2526.86	27.2	0.4	36.2	29.6	2.1	1.1	3.26	0.2
2527.06	33.2	0.4	34.0	27.4	2.2	0.7	2.03	0.2
2527.26	21.0	0.1	14.6	33.5	1.7	26.5	2.30	0.4
2527.44	28.7	0.4	35.5	30.0	2.1	1.3	1.90	0.2
2527.67	27.5	0.4	36.4	29.4	3.5	1.1	1.60	0.2
2527.88	26.9	0.4	39.6	26.1	2.3	1.4	3.06	0.2
2528.13	27.9	0.4	35.7	27.8	2.2	2.3	3.43	0.2
2528.33	26.2	0.4	38.2	27.3	2.5	1.3	3.87	0.2
2528.53	26.7	0.4	38.0	25.9	2.4	3.1	3.31	0.2
2528.72	29.0	0.5	39.0	23.9	2.2	2.1	3.07	0.2
2528.91	28.6	0.4	38.2	25.7	3.0	1.2	2.75	0.2
2529.11	28.4	0.3	30.5	35.5	1.9	0.8	2.34	0.2
2529.31	23.2	0.4	31.8	39.7	1.9	1.1	1.77	0.2
2529.51	19.2	0.4	35.3	37.4	2.9	0.8	3.78	0.2
2529.71	17.8	0.1	21.5	29.4	1.8	24.7	4.25	0.3
2529.90	21.4	0.4	33.6	33.1	2.2	4.2	4.82	0.3
2530.09	24.0	0.4	33.2	30.1	3.1	5.9	3.04	0.2
2530.29	25.3	0.4	38.0	26.9	3.0	2.3	3.97	0.2
2530.49	27.0	0.5	39.6	23.7	2.8	1.4	4.75	0.2
2530.69	24.1	0.5	40.8	24.4	3.0	2.5	4.46	0.2
n=51								
Minimum	17.8	0.1	14.6	19.8	1.3	0.7	1.47	0.2
Maximum	33.2	0.5	40.8	53.9	9.7	26.5	4.82	0.4
Median	27.2	0.4	33.8	28.3	2.4	2.3	3.20	0.2

Table 4.3

Sample	Light HC	FHR	Light HC	FHR	Kerogen & Solid Bitumen	Light HC	FHR	Kerogen & Solid Bitumen	TOC	Porosity	Bulk Density	Grain Density
	mg HC/g Rock	mg HC/g Rock	wt%	wt%	wt%	vol%	vol%	vol%	wt%	%	g/cm^3	g/cm^3
2520.45 m	0.10	0.88	0.01	0.08	1.45	0.02	0.22	3.07	1.54	5.91	2.54	2.70
2520.87 m	0.40	1.93	0.04	0.17	4.32	0.10	0.48	9.13	4.53	4.63	2.53	2.66
2521.85 m	0.22	0.99	0.02	0.09	3.15	0.05	0.25	6.61	3.26	2.86	2.52	2.59
2522.07 m	0.08	0.73	0.01	0.06	1.55	0.02	0.18	3.30	1.62	6.92	2.56	2.75
2523.65 m	0.17	0.96	0.02	0.09	2.85	0.04	0.24	6.00	2.95	4.68	2.53	2.65
2524.13 m	0.27	1.19	0.02	0.11	4.44	0.07	0.29	9.16	4.57	2.79	2.48	2.55
2524.33 m	0.14	1.75	0.01	0.15	1.90	0.03	0.44	4.04	2.07	10.88	2.55	2.86
2526.26 m	0.19	1.06	0.02	0.09	2.35	0.05	0.27	5.02	2.46	2.66	2.56	2.63
2527.26 m	0.16	4.44	0.01	0.38	1.81	0.04	1.10	3.91	2.21	5.57	2.59	2.74
2528.33 m	0.26	1.46	0.02	0.13	3.46	0.06	0.36	7.16	3.61	3.12	2.48	2.56
2529.90 m	0.29	1.70	0.03	0.15	4.59	0.07	0.41	9.46	4.77	2.74	2.47	2.54
2530.69 m	0.18	1.14	0.02	0.10	4.07	0.05	0.28	8.44	4.19	1.66	2.49	2.53
n=12												
Minimum	0.08	0.73	0.01	0.06	1.45	0.02	0.18	3.07	1.54	1.66	2.47	2.53
Maximum	0.40	4.44	0.04	0.38	4.59	0.10	1.10	9.46	4.77	10.88	2.59	2.86
Median	0.19	1.17	0.02	0.10	3.00	0.05	0.28	6.31	3.11	3.88	2.53	2.64
Mean	0.21	1.52	0.02	0.13	3.00	0.05	0.38	6.28	3.15	4.54	2.52	2.65
Stdev	0.09	0.95	0.01	0.08	1.13	0.02	0.23	2.30	1.13	2.45	0.04	0.10

Figure Captions

Figure 4.1: Map showing the regional thermal maturity of Middle Triassic strata in the Sverdrup Basin (after Dewing and Obermajer, 2011; Embry, 2011). Black dot shows location of the studied core from well Skybattle Bay M-11. Inset shows location of study area within North America.

Figure 4.2: Graphical log and core description of the base of the Cape Caledonia Member of the Murray Harbour Formation from core extracted from Skybattle Bay M-11. Photo of a representative section of core is shown on the right; thick, blue outline denotes location of core section within the litholog portion of the figure. Each scale block in core photo equates to 10 cm.

Figure 4.3: Rock-Eval 6 data from Murray Harbour Formation samples (n=51): a) Depth versus total organic carbon; b) Depth versus S2; c) Hydrogen Index versus T_{max}.

Figure 4.4: Pyrograms generated from Rock-Eval 6 analysis pyrolysis stage from a representative Murray Harbour Formation sample (2524.33 m) during a) standard cycle and b) extended slow heating (ESH) cycle. a) The S1 peak consists of all free hydrocarbons within the rock, and the S2 peak shows a poorly resolved bimodal peak, commonly observed in unconventional hydrocarbon rocks containing multiple fractions of organic matter. b) Three distinct peaks are resolved using the ESH cycle. The $S1_{ESH}$ peak consists only of light free hydrocarbons, the $S2a_{ESH}$ peak consists of medium and heavy fluid-like hydrocarbon residue (FHR), and the $S2b_{ESH}$ peak consists of hydrocarbons generated from the kerogen and solid bitumen fraction of the rock that includes remnant primary kerogen, solid bitumen, and detrital and refractory organic matter. HC = hydrocarbons.

Figure 4.5: Gas chromatography traces from TD/Py-GC-MS/FID analysis of a Murray Harbour Formation sample (2527.26 m). a) Hydrocarbons thermally desorbed at 300°C for 3 minutes followed by b) thermal desorption at 350°C for 3 minutes. c) Hydrocarbons generated during flash-pyrolysis of sample at 650°C for 30 seconds following thermal desorption at 350°C for 3 minutes.

Figure 4.6: Photomicrographs exemplifying different organic matter fractions observed within Murray Harbour Formation samples. All photomicrographs are taken under reflected white light and oil immersion unless specified. a) Dark grey, low-reflecting matrix bitumen (MB) disseminated throughout clay-rich matrix; b) Higher-reflecting lump solid bitumen (LSB) containing carbonate crystals; c) (Ultraviolet light) Well-defined, fine-grained dull-orange fluorescing zone (phosphate nodule) exuding bright-blue fluorescing free hydrocarbons (HC); d) Same image as c) showing fluid-like hydrocarbon residue (FHR) filling or coating porosity within the phosphate nodule

Figure 4.7: a) Back-scattered electron (BSE) image of a phosphate nodule within a mudstone and siltstone matrix (image in grey, top left). Energy Dispersive X-ray Spectrometry (EDXS) chemical element maps of the same phosphate nodule showing the presence of Ca (magenta), Si (yellow), P (orange), C (red), K (dark purple), Al (purple), and O (green), Na (blue); b) BSE image of the phosphate nodule in EDXS maps under higher magnification illustrating crystal form and porosity (Sample 2527.26 m).

Figure 4.8: Cross plots from Murray Harbour Formation samples (n=12): a) porosity versus grain density; bubble size indicates relative concentration of apatite within each sample (Pearson's r correlation coefficient = 0.95; $p<0.05$; Microsoft Excel Analysis ToolPak™); b) porosity versus

total organic carbon; bubble size indicates relative volume percentage of the kerogen and solid bitumen fraction in each sample (Pearson's r correlation coefficient = -0.65; $p<0.05$; Microsoft Excel Analysis ToolPak™); c) porosity versus clay mineral concentration; bubble size indicates relative volume percentage of the kerogen and solid bitumen fraction in each sample (Pearson's r correlation coefficient = -0.80; $p<0.05$; Microsoft Excel Analysis ToolPak™).

Figure 4.9: a) Representative low pressure nitrogen gas adsorption isotherm from sample 2524.33 m. p = equilibrium pressure; p° = saturation pressure of nitrogen (~89.6 kPa); b), c), d) Pore-size distributions derived from the adsorption branch of isotherms using Barret-Joyner-Halenda method for Murray Harbour Formation samples. Each plot shows samples on an appropriate vertical scale. Bimodal samples = solid line, open symbol; Unimodal samples = dashed line, open symbol; Multimodal samples = solid line, solid symbol.

Figures

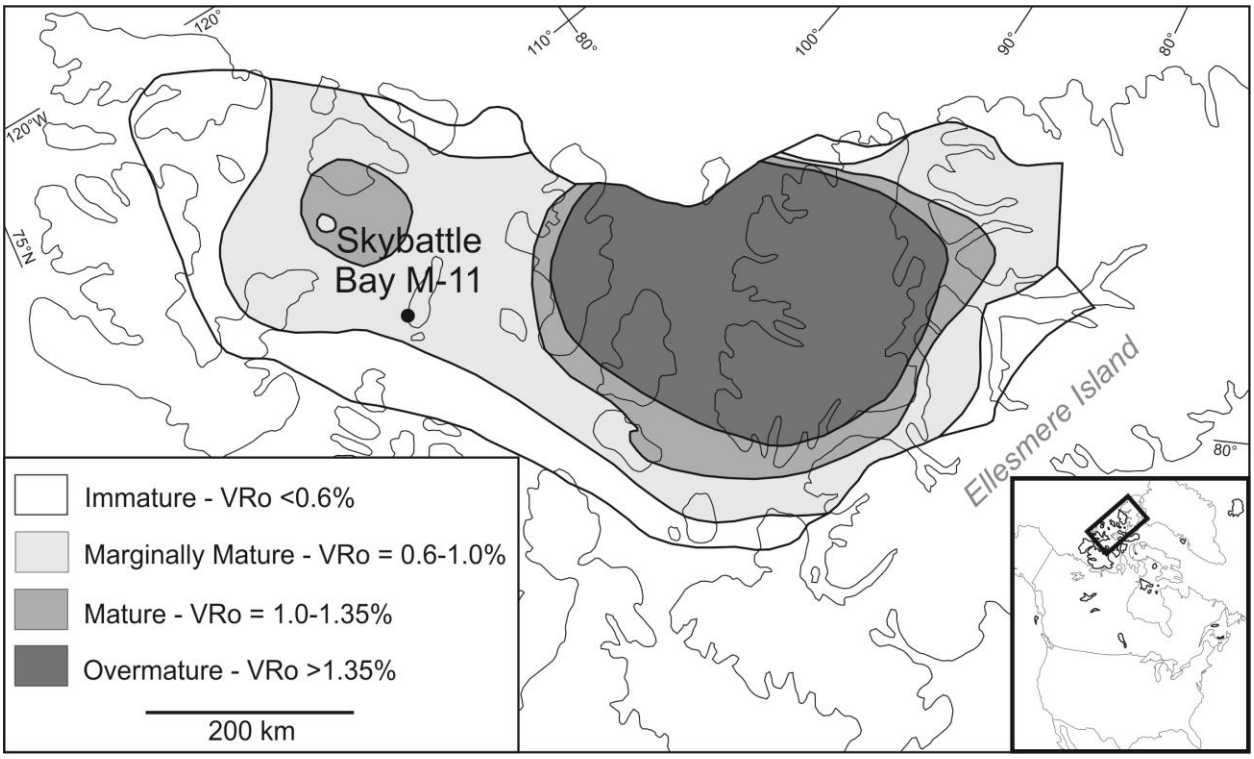

Figure 4.1

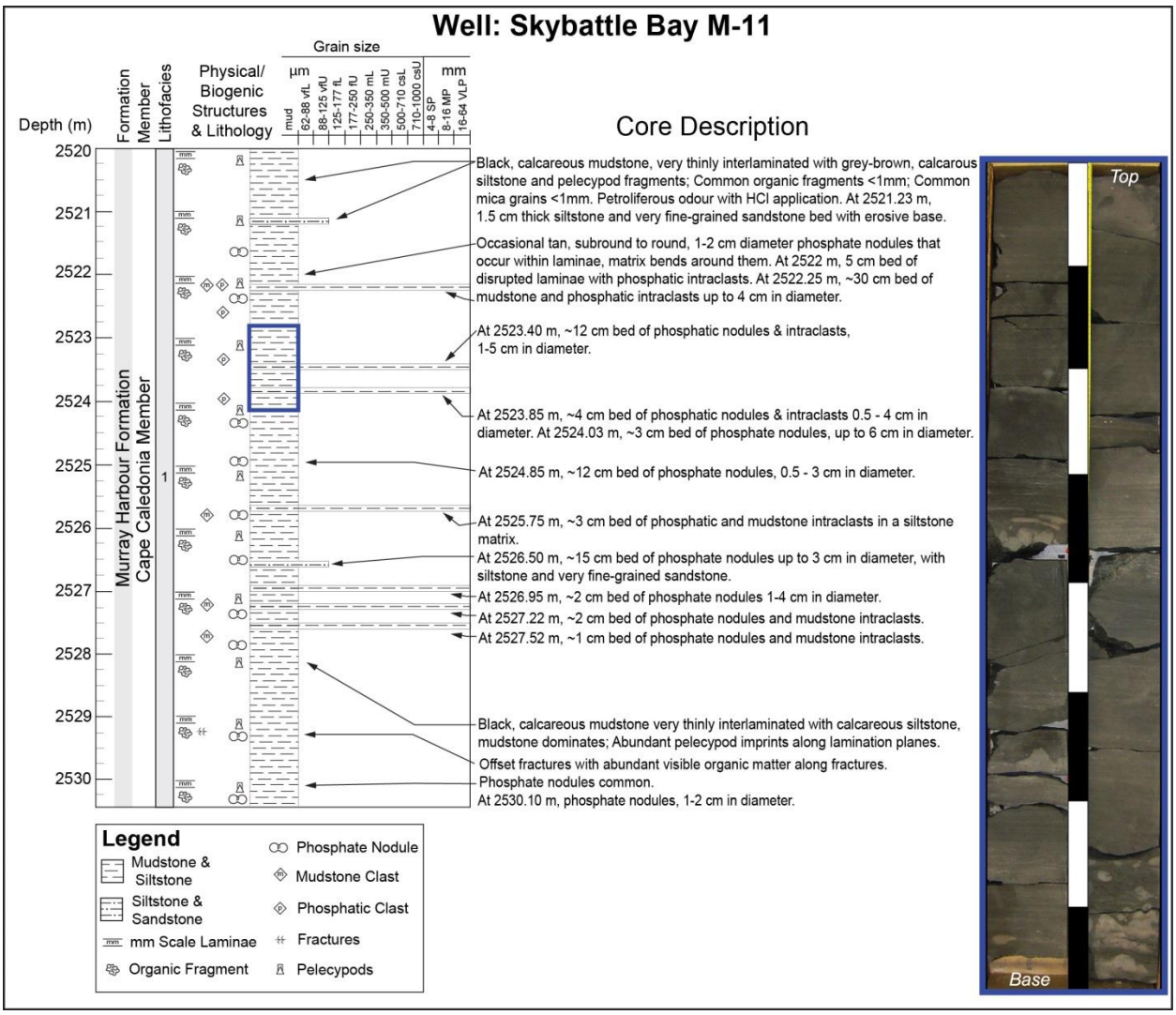
Well: Skybattle Bay M-11
Grain size
µm
mm
Depth (m)
Formation
Member
Lithofacies
Physical/ Biogenic Structures & Lithology
mud
62-88 vfL
88-125 vfU
125-177 fL
177-250 fU
250-350 mL
350-500 mU
500-710 csL
710-1000 csU
4-8 SP
8-16 MP
16-64 VLP
Core Description
2520
2521
2522
2523
2524
2525
2526
2527
2528
2529
2530
Murray Harbour Formation
Cape Caledonia Member
1
Black, calcareous mudstone, very thinly interlaminated with grey-brown, calcarous siltstone and pelecypod fragments; Common organic fragments <1mm; Common mica grains <1mm. Petroliferous odour with HCl application. At 2521.23 m, 1.5 cm thick siltstone and very fine-grained sandstone bed with erosive base.
Occasional tan, subround to round, 1-2 cm diameter phosphate nodules that occur within laminae, matrix bends around them. At 2522 m, 5 cm bed of disrupted laminae with phosphatic intraclasts. At 2522.25 m, ~30 cm bed of mudstone and phosphatic intraclasts up to 4 cm in diameter.
At 2523.40 m, ~12 cm bed of phosphatic nodules & intraclasts, 1-5 cm in diameter.
At 2523.85 m, ~4 cm bed of phosphatic nodules & intraclasts 0.5 - 4 cm in diameter. At 2524.03 m, ~3 cm bed of phosphate nodules, up to 6 cm in diameter.
At 2524.85 m, ~12 cm bed of phosphate nodules, 0.5 - 3 cm in diameter.
At 2525.75 m, ~3 cm bed of phosphatic and mudstone intraclasts in a siltstone matrix.
At 2526.50 m, ~15 cm bed of phosphate nodules up to 3 cm in diameter, with siltstone and very fine-grained sandstone.
At 2526.95 m, ~2 cm bed of phosphate nodules 1-4 cm in diameter.
At 2527.22 m, ~2 cm bed of phosphate nodules and mudstone intraclasts.
At 2527.52 m, ~1 cm bed of phosphate nodules and mudstone intraclasts.
Black, calcareous mudstone very thinly interlaminated with calcareous siltstone, mudstone dominates; Abundant pelecypod imprints along lamination planes.
Offset fractures with abundant visible organic matter along fractures.
Phosphate nodules common.
At 2530.10 m, phosphate nodules, 1-2 cm in diameter.
Top
Base
Legend
Mudstone & Siltstone
Siltstone & Sandstone
mm Scale Laminae
Organic Fragment
Phosphate Nodule
Mudstone Clast
Phosphatic Clast
Fractures
Pelecypods

Figure 4.2

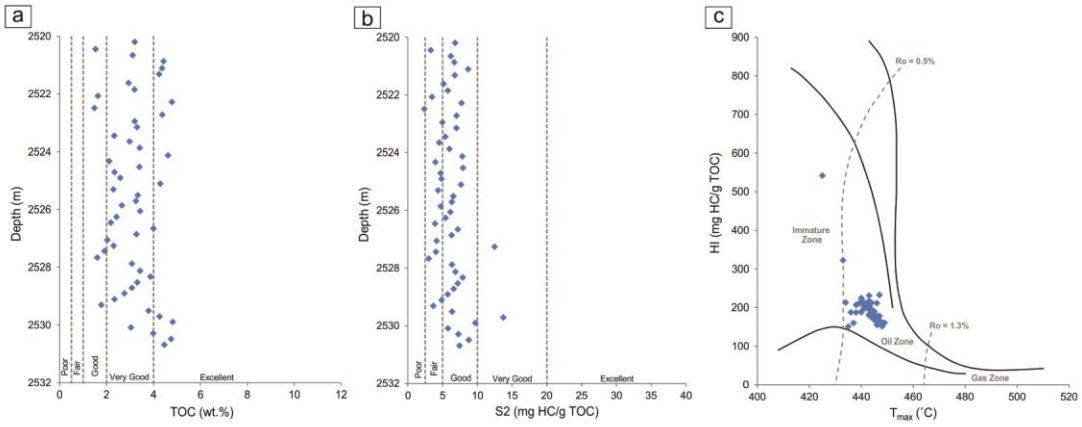
a
b
c
Depth (m)
TOC (wt.%)
S2 (mg HC/g TOC)
HI (mg HC/g TOC)
T_{max} (°C)
Poor
Fair
Good
Very Good
Excellent
Immature Zone
Oil Zone
Gas Zone
Ro = 0.5%
Ro = 1.3%

Figure 4.3

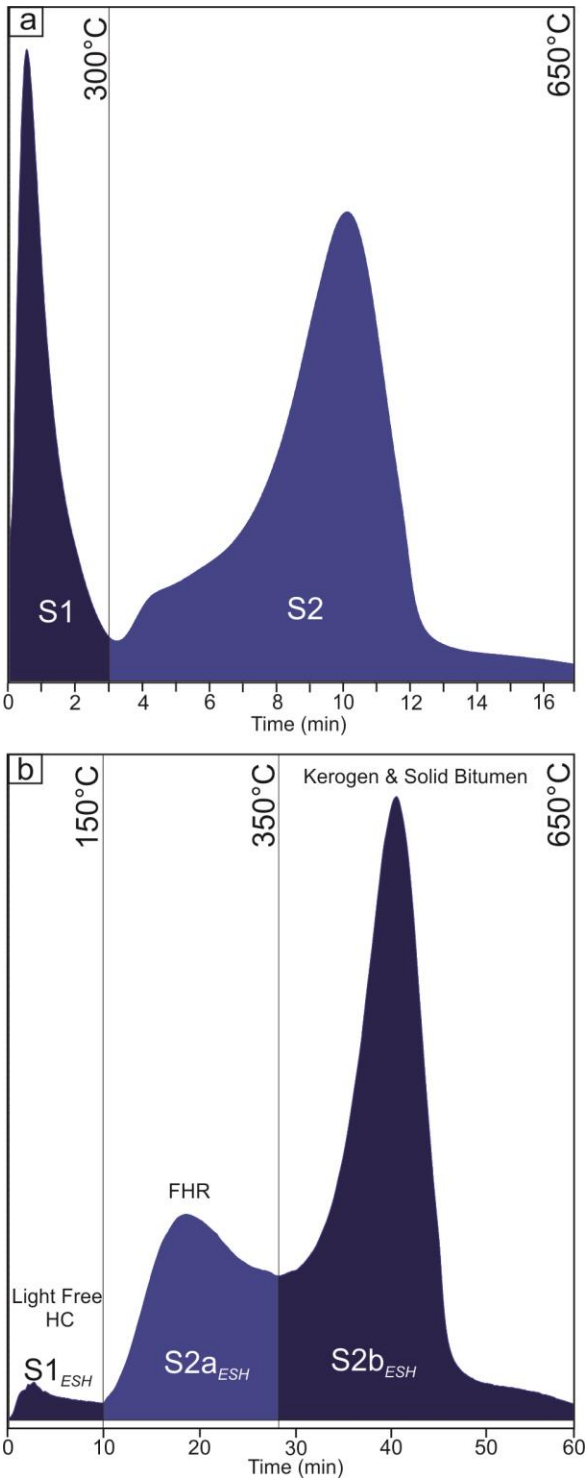
a
300°C
650°C
S1
S2
0
2
4
6
8
10
12
14
16
Time (min)
b
150°C
350°C
650°C
Kerogen & Solid Bitumen
FHR
Light Free HC
S1ESH
S2aESH
S2bESH
0
10
20
30
40
50
60
Time (min)

Figure 4.4

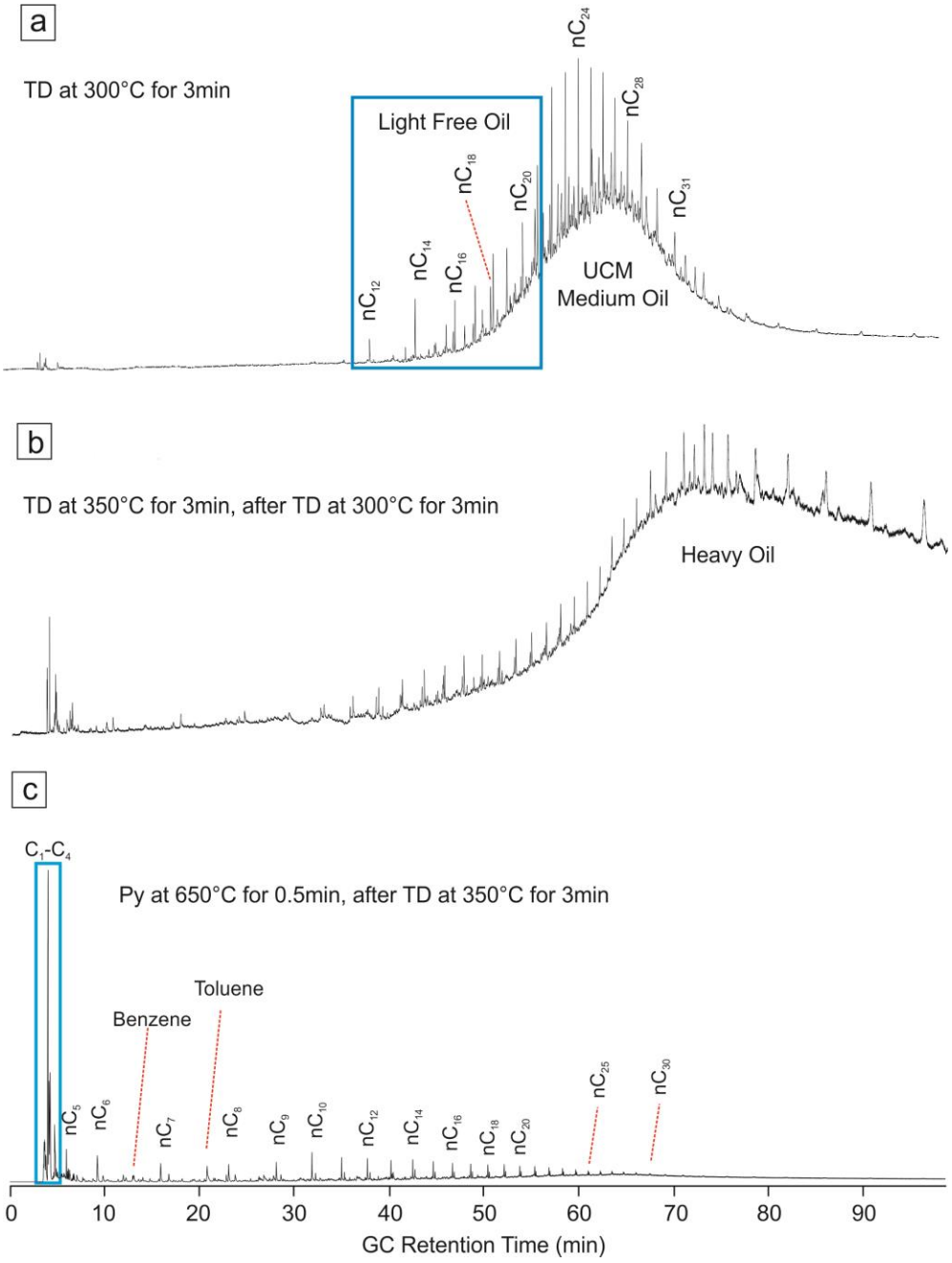
a
TD at 300°C for 3min
Light Free Oil
nC12
nC14
nC16
nC18
nC20
nC24
nC28
nC31
UCM
Medium Oil
b
TD at 350°C for 3min, after TD at 300°C for 3min
Heavy Oil
c
C1-C4
Py at 650°C for 0.5min, after TD at 350°C for 3min
Toluene
Benzene
nC5
nC6
nC7
nC8
nC9
nC10
nC12
nC14
nC16
nC18
nC20
nC25
nC30
0
10
20
30
40
50
60
70
80
90
GC Retention Time (min)

Figure 4.5

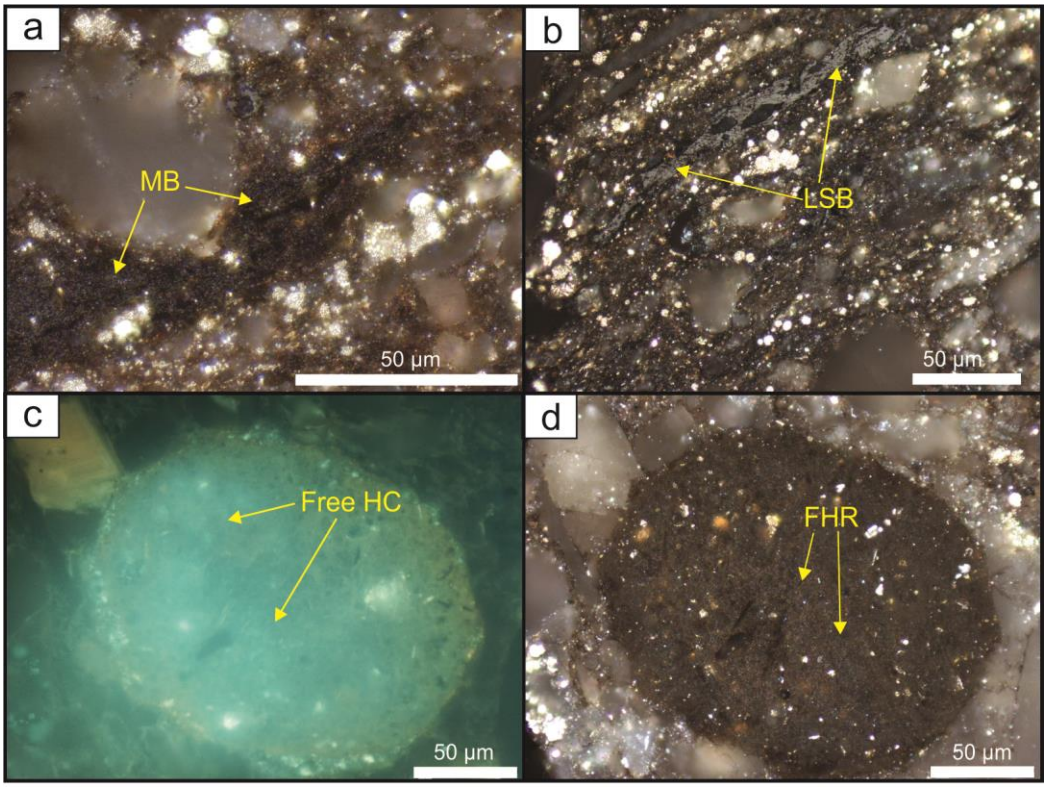

Figure 4.6

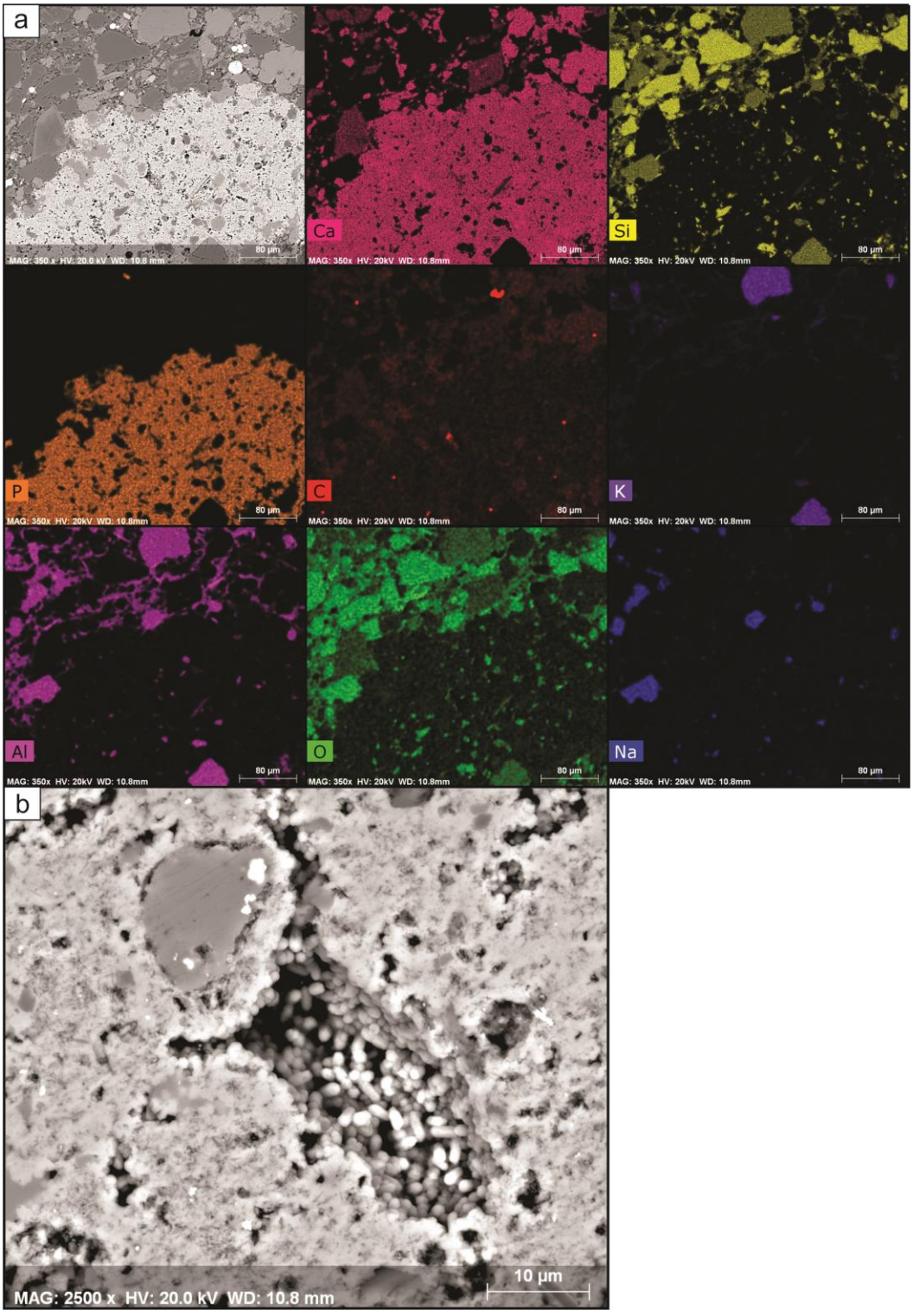
a
Ca
Si
P
C
K
Al
O
Na
80 µm
MAG: 350x HV: 20kV WD: 10.8mm
b
10 µm
MAG: 2500 x HV: 20.0 kV WD: 10.8 mm

Figure 4.7

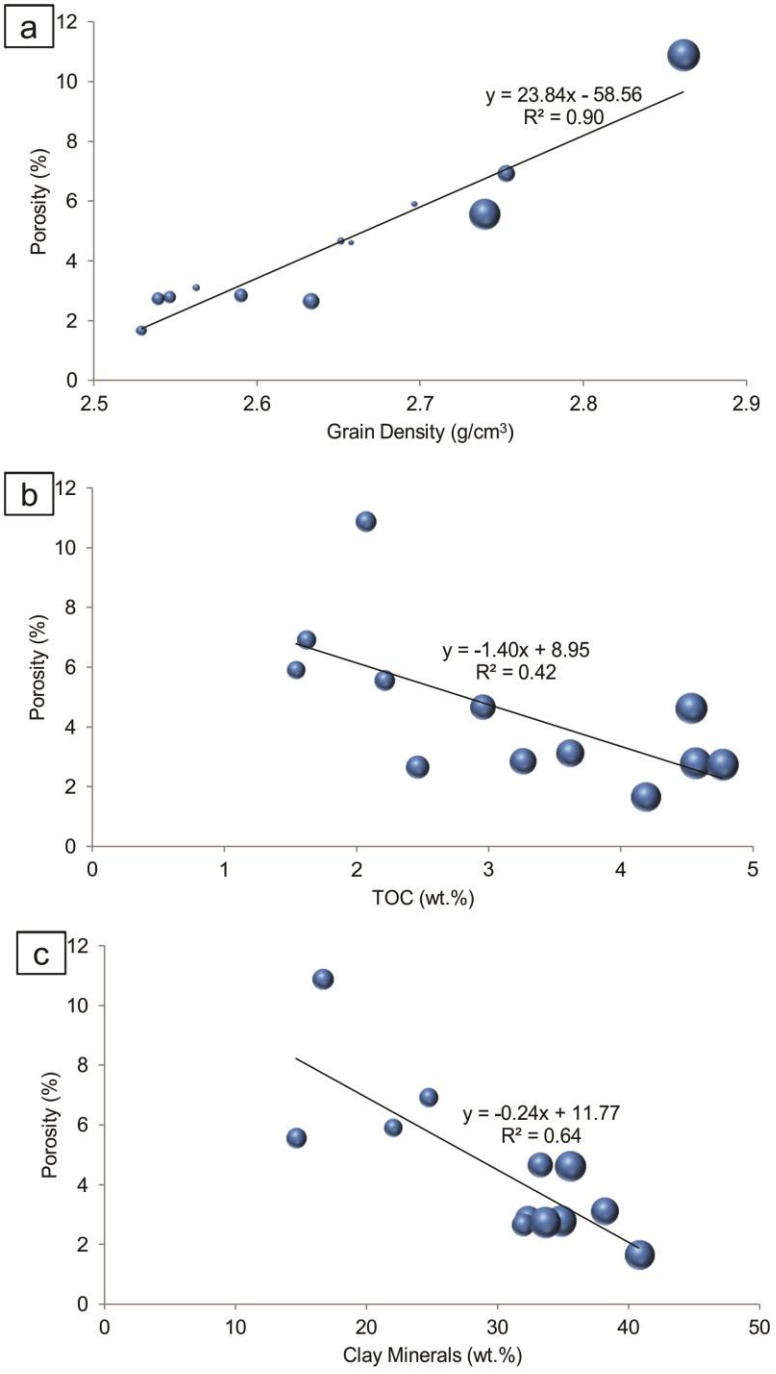
a
y = 23.84x - 58.56
R² = 0.90
Porosity (%)
Grain Density (g/cm³)
b
y = -1.40x + 8.95
R² = 0.42
Porosity (%)
TOC (wt.%)
c
y = -0.24x + 11.77
R² = 0.64
Porosity (%)
Clay Minerals (wt.%)

Figure 4.8

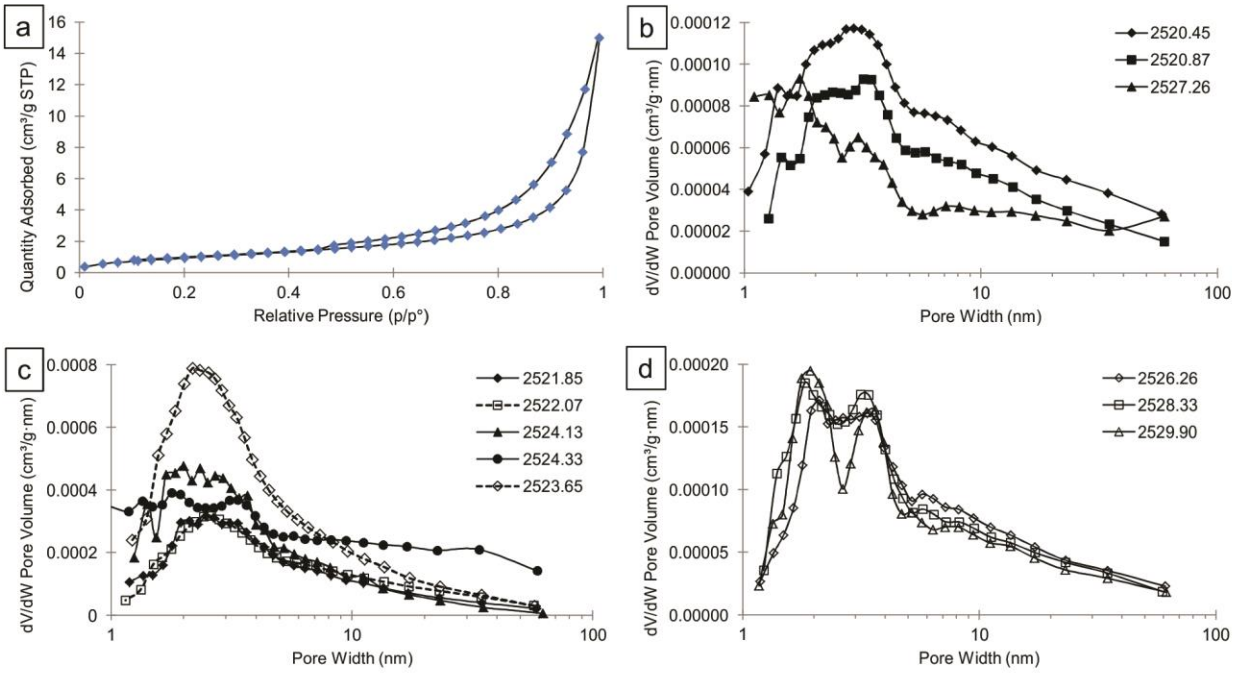
a
Quantity Adsorbed (cm³/g STP)
Relative Pressure (p/p°)
b
dV/dW Pore Volume (cm³/g·nm)
Pore Width (nm)
2520.45
2520.87
2527.26
c
dV/dW Pore Volume (cm³/g·nm)
Pore Width (nm)
2521.85
2522.07
2524.13
2524.33
2523.65
d
dV/dW Pore Volume (cm³/g·nm)
Pore Width (nm)
2526.26
2528.33
2529.90

Figure 4.9

Chapter Five: **Conclusions**

5.1 Concluding Remarks

This study provides a detailed assessment of dispersed organic matter (OM) within three cores of Middle Triassic strata from the west-central Sverdrup Basin. The three cores represent strata from three locations across the basin as well as from different episodes of geologic time: Collingwood K-33 (southern basin margin, Ladinian regressive systems tract), Skybattle Bay M-11 (basin centre, Anisian regressive systems tract and transgressive systems tract, Ladinian regressive systems tract), Pollux G-60 (northern basin margin, Anisian regressive systems tract). Chapters 3 and 4 each investigate OM within the strata, but each with a different strategy and emphasis. Chapter 3 focuses on the relationship between OM and depositional environment, while Chapter 4 addresses the contribution of OM to hydrocarbon potential and reservoir quality of the unit. The conclusions from both chapters can be combined to illustrate the overall construction of the petroleum system of the Middle Triassic strata in the Sverdrup Basin, albeit on a localized scale.

The main conclusions of Chapter 3 relate to the characterization of OM and the spatial and temporal distribution of it within the sequence stratigraphic framework of the Middle Triassic strata. The type and abundance of OM within the rocks results from a combination of three factors: (i) level of primary production of marine biomass, (ii) the extent of preservation of deposited OM, and (iii) the amount of dilution of autochthonous OM by mineral matter and allochthonous OM. These factors appear to be controlled predominantly by the 3rd order stratigraphic sequences resulting from base level rise and fall in the basin. Chapter 4 conclusions highlight initial findings regarding the hydrocarbon potential and reservoir quality of the organic

rich Ladinian regressive systems tract in the west-central part of the Sverdrup Basin. The general conclusions from both Chapters 3 and 4 are:

1) Collingwood K-33 samples are low in TOC and consist of a mixture of marine Type II and reworked or detrital terrestrial Type III kerogen. The Anisian portion of the Skybattle Bay M-11 core is also low in TOC, consisting of mainly allochthonous Type III kerogen. The organic lean nature of samples from these intervals is due to both oxic depositional conditions, limiting OM preservation, as well as dilution of primary OM by coarser clastic material and allochthonous OM.

2) Pollux G-60 samples display cycles of low to high TOC values throughout the core. The OM is mainly marine Type II, and the richest intervals were deposited under suboxic bottom water conditions. The organic lean intervals were deposited under oxic conditions and demonstrate substantial dilution from coarser-grained clastic influx. These organic lean, coarser-grained intervals may be evidence of distally-deposited sediment sourced from the northerly-situated Crockerland.

3) The Ladinian portion of the Skybattle Bay M-11 core is the most prospective interval in terms of hydrocarbon exploration. These samples are organic rich (Type II kerogen) as a consequence of anoxic depositional conditions facilitating preservation of primary biomass, with limited dilution effects. OM within the core can be divided into three fractions: (i) light free hydrocarbons, (ii) medium and heavy molecular-weight fluid-like hydrocarbon residue (FHR), and (iii) kerogen and solid bitumen.

4) The kerogen and solid bitumen fraction, which includes solid bitumen and degraded kerogen, is dominated by solid bitumen. Solid bitumen is present in two petrographically discernable forms: (i) matrix bitumen, and (ii) lump solid bitumen, both of which have

detrimental effects on reservoir quality due their pore-filling character. However, overmature areas of the basin may have improved reservoir quality as a result of microporosity development within solid bitumen that could provide additional adsorption sites for generated gaseous hydrocarbons.

5) Phosphatic nodules are present in variable abundance throughout the core, both micro- and macroscopically. These nodules contain porosity, which in some instances, contains light free hydrocarbons and FHR, contributing to the total porosity and hydrocarbon storage potential of the interval.

Findings from the research summarized in both Chapters 3 and 4 are not only useful for the Middle Triassic strata of the Sverdrup Basin, but also for application to other self-sourced reservoirs. The relationships established between OM, depositional environment, and stratigraphic sequences in these rocks can be used to better understand depositional systems in other fine-grained marine basins. The use of a suite of redox-sensitive trace elements to infer the depositional conditions of these samples is particularly useful when supported by petrographic and core evidence. Reservoir quality and hydrocarbon potential of self-sourced reservoirs can be affected negatively (e.g., Sanei et al., 2015) or positively (e.g., Jarvie et al., 2007) by OM fractions, highlighting the need to treat each reservoir uniquely. Use of the extended slow heating (ESH) cycle for Rock-Eval analysis facilitated identification of chemically distinct OM fractions, which were then aligned with petrographically observed characteristics of OM, a novel method that can be applied to other organic-rich units.

These systems are complex and difficult to study, making it important to have a variety of research tools to select from. Each new study of fine-grained, organic-rich rocks can develop ideas and methods that can be used to further the understanding of these increasingly important

resources. The integration of organic and inorganic geochemistry with petrology, SEM, petrophysics, and core examination in this study has been shown to be a powerful combination to characterize OM and its relationship with the mineral fraction of the rock.

5.2 Future Work

A number of opportunities for further research have evolved over the course of study for this thesis. Moreover, some of the conclusions from the two research chapters could be substantiated with additional analyses. Areas for further investigation include:

1) The lump solid bitumen identified in Chapter 4, is synonymous with the high-reflecting, larger-pore-filling solid bitumen described in Chapter 3, and is inferred to be the result of degradation of OM during the early stages of diagenesis. More specifically, it is inferred to be a product of bacterial sulphate reduction (BSR) of OM. The most promising approach to determine if this form of bitumen is a product of BSR is to analyse the associated framboidal pyrite for the stable isotopes of sulphur. However, isotopic fractionation would only be apparent if the system was open, allowing preferential use of light isotopes by the bacteria, so even this analysis may not be conclusive (Machel et al., 1995 and references therein).

2) Porosity measurements of the Skybattle Bay M-11 samples were conducted on "as received" material and correlations were made with other parameters based on this data. As a result of this, any porosity that was filled with fluids (i.e., hydrocarbons, water) was not measured, potentially affecting the correlations. Re-analysing the samples after cleaning with solvents to remove any fluids within pore spaces would likely result in stronger correlations and potentially reveal new links between porosity and other parameters.

3) The mineralogy of the Skybattle Bay M-11 samples was derived based on bulk elemental values of the rock. While this method has proved quite accurate on other samples sets,

confirmation of mineralogy via X-ray diffraction (XRD) is required to validate the conclusions derived from bulk elemental values.

4) The association of porosity with phosphatic nodules in the Skybattle Bay M-11 samples is interesting but certainly requires further investigation to determine how substantial it is in terms of affecting reservoir quality. Study of porosity and geochemistry of other samples within phosphatic Middle Triassic strata in the Sverdrup Basin could establish the extent to which phosphate nodules contribute to porosity on a more regional scale. Additionally, investigation of other phosphatic self-sourced reservoirs could determine if similar associations between porosity and phosphate nodules or laminae exist elsewhere.

5) Examination of Middle Triassic strata in more thermally mature areas of the basin may identify areas of greater prospectivity for hydrocarbon exploration. The organic-rich Skybattle Bay M-11 samples are likely to have developed increased microporosity within the pervasive solid bitumen network in overmature areas, providing additional gas adsorption sites (e.g., Chalmers and Bustin, 2007; Jarvie et al., 2007). The Pollux G-60 samples also showed substantial organic richness, albeit at immature thermal maturity; tracing this interval further basinward (to limit effects from clastic dilution) and to areas of increased thermal maturity may lead to discovery of hydrocarbon-rich zones similar to the Ladinian Skybattle Bay M-11 interval.

References

Abanda, P.A., and Hannigan, R.E., 2006, Effect of diagenesis on trace element partitioning in shales: Chemical Geology, v. 230, p. 42-49, doi:10.1016/j.chemgeo.2005.11.011.

Algeo, T.J., and Maynard, J.B., 2004, Trace-element behavior and redox facies in core shales of Upper Pennsylvanian Kansas-type cyclothems: Chemical Geology, v. 206, p. 289-318, doi: 10.1016/j.chemgeo.2003.12.009.

Algeo, T.J., and Tribovillard, N., 2009, Environmental analysis of paleoceanographic systems based on molybdenum-uranium covariation: Chemical Geology, v. 268, p. 211-225, doi: 10.1016/j.chemgeo.2009.09.001.

Balkwill, H.R., 1978, Evolution of Sverdrup Basin, Arctic Canada: AAPG Bulletin, v. 62, p. 1004-1028, doi: 10.1306/C1EA4F86-16C9-11D7-8645000102C1865D.

Barker, C.E., and Pawlewicz, M.J., 1993, An empirical determination of the minimum number of measurements needed to estimate the mean random vitrinite reflectance of disseminated organic matter: Organic Geochemistry, v. 20, p. 643-651.

Bertrand, R., and Malo, M., 2001, Source rock analysis, thermal maturation and hydrocarbon generation in the Siluro-Devonian rocks of the Gasps Belt basin, Canada. Bulletin of Canadian Petroleum Geology, v. 49, p. 238–261.

Brooks, P.W., Embry, A.F., Goodarzi, F., and Stewart, R., 1992, Organic geochemistry and biological marker geochemistry of Schei Point Group (Triassic) and recovered oils from

the Sverdrup Basin (Arctic Islands, Canada): Bulletin of Canadian Petroleum Geology, v. 40, p. 173-187.

Canadian Association of Petroleum Producers (CAPP), 1999, CAPP Statistical Handbook – 1998, Canadian Association of Petroleum Producers, Calgary.

Chalmers, G.R., Bustin, R.M., and Power, I.M., 2012, Characterization of gas shale pore systems by porosimetry, pycnometry, surface area, and field emission scanning electron microscopy/transmission electron microscopy image analyses: Examples from the Barnett, Woodford, Haynesville, Marcellus, and Doig units: AAPG Bulletin, v. 96, p. 1099-1119.

Chalmers, G.R.L., and Bustin, R.M., 2008, Lower Cretaceous gas shales in northeastern British Columbia, Part I: geological controls on methane sorption capacity: Bulletin of Canadian Petroleum Geology, v. 56, p. 1-21.

Chalmers, G.R.L., and Bustin, R.M., 2007, The organic matter distribution and methane capacity of the Lower Cretaceous strata of Northeastern British Columbia, Canada: International Journal of Coal Geology, v. 70, p. 223-239, doi: 10.1016/j.coal.2006.05.001.

Chen, Z., and Osadetz, K.G., 2011, Chapter 39 Using discovery process and accumulation volumetric models to improve petroleum resource assessment in Sverdrup Basin, Canadian Arctic Archipelago, in Spencer, A.M., Embry, A.F., Gautier, D.L., Stroupakova, A.V. and Sorensen, K., eds., Arctic Petroleum Geology: London, Geological Society of London, Memoirs, p. 581-593, doi: 10.1144/M35.39.

Chen, Z., Osadetz, K.G., Embry, A.F., Gao, H., and Hannigan, P.K., 2000, Petroleum potential in western Sverdrup Basin, Canadian Arctic Archipelago: Bulletin of Canadian Petroleum Geology, v. 48, p. 323-338.

Cornford, C., Gardner, P., and Burgess, C., 1998, Geochemical truths in large data sets. I: Geochemical screening data: Organic Geochemistry, v. 29, p. 519-530.

Dewing, K., and Obermajer, M., 2011, Chapter 38 Thermal maturity of the Sverdrup Basin, Arctic Canada and its bearing on hydrocarbon potential, in Spencer, A.M., Embry, A.F., Gautier, D.L., Stroupakova, A.V. and Sorensen, K., eds., Arctic Petroleum Geology: London, Geological Society of London, Memoirs, p. 567-580.

Edwards, D.E., Barclay, J.E., Gibson, D.W., Kvill, G.E., and Halton, E., 1994, Triassic strata of the Western Canada Sedimentary Basin, in Mossop, G.D. and Shetsen, I., eds., Geological Atlas of the Western Canada Sedimentary Basin: Calgary, Canadian Society of Petroleum Geologists and Alberta Research Council, p. 259-275.

Embry, A.F., 2011, Petroleum prospectivity of the Triassic-Jurassic succession of Sverdrup Basin, Canadian Arctic Archipelago, in Spencer, A.M., Embry, A.F., Gautier, D.L., Stroupakova, A.V. and Sorensen, K., eds., Arctic Petroleum Geology: London, Geological Society of London, Memoirs, p. 545-558.

Embry, A.F., 2009, Crockerland – The Source Area for the Triassic to Middle Jurassic Strata of Northern Axel Heiberg Island, Canadian Arctic Islands: Bulletin of Canadian Petroleum Geology, v. 57, p. 129-140.

Embry, A.F., 1993, Crockerland - the northern source area for the Sverdrup Basin, Canadian Arctic Archipelago, in Vorren, T., Blackadar, R., Glenister, B., Greiner, H., McLaren, D., McMillan, N., Norris, A., Roots, E., Souther, J., Thorsteinsson, R. and Tozer, T., eds., Arctic geology and petroleum potential: Amsterdam, The Netherlands, Norwegian Petroleum (Special Publication), p. 205-216.

Embry, A.F., 1991, Chapter 14: Mesozoic History of the Arctic Islands, in Trettin, H.P., ed., Geology of the Innuitian orogen and arctic platform of Canada and Greenland: Ottawa, Geological Survey of Canada, p. 371-434.

Embry, A.F., 1984a, The Schei Point and Blaa Mountain groups (Middle-Upper Triassic), Sverdrup Basin, Canadian Arctic Archipelago: Current Research, Part B, Geological Survey of Canada, v. Paper 84-1B, p. 327-336.

Embry, A.F., 1984b, Stratigraphic Subdivision of the Roche Point, Hoyle Bay and Barrow formations (Schei Point Group), Western Sverdrup Basin, Arctic Islands: Current Research, Part B, Geological Survey of Canada, v. Paper 84-1B, p. 275-283.

Embry, A.F., and Beauchamp, B., 2008, Sverdrup Basin, in Hsu, K.J., ed., Sedimentary Basins of the World, Vol 5, The Sedimentary Basins of the United States and Canada: Andrew D. Miall, Elsevier, The Netherlands, p. 451-471.

Embry, A.F., and Podruski, J.A., 1988, Third-order depositional sequences of the Mesozoic succession of Sverdrup Basin: Canadian Society of Petroleum Geologists, v. Memoir 15, p. 73-84.

Espitalie, J., Derro, G., and Marquis, F., 1985, Rock Eval pyrolysis and its applications : Revue de l'Institut Français du Petrole, v. 40, p. 563-579.

Föllmi, K.B., 1996, The phosphorus cycle, phosphogenesis and marine phosphate-rich deposits: Earth-Science Reviews, v. 40, p. 55-124.

Fraenkel, J.R., Wallen, N.E., and Hyun, H.H., 1993, How to design and evaluate research in education: v. 7, New York, McGraw-Hill, p. 706.

Gentzis, T., and Goodarzi, F., 1993, Thermal maturity and source-rock potential of the sedimentary succession from the Drake field, Sverdrup Basin, Arctic Canada: Journal of Petroleum Geology, v. 16, p. 33-54, doi: 10.1111/j.1747-5457.1993.tb00729.x.

Gentzis, T., and Goodarzi, F., 1991, Thermal maturity and hydrocarbon potential of the sedimentary succession from the Hecla field in Sverdrup Basin, Arctic Canada: International Journal of Coal Geology, v. 19, p. 483-517, doi: 10.1016/0166-5162(91)90031-D.

Gentzis, T., Goodarzi, F., and Embry, A.F., 1996, Thermal maturation, potential source rocks and hydrocarbon generation in Mesozoic rocks, Lougheed Island area, Central Canadian Arctic archipelago: Marine and Petroleum Geology, v. 13, p. 879-905, doi: 10.1016/S0264-8172(96)00028-1.

Ghanizadeh, A., Clarkson, C.R., Aquino, S., Ardakani, O.H., and Sanei, H., 2014, Petrophysical and geomechanical characteristics of Canadian tight oil and liquid-rich gas reservoirs: I. Pore network and permeability characterization: Fuel, v. 153, p. 664-681.

Ghanizadeh, A., Bhowmik, S., Ardakani, O.H., Sanei, H., and Clarkson, C.R., 2015, A comparison of shale permeability coefficients derived using multiple non-steady-state measurement techniques: Examples from the Duvernay Formation, Alberta (Canada): Fuel, v. 140, p. 371-387.

Gibson, D.W., and Barclay, J.E., 1989, Middle Absaroka Sequence – the Triassic stable craton, in Ricketts, B.D., ed., Western Canada Sedimentary Basin – a Case History: Canadian Society of Petroleum Geologists, Special Publication, p. 219-232.

Golding, M.L., Orchard, M.J., Zonneveld, J.-P., Henderson, C.M., and Dunn, L., 2014, An exceptional record of the sedimentology and biostratigraphy of the Montney and Doig formations in British Columbia: Bulletin of Canadian Petroleum Geology, v. 62, p. 157-176.

Goodarzi, F., Brooks, P.W., and Embry, A.F., 1989, Regional maturity as determined by organic petrography and geochemistry of the Schei Point Group (Triassic) in the western Sverdrup Basin, Canadian Arctic Archipelago: Marine and Petroleum Geology, v. 6, p. 290-302, doi: 10.1016/0264-8172(89)90026-3.

Gough, M.A., and Rowland, S.J., 1990, Characterization of unresolved complex mixtures of hydrocarbons in petroleum: Nature, v. 344, p. 648-650.

Gregg, S.J., and Sing, K.S.W., 1982, Adsorption, surface area and porosity: New York, Academic Press, p. 303.

Jarvie, D.M., Hill, R.J., Ruble, T.E., and Pollastro, R.M., 2007, Unconventional shale-gas systems: The Mississippian Barnett Shale of north-central Texas as one model for thermogenic shale-gas assessment: AAPG Bulletin, v. 91, p. 475-499, doi: 10.1306/12190606068.

Jarvis, I., Burnett, W.C., Nathan. Y., Almbaydin, F., Attia, K.M., Castro, L.N., Flicoteaux, R., Hilmy, M.E., Husain, V., Qutawna, A.A., Serjani, A., and Zanin, Y.N., 1994, Phosphorite geochemistry: state-of-the-art and environmental concerns, in Föllmi, K.B., ed., Concepts and Controversies in Phosphogenesis: Eclogae Geologicae Helvetiae, p. 643-700.

Jones, P.J., and Tobey, M.H., 1999, Pyrolitic oil-productivity index method for characterizing reservoir rock, U.S. Patent Number 5866814.

Jones, S.F., Wielens, H., Williamson, M-C., and Zentilli, M., 2007, Impact of magmatism on petroleum systems in the Sverdrup Basin, Canadian Arctic Islands, Nunavut: a numerical modelling study: Journal of Petroleum Geology, v. 30, p. 237-256.

Kondla, D., Sanei, H., Embry, A., Ardakani, O.H., and Clarkson, C.R., 2015, Depositional environment and hydrocarbon potential of the Middle Triassic strata of the Sverdrup Basin, Canada: International Journal of Coal Geology, v. 147-148, p. 71-84, doi: 10.1016/j.coal.2015.06.010.

Kuila, U., and Prasad, M., 2013, Specific surface area and pore-size distribution in clays and shales: Geophysical Prospecting, v. 61, p. 341-362, doi: 10.1111/1365-2478.12028.

Lafargue, E., Espitalie, J., Marquis, F., and Pillot, D., 1998, Rock-Eval 6 applications in hydrocarbon exploration, production and in soil contamination studies: Revue De l'Institut Français Du Pétrole, v. 53, p. 421-437.

Langford, F.F., and Blanc-Valleron, M. –M., 1990, Interpreting Rock-Eval pyrolysis data using graphs of pyrolizable hydrocarbons vs. total organic carbon: AAPG Bulletin, v. 74, p. 799-804.

Li, H., and Bennett, R.H., 1991, The significance of sediment-flow dynamics on clay microstructure development: riverine and continental shelf environments, in Bennett, R.H., Iryant, W.R., Hulbert, M.H., eds., Microstructure of Fine-Grained Sediments From Mud to Shale: Springer-Verlag, New York, p 193-202.

Loucks, R.G., Reed, R.M., Ruppel, C., and Hammes, U., 2012, Spectrum of pore types and networks in mudrocks and a descriptive classification for matrix-related mudrock pores: AAPG Bulletin, v. 96, p. 1071-1098, doi: 10.1306/08171111061.

Machel, H.G., 2001, Bacterial and thermochemical sulfate reduction in diagenetic settings - old and new insights: Sedimentary Geology, v. 140, p. 143-175.

Machel, H.G., Krouse, H.R., and Sassen, R., 1995, Products and distinguishing criteria of bacterial and thermochemical sulfate reduction: Applied Geochemistry, v. 10, p. 373-389.

Mukhopadhyay, P.K., Goodarzi, F., Kruge, M.A., and Alimi, M.H., 1997, Comparison of source rock geochemistry of selected rocks from the Schei Point group and Ringnes formation,

Sverdrup basin, arctic Canada: International Journal of Coal Geology, v. 34, p. 225-260, doi: 10.1016/S0166-5162(97)00024-4.

Parrish, J.Y., 1995, Paleogeography of Corg-rich rocks and the preservation versus production controversy, in Huc, A.-Y., ed., Paleogeography, paleoclimate, and source rocks: AAPG Studies in Geology, v. 40, p. 1-20.

Patchett, P.J., Embry, A.F., Ross, G.M., Beauchamp, B., Harrison, J.C., and Mayr, U., 2004, Sedimentary Cover of the Canadian Shield through Mesozoic Time Reflected by Nd Isotopic and Geochemical Results for the Sverdrup Basin, Arctic Canada The Journal of Geology, v. 112, p. 39-57.

Poulson Brucker, R.L., McManus, J., Severmann, S., and Berelson, W.M., 2009, Molybdenum behavior during early diagenesis: Insights from Mo isotopes: Geochemistry Geophysics Geosystems, v. 10, p. 1-25, doi: 10.1029/2008GC002180.

Riediger, C.L., Fowler, M.G., Brooks, P.W., and Snowdon, L.R., 1990, Triassic oils and potential Mesozoic source rocks, Peace River Arch area, Western Canada Basin: Organic Geochemistry, v. 16, p. 295-305.

Rouquerol, J., Avnir, D., Sing, K.S.W., Everett, D.H., Haynes, J.H., Pernicone, N., Ramsay, J.D.F., Sing, K.S.W., and Ungar, K.K., 1994, Recommendations for the characterization of porous solids: Pure and Applied Chemistry, v. 66, p. 1739-1758.

Sageman, B.B., and Lyons, T.W., 2004, Geochemistry of Fine-grained Sediments and Sedimentary Rocks, in MacKenzie, F., ed., Sediments, Diagenesis, and Sedimentary Rocks, Treatise on Geochemistry: New York, Elsevier, p. 115-158.

Sanei, H., Wood, J.M., Ardakani, O.H., Clarkson, C.R., and Jiang, C., 2015, Characterization of organic matter fractions in an unconventional tight gas siltstone reservoir: International Journal of Coal Geology. (In press)

Sing, K.S.W., Everett, D.H., Haul, R.A.W., Moscou, L., Pierotti, R.A., Rouquérol, J., and Siemieniewska, T., 1985, Reporting physisorption data for gas/solid systems with special reference to the determination of surface area and porosity: Pure and Applied Chemistry, v. 57, p. 603-619.

Taylor, S.R., and McLennan, S.M., 1985, The continental crust: its composition and evolution: Blackwell, Oxford. p. 312.

Taylor, G.H., Teichmüller, M., Davis, A., Diessel, C.F.K., Littke, R., and Robert, P., 1998, Organic Petrology: Berlin, Stuttgart, Gebrüder Borntraeger, p. 704.

Teichmüller, M., 1989, The genesis of coal from the viewpoint of coal petrology: International Journal of Coal Geology, v. 12, p. 1-87.

Tissot, B.P., Pelet, R., and Ungerer, P., 1987, Thermal History of sedimentary basins, maturation indices, and kinetics of oil and gas generation: AAPG Bulletin, v. 71, p. 1445-1466.

Tozer, E.T., 1970, Marine Triassic faunas, in Douglas, R.J.W., ed., Geology and Economic Minerals of Canada: Geological Survey of Canada, Economic Geology Report v. 1, p. 633-640.

Tozer, E.T., 1967, A standard for Triassic time: Geological Survey of Canada, Bulletin 156, p. 103.

Tozer, E.T., 1963, Mesozoic and Tertiary stratigraphy, western Ellesmere Island and Axel Heiberg Island, District of Franklin: Geological Survey of Canada, v. 63-30.

Tozer, E.T., 1961a, Summary account of Mesozoic and Tertiary stratigraphy, Canadian Arctic Archipelago, in Raasch, G.O., ed., Geology of the Arctic Geological Survey of Canada: Alberta Society of Petroleum Geologists, p. 381-402.

Tozer, E.T., 1961b, Triassic stratigraphy and faunas, Queen Elizabeth Islands, Arctic Archipelago: Geological Survey of Canada, v. Memoir 316.

Wood, J.M., Sanei, H., Curtis, M.E., and Clarkson, C.R., 2015, Solid bitumen as a determinant of reservoir quality in an unconventional tight gas siltstone play: International Journal of Coal Geology. (In press)

Waylett, D.C., and Embry, A.F., 1992, Hydrocarbon loss from oil and gas fields of the Sverdrup Basin, Canadian Arctic Islands, in Vorren, T.O., Bergsager, E., Dahl-Stannes, Ø.A., Holter, E., Johansen, B., Lie, E., and Lund, T.B., eds., Arctic Geology and Petroleum Potential: NPF Special Publication v. 2, Elsevier, Amsterdam, p. 195-204.

Yakushev, E.V., 2013, Chemical Structure of Pelagic Redox Interfaces: Observation and Modeling: Berlin Heidelberg, Springer-Verlag, p. 287.

APPENDIX A: CORE LOGS & LITHOFACIES DESCRIPTIONS

GRAPHIC LOGGING FORM SILICICLASTIC FACIES

DATE: August 2013 Page 1 of 1

STRAT. INTERVAL: Cape Caledonia Member - Roche Point Formation
WELL NAME: Collingwood K-33
LOCATION: Geological Survey of Canada - Calgary

COORDINATES: 300/K-33-7640-10830/0
LOGGED BY: Danielle Kondla
SLABBED: YES

K.B.: 53.9 m
DEPTH INTERVAL: Core 1: 1898.9-1917.2m (6.9m recovered)
DEVIATION: None

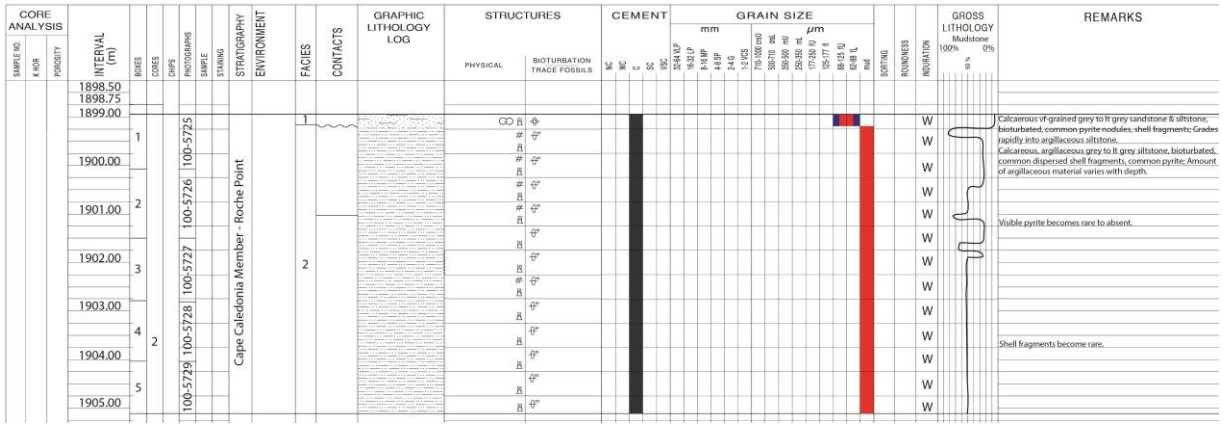

GRAPHIC LOGGING FORM SILICICLASTIC FACIES

DATE: August 2013 Page 1 of 1

STRAT. INTERVAL: Murray Harbour Formation WELL NAME: Skybattle Bay M-11 LOCATION: Geological Survey of Canada - Calgary

COORDINATES: 300/M-11-7720-10500/0 LOGGED BY: Danielle Kondla SLABBED: YES

K.B.: 19.7 m DEPTH INTERVAL: Core 3: 2520.0-2538.2m DEVIATION: None

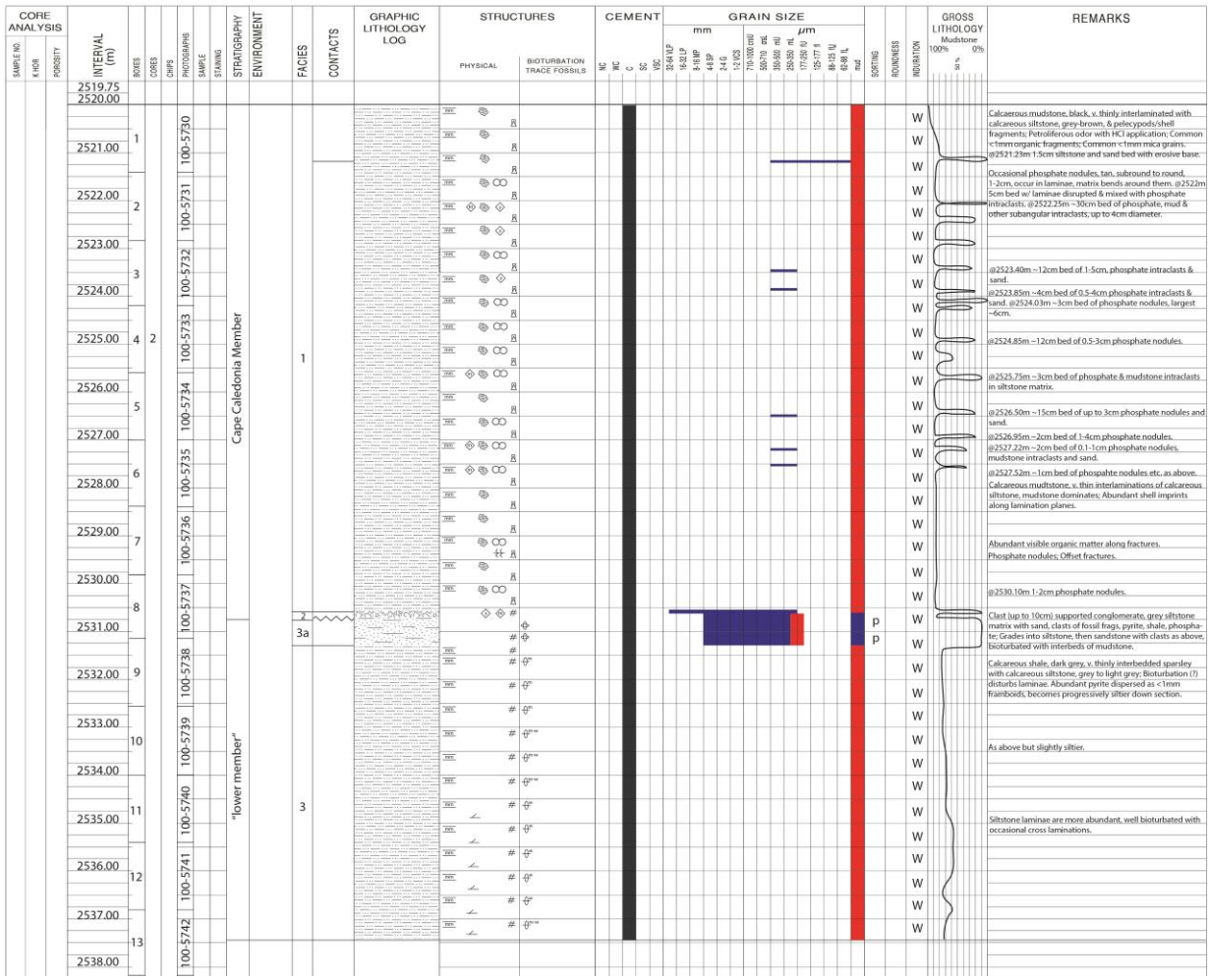

GRAPHIC LOGGING FORM SILICICLASTIC FACIES

DATE: August 2013 Page 1 of 1

STRAT. INTERVAL: "lower member" - Murray Harbour Formation WELL NAME: Pollux G-60 LOCATION: Geological Survey of Canada - Calgary

COORDINATES: 300/G-60-7910-10430/0 LOGGED BY: Danielle Kondla SLABBED: YES

K.B.: 59.7 m DEPTH INTERVAL: Core 2: 1371.6-1380.7m DEVIATION: None

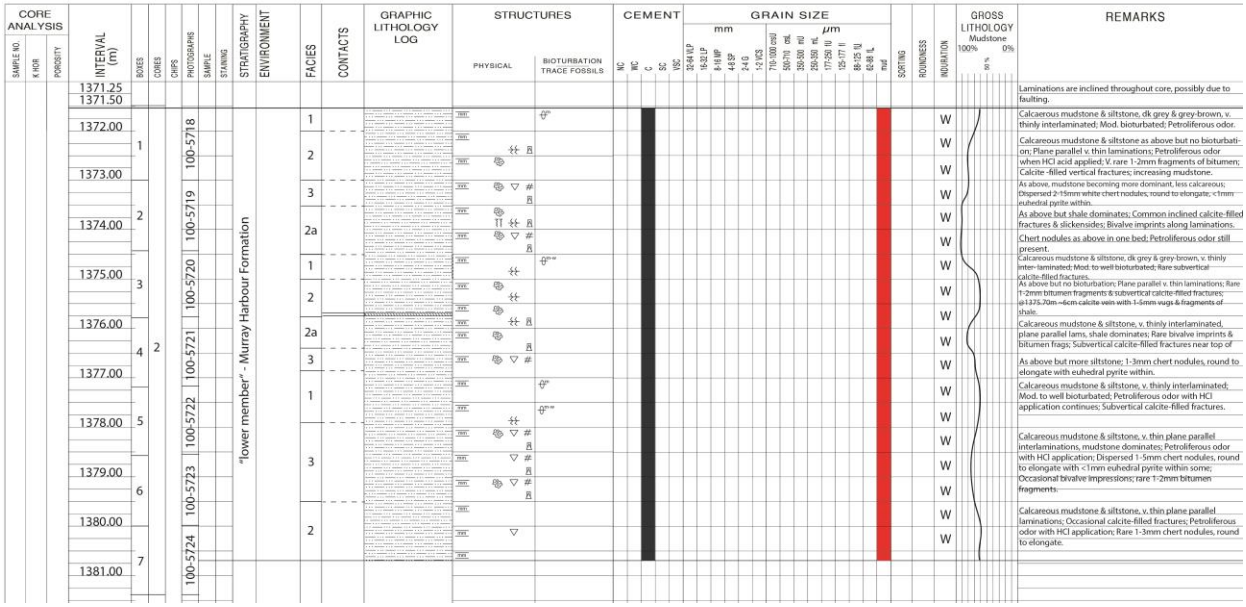

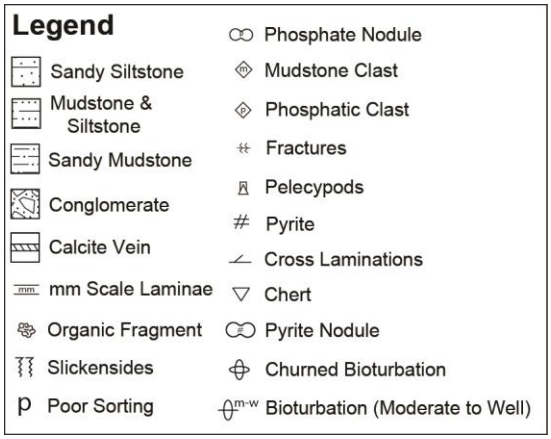

Collingwood K-33

Lithofacies	Lithofacies Description	Interpreted Depositional Setting
1	Calcareous grey to light grey siltstone and very fine-grained sandstone, churned bioturbation, common pyrite nodules and dispersed shell fragments	Marine inner-shelf
2	Calcareous, argillaceous, grey to light grey siltstone, moderately to well bioturbated, common to rare dispersed shell fragments and pyrite framboids	Marine mid-shelf

Skybattle Bay M-11

Lithofacies	Lithofacies Description	Interpreted Depositional Setting
1	Calcareous, black mudstone, very thinly interlaminated with calcareous grey-brown siltstone, occasional beds containing phosphate nodules, phosphate intraclasts, and mudstone clasts, common pelecypod fragments, micaceous grains, and organic fragments	Marine outer shelf to slope
2	Clast-supported conglomerate with grey siltstone and fine- to medium-grained sandstone matrix, clasts are up to 10 cm in length and composed of fossil fragments, pyrite, mudstone, and phosphate, poorly sorted, angular to rounded clasts	Marine mid- to outer shelf
3	Calcareous dark grey mudstone, very thinly interbedded with calcareous grey to light grey siltstone, moderately to well bioturbated, moderate to abundant dispersed pyrite framboids (<1 mm in diameter), some siltstone interbeds show cross laminations.	Marine inner to mid-shelf
3a	Calcareous, silty, fine- to lower medium-grained sandstone, well bioturbated, occasional clasts of fossil fragments, pyrite, mudstone, and phosphate	Marine inner to mid-shelf

Pollux G-60

Lithofacies	Lithofacies Description	Interpreted Depositional Setting
1	Calcareous dark grey mudstone, very thinly interlaminated with grey-brown siltstone, moderately to well bioturbated	Marine mid-shelf
2	Calcareous dark grey mudstone, very thinly interlaminated with grey-brown siltstone, very thin plane parallel laminations, rare 1-2 mm fragments of organic matter and pelecypod impressions	Marine outer shelf
2a	Calcareous dark grey mudstone, very thinly interlaminated with grey-brown siltstone, dark grey mudstone interlaminations dominate, very thin plane parallel laminations, rare 1-2 mm fragments of organic matter and pelecypod impressions	Marine outer shelf
3	Calcareous dark grey mudstone, very thinly interlaminated with grey-brown siltstone, dark grey mudstone interlaminations dominate, very thin plane parallel laminations, rare to occasional 1-2 mm fragments of organic matter and pelecypod impressions, dispersed white chert nodules, 1-15 mm in diameter, rounded to elongate in shape and often with euhedral pyrite crystals in the centre	Marine outer shelf

APPENDIX B: ROCK-EVAL 6 DATA – STANDARD CYCLE

Collingwood K-33

Sample Depth	S1	S2	S3	T_{max}	HI	OI	TOC	PC	RC	Mineral Carbon
m	mg HC/g rock	mg HC/g rock	mg CO_2/g rock	°C	mg HC/g TOC	mg CO_2/g TOC	wt.%	wt.%	wt.%	wt.%
1898.90	0.02	0.08	0.23	433	89	256	0.09	0.02	0.07	3.0
1899.18	0.14	2.24	0.29	432	315	41	0.71	0.21	0.50	2.8
1899.39	0.17	2.69	0.29	434	324	35	0.83	0.25	0.58	2.8
1899.60	0.06	1.08	0.24	433	251	56	0.43	0.11	0.32	2.7
1899.84	0.03	0.38	0.21	430	136	75	0.28	0.04	0.24	2.5
1900.04	0.07	1.03	0.24	435	264	62	0.39	0.10	0.29	3.3
1900.38	0.01	0.08	0.22	428	89	244	0.09	0.01	0.08	7.5
1900.66	0.06	0.80	0.22	434	205	56	0.39	0.08	0.31	4.4
1900.86	0.09	0.92	0.28	433	230	70	0.40	0.10	0.30	2.8
1901.10	0.04	0.70	0.24	435	189	65	0.37	0.07	0.30	3.3
1901.29	0.06	1.01	0.21	435	220	46	0.46	0.10	0.36	4.0
1901.51	0.05	0.46	0.20	432	170	74	0.27	0.05	0.22	3.4
1901.80	0.05	0.61	0.24	434	165	65	0.37	0.07	0.30	5.5
1902.05	0.07	1.14	0.24	436	243	51	0.47	0.11	0.36	6.0
1902.27	0.14	1.76	0.30	435	309	53	0.57	0.17	0.40	5.0
1902.45	0.10	1.62	0.26	435	275	44	0.59	0.16	0.43	4.5
1902.65	0.06	1.12	0.25	434	233	52	0.48	0.11	0.37	3.0
1902.91	0.11	1.60	0.28	433	271	47	0.59	0.16	0.43	3.8
1903.14	0.05	0.78	0.24	434	205	63	0.38	0.08	0.30	3.2
1903.41	0.09	1.04	0.29	434	208	58	0.50	0.11	0.39	3.1
1903.59	0.05	0.96	0.26	435	204	55	0.47	0.10	0.37	3.1
1903.89	0.10	1.81	0.28	436	278	43	0.65	0.17	0.48	3.6
1904.09	0.09	1.17	0.28	435	244	58	0.48	0.12	0.36	3.2
1904.33	0.08	1.30	0.25	435	245	47	0.53	0.13	0.40	3.4
1904.52	0.14	2.15	0.34	435	291	46	0.74	0.21	0.53	3.8
1904.79	0.10	1.37	0.38	433	249	69	0.55	0.14	0.41	3.3
1904.98	0.06	1.06	0.25	435	230	54	0.46	0.11	0.35	4.0
1905.21	0.15	1.84	0.33	436	302	54	0.61	0.18	0.43	3.4

Skybattle Bay M-11 (Upper)

Sample Depth	S1	S2	S3	T_{max}	HI	OI	TOC	PC	RC	Mineral Carbon
m	mg HC/g rock	mg HC/g rock	mg CO_2/g rock	°C	mg HC/g TOC	mg CO_2/g TOC	wt.%	wt.%	wt.%	wt.%
2520.20	1.44	6.79	0.35	444	212	11	3.20	0.70	2.50	3.8
2520.45	0.80	3.30	0.26	440	216	17	1.53	0.35	1.18	7.1
2520.66	1.24	6.16	0.36	441	198	12	3.11	0.64	2.47	4.9
2520.87	1.53	6.68	0.35	435	151	8	4.43	0.70	3.73	2.5
2521.11	1.30	8.66	0.40	442	199	9	4.36	0.85	3.51	3.1
2521.32	1.72	6.75	0.46	448	159	11	4.24	0.73	3.51	3.3
2521.62	0.79	5.13	0.36	444	174	12	2.94	0.51	2.43	3.5
2521.85	0.75	5.75	0.36	445	180	11	3.19	0.56	2.63	4.1
2522.07	0.67	3.47	0.33	434	213	20	1.63	0.36	1.27	4.3
2522.28	0.85	7.72	0.40	448	161	8	4.79	0.74	4.05	3.8
2522.49	0.55	2.37	0.38	437	160	26	1.48	0.26	1.22	5.8
2522.72	1.04	7.01	0.51	449	160	12	4.37	0.70	3.67	3.7
2522.95	0.73	4.95	0.61	446	155	19	3.20	0.50	2.70	4.5
2523.15	0.42	6.98	0.36	446	212	11	3.30	0.64	2.66	3.9
2523.45	0.39	5.38	0.34	443	231	15	2.33	0.50	1.83	4.2
2523.65	0.69	4.50	0.48	448	151	16	2.98	0.46	2.52	4.1
2523.87	0.57	5.97	0.36	444	175	11	3.41	0.57	2.84	3.7
2524.13	0.90	7.82	0.42	446	169	9	4.62	0.75	3.87	3.2
2524.33	1.47	3.96	0.42	440	188	20	2.11	0.47	1.64	3.0
2524.53	0.44	7.91	0.34	447	233	10	3.40	0.71	2.69	4.0
2524.71	0.38	4.69	0.37	443	200	16	2.34	0.44	1.90	4.7
2524.91	0.54	4.83	0.32	438	187	12	2.58	0.46	2.12	3.4
2525.11	0.86	7.63	0.40	447	178	9	4.29	0.73	3.56	3.6
2525.31	0.39	4.35	0.28	445	190	12	2.29	0.41	1.88	3.8
2525.51	0.54	6.53	0.37	443	196	11	3.33	0.61	2.72	3.4
2525.71	0.51	6.33	0.38	444	195	12	3.25	0.59	2.66	3.7
2525.86	0.90	4.73	0.49	445	178	18	2.65	0.49	2.16	4.0
2526.06	0.55	6.11	0.41	447	178	12	3.43	0.57	2.86	3.8
2526.26	0.71	5.43	0.37	440	224	15	2.42	0.53	1.89	3.5
2526.46	0.49	3.91	0.34	443	179	16	2.18	0.38	1.80	3.7
2526.66	1.01	7.18	0.42	444	180	11	4.00	0.71	3.29	3.9
2526.86	0.68	6.28	0.36	444	192	11	3.27	0.60	2.67	4.0
2527.06	0.64	4.13	0.32	441	203	16	2.03	0.41	1.62	3.8
2527.26	3.50	12.46	0.36	425	542	16	2.30	1.34	0.96	4.0
2527.44	0.73	4.02	0.35	439	210	18	1.91	0.41	1.50	4.2
2527.67	0.53	3.00	0.38	436	188	24	1.60	0.31	1.29	4.1
2527.88	0.81	6.34	0.38	443	206	12	3.08	0.62	2.46	3.5
2528.13	0.90	6.83	0.35	443	199	10	3.43	0.66	2.77	3.9
2528.33	1.04	7.88	0.39	443	204	10	3.87	0.76	3.11	3.8
2528.53	0.94	7.18	0.36	443	217	11	3.31	0.69	2.62	3.4
2528.72	0.90	6.58	0.39	441	214	13	3.08	0.64	2.44	3.2
2528.91	0.88	5.73	0.35	442	208	13	2.76	0.57	2.19	3.5
2529.11	0.71	4.85	0.29	441	207	12	2.34	0.48	1.86	4.9
2529.31	0.59	3.66	0.31	438	207	18	1.77	0.37	1.40	5.5
2529.51	0.95	6.36	0.36	445	168	9	3.79	0.63	3.16	4.9
2529.71	2.73	13.73	0.46	433	322	11	4.26	1.39	2.87	4.2
2529.90	1.34	9.70	0.44	443	201	9	4.82	0.94	3.88	4.4
2530.09	0.87	5.76	0.39	440	189	13	3.04	0.57	2.47	4.0
2530.29	0.83	7.27	0.42	443	182	11	3.99	0.70	3.29	3.6
2530.49	0.94	8.76	0.41	445	184	9	4.75	0.83	3.92	3.2
2530.69	0.76	7.43	0.42	447	167	9	4.46	0.70	3.76	3.3

Skybattle Bay M-11 (Lower)

Sample Depth	S1	S2	S3	T_{max}	HI	OI	TOC	PC	RC	Mineral Carbon
m	mg HC/g rock	mg HC/g rock	mg CO_2/g rock	°C	mg HC/g TOC	mg CO_2/g TOC	wt.%	wt.%	wt.%	wt.%
2530.96	0.09	0.37	0.25	434	106	71	0.35	0.05	0.30	4.2
2531.17	0.05	0.20	0.35	442	91	159	0.22	0.03	0.19	4.3
2531.37	0.10	0.37	0.44	437	70	83	0.53	0.05	0.48	5.5
2531.64	0.13	0.47	0.39	437	71	59	0.66	0.06	0.60	4.2
2531.86	0.12	0.46	0.42	438	68	62	0.68	0.06	0.62	4.0
2532.09	0.16	0.62	0.40	441	71	46	0.87	0.08	0.79	3.2
2532.31	0.12	0.43	0.41	439	64	61	0.67	0.06	0.61	3.4
2532.54	0.23	0.73	0.42	438	81	47	0.90	0.10	0.80	3.2
2532.82	0.10	0.38	0.34	438	66	59	0.58	0.05	0.53	2.3
2533.02	0.09	0.40	0.37	440	69	64	0.58	0.05	0.53	2.8
2533.22	0.08	0.29	0.42	438	56	81	0.52	0.05	0.47	3.0
2533.42	0.11	0.52	0.38	439	79	58	0.66	0.07	0.59	2.1
2533.70	0.06	0.28	0.40	437	54	77	0.52	0.04	0.48	2.8
2533.90	0.10	0.38	0.38	438	78	78	0.49	0.05	0.44	3.0
2534.10	0.12	0.39	0.36	437	74	68	0.53	0.05	0.48	2.8
2534.29	0.11	0.44	0.43	437	69	67	0.64	0.06	0.58	2.4
2534.56	0.10	0.41	0.37	439	68	62	0.60	0.06	0.54	2.6
2534.73	0.09	0.40	0.35	438	69	60	0.58	0.05	0.53	2.9
2534.95	0.11	0.46	0.37	438	74	60	0.62	0.06	0.56	2.6
2535.18	0.12	0.47	0.34	440	80	58	0.59	0.06	0.53	2.4
2535.38	0.20	0.76	0.33	445	95	41	0.80	0.09	0.71	1.9
2535.55	0.14	0.55	0.33	439	85	51	0.65	0.07	0.58	2.0
2535.81	0.20	0.94	0.38	443	101	41	0.93	0.11	0.82	1.7
2536.08	0.17	0.59	0.29	437	97	48	0.61	0.07	0.54	2.0
2536.28	0.16	0.67	0.32	438	92	44	0.73	0.08	0.65	1.8
2536.56	0.13	0.60	0.34	440	85	48	0.71	0.07	0.64	1.8
2536.72	0.17	0.73	0.35	439	89	43	0.82	0.09	0.73	1.6
2536.95	0.21	0.90	0.30	440	110	37	0.82	0.11	0.71	1.6
2537.15	0.13	0.53	0.35	441	82	54	0.65	0.07	0.58	1.9
2537.37	0.07	0.24	0.36	438	51	77	0.47	0.04	0.43	1.6

Pollux G-60

Sample Depth	S1	S2	S3	T_{max}	HI	OI	TOC	PC	RC	Mineral Carbon
m	mg HC/g rock	mg HC/g rock	mg CO_2/g rock	°C	mg HC/g TOC	mg CO_2/g TOC	wt.%	wt.%	wt.%	wt.%
1371.80	0.33	2.27	0.28	439	324	7	0.70	0.23	0.47	4.9
1372.07	0.55	5.17	0.35	441	407	7	1.27	0.49	0.78	4.0
1372.28	0.45	5.34	0.29	441	402	5	1.33	0.50	0.83	3.5
1372.50	0.56	9.03	0.29	442	434	5	2.08	0.81	1.27	3.0
1372.70	0.57	8.63	0.21	442	440	3	1.96	0.78	1.18	4.0
1372.90	0.54	9.10	0.25	441	448	3	2.03	0.81	1.22	3.8
1373.11	0.68	13.43	0.30	441	460	4	2.92	1.19	1.73	2.7
1373.32	0.76	17.51	0.27	440	492	4	3.56	1.54	2.02	2.4
1373.53	0.69	15.95	0.30	441	473	4	3.37	1.40	1.97	2.4
1373.67	0.81	14.86	0.27	443	479	4	3.10	1.32	1.78	1.6
1373.86	0.73	10.21	0.29	442	454	6	2.25	0.93	1.32	1.7
1374.07	0.57	7.72	0.22	441	427	4	1.81	0.70	1.11	1.8
1374.27	0.60	7.68	0.27	440	457	8	1.68	0.70	0.98	2.7
1374.51	0.17	1.85	0.19	438	325	5	0.57	0.18	0.39	3.8
1374.74	0.11	1.08	0.23	437	277	5	0.39	0.11	0.28	5.8
1375.02	0.13	1.18	0.22	437	288	7	0.41	0.12	0.29	4.1
1375.22	0.18	1.91	0.25	440	313	5	0.61	0.18	0.43	4.2
1375.45	0.46	4.24	0.28	440	396	6	1.07	0.40	0.67	3.6
1375.76	0.89	11.50	0.32	442	442	5	2.60	1.05	1.55	1.6
1375.86	0.89	10.88	0.27	443	442	6	2.46	0.99	1.47	1.7
1376.08	1.17	8.57	0.43	439	463	4	1.85	0.83	1.02	1.5
1376.31	0.73	6.46	0.31	441	411	8	1.57	0.61	0.96	1.7
1376.55	0.35	2.19	0.20	438	348	5	0.63	0.22	0.41	3.4
1376.75	0.19	1.70	0.27	439	293	5	0.58	0.17	0.41	3.3
1376.97	0.17	1.01	0.25	439	266	11	0.38	0.11	0.27	4.3
1377.50	0.12	0.80	0.26	439	235	6	0.34	0.09	0.25	8.0
1377.69	0.06	0.47	0.30	440	196	21	0.24	0.06	0.18	8.4
1377.97	0.27	1.93	0.42	440	306	11	0.63	0.20	0.43	5.9
1378.21	0.45	4.26	0.34	441	377	6	1.13	0.41	0.72	2.5
1378.48	0.62	7.12	0.27	441	426	5	1.67	0.66	1.01	1.9
1378.72	0.65	6.89	0.23	441	428	6	1.61	0.64	0.97	1.9
1378.95	0.70	8.29	0.19	442	451	4	1.84	0.76	1.08	1.8
1379.16	0.66	7.57	0.24	441	435	6	1.74	0.70	1.04	1.8
1379.37	0.67	7.62	0.19	441	443	6	1.72	0.70	1.02	1.7
1379.58	0.47	6.00	0.26	439	414	9	1.45	0.55	0.90	1.8
1379.78	0.52	5.76	0.22	440	420	6	1.37	0.53	0.84	2.3
1379.88	0.36	3.04	0.25	439	366	6	0.83	0.29	0.54	3.4
1380.18	0.31	2.98	0.25	441	359	6	0.83	0.29	0.54	3.9
1380.38	0.44	2.65	0.36	439	363	5	0.73	0.27	0.46	4.3
1380.59	0.32	3.05	0.28	439	363	7	0.84	0.29	0.55	4.7
1380.70	0.27	2.06	0.27	441	327	8	0.63	0.21	0.42	3.3

APPENDIX C: ADDITIONAL ONLINE THERMAL DESORPTION- GAS CHROMATOGRAPHY-FLAME IONIZATION DETECTION (TD-GC-FID) ANALYSES

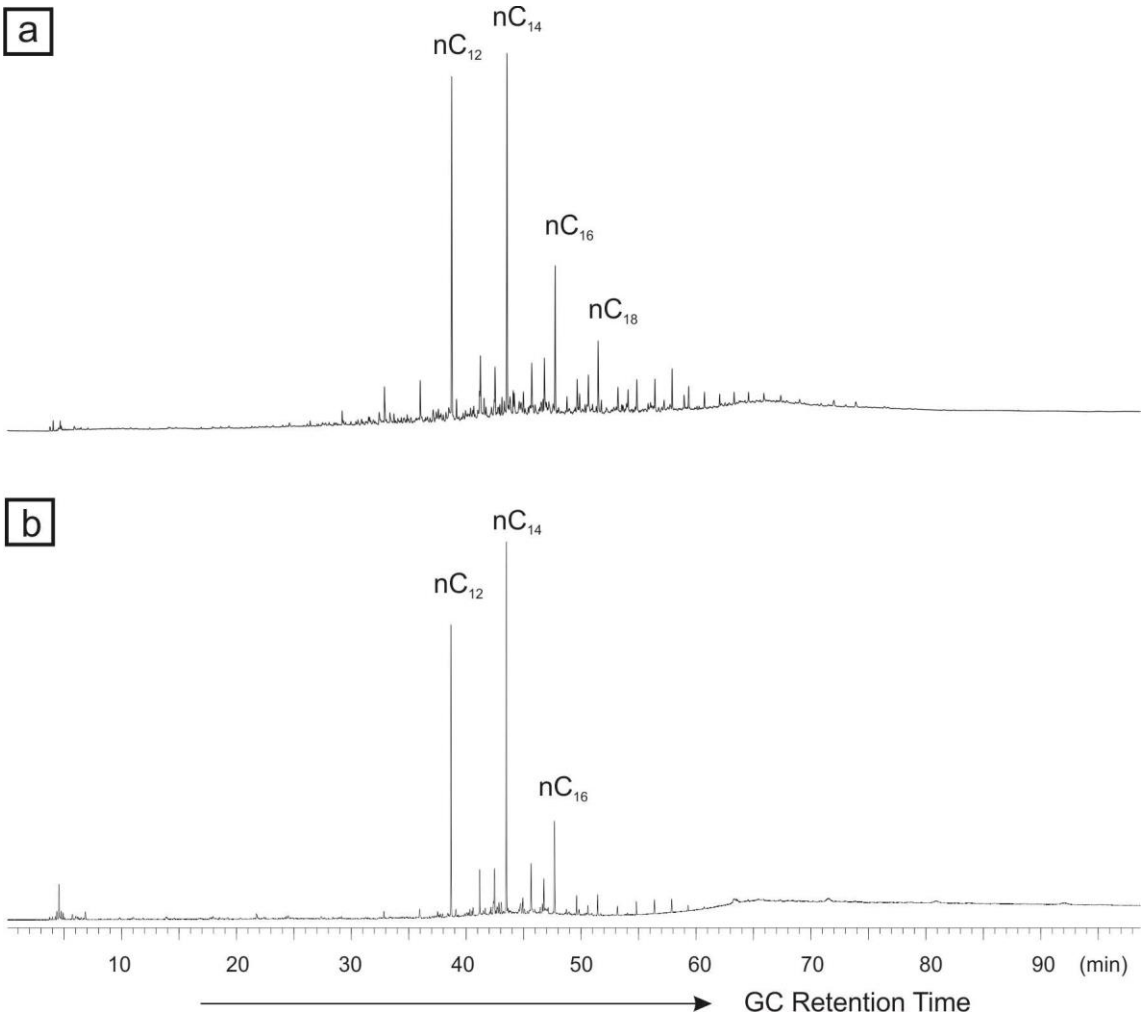

a) TD-GC-FID trace of Skybattle Bay M-11 sample 2525.51 m, organic rich, no front shoulder on S2 peak of standard Rock-Eval cycle pyrogram; b) TD-GC-FID trace of Skybattle Bay M-11 sample 2533.42 m, organic lean.

APPENDIX D: INDUCTIVELY COUPLED PLASMA-MASS SPECTROMETRY DATA

Collingwood K-33

Sample Depth	Mo	Cu	Pb	Zn	Ag	Ni	Co	Mn	Fe	As	U	Th	Sr	Cd	Sb	Bi
m	PPM	PPM	PPM	PPM	PPB	PPM	PPM	PPM	%	PPM	PPM	PPM	PPM	PPM	PPM	PPM
1898.90	0.74	2.69	11.88	17.6	75	4.8	1.20	79	0.45	2.3	1.6	3.3	195	0.17	0.26	0.71
1899.18	11.39	20.16	10.55	43.7	194	36.7	7.50	90	2.47	20.5	5.8	9.7	289	0.39	0.89	0.54
1899.39	6.84	19.80	9.37	36.8	134	32.7	7.20	98	2.07	17.4	5.1	8.6	263	0.29	0.66	0.14
1899.60	2.77	16.29	10.90	55.9	143	28.6	8.50	107	1.61	9.4	4.2	9.7	256	0.29	0.49	0.50
1899.84	3.23	20.31	12.82	54.7	142	37.4	10.20	118	3.28	20.4	3.0	9.1	245	0.27	0.65	0.14
1900.04	2.24	11.41	7.38	41.7	105	21.8	5.10	110	1.18	10.2	2.6	7.0	249	0.33	0.49	0.11
1900.38	0.94	4.26	4.33	18.5	75	7.2	1.80	147	0.53	6.8	4.0	4.1	313	0.15	0.18	0.08
1900.66	7.97	12.56	7.83	24.0	97	25.8	4.30	117	1.71	17.0	3.7	6.7	332	0.34	0.54	0.06
1900.86	3.96	17.38	11.93	43.8	153	30.6	9.30	117	1.62	13.8	4.5	9.6	280	0.22	0.68	0.13
1901.10	3.20	13.60	8.86	46.4	83	25.9	7.40	117	2.10	11.1	3.1	7.6	254	0.32	0.56	0.11
1901.29	3.45	14.02	8.99	48.3	111	25.7	6.50	135	1.41	6.7	3.3	7.0	285	0.38	0.45	0.26
1901.51	2.17	13.56	10.14	34.9	103	23.3	6.60	130	1.39	11.7	4.0	8.5	245	0.22	0.58	0.17
1901.80	9.58	26.09	7.74	96.0	173	28.3	5.90	141	1.78	18.5	3.3	6.5	360	0.79	0.80	0.14
1902.05	2.84	13.78	7.29	36.2	115	21.7	5.70	166	1.31	10.3	4.6	6.5	283	0.21	0.38	0.28
1902.27	2.61	13.41	6.52	49.2	129	22.1	4.70	142	1.31	7.6	3.9	6.8	309	0.34	0.46	0.02
1902.45	2.90	14.39	7.80	37.8	116	26.3	5.80	133	1.67	16.3	3.9	7.1	277	0.23	0.46	0.16
1902.65	1.98	19.34	12.69	47.0	161	39.6	9.70	144	2.22	7.6	4.0	8.8	246	0.21	0.65	0.11
1902.91	3.64	11.49	6.48	44.7	102	21.4	4.30	145	1.26	6.0	2.9	7.1	239	0.25	0.43	0.08
1903.14	0.75	16.47	11.88	42.6	102	30.0	7.90	142	1.88	13.9	4.1	9.1	247	0.19	0.51	0.11
1903.41	1.21	17.97	11.79	76.7	128	33.2	8.20	161	1.97	14.5	3.9	9.5	246	0.36	0.70	0.20
1903.59	1.81	15.05	10.66	35.4	114	26.5	8.90	148	1.72	12.3	3.5	9.0	233	0.22	0.75	0.26
1903.89	2.16	15.79	8.23	52.6	123	33.4	7.70	148	1.92	18.7	3.2	7.7	263	0.32	0.61	0.16
1904.09	2.16	15.46	9.98	56.6	140	28.1	7.00	151	1.73	11.7	3.3	8.4	222	0.23	0.84	0.30
1904.33	2.25	17.93	9.94	41.9	103	31.6	6.90	151	1.83	13.2	3.3	9.0	239	0.26	0.58	0.37
1904.52	2.30	18.35	8.17	62.5	120	32.3	6.40	160	1.70	13.1	3.8	8.1	252	0.25	0.56	0.25
1904.79	2.17	17.01	10.25	31.5	116	30.7	7.50	159	1.87	13.6	3.0	8.8	254	0.21	0.53	0.25
1904.98	1.97	13.97	9.32	35.4	111	27.0	6.80	154	1.63	10.6	3.0	8.3	251	0.19	0.53	0.13
1905.21	2.25	17.86	10.71	42.1	108	34.3	8.00	165	1.79	7.8	3.4	9.1	253	0.22	0.69	0.21

Collingwood K-33

Sample Depth	V	Ca	P	La	Cr	Mg	Ba	Ti	Al	Na	K	W	Zr	Sn	Be	Sc
m	PPM	%	%	PPM	PPM	%	PPM	%	%	%	%	PPM	PPM	PPM	PPM	PPM
1898.90	21	9.15	0.08	14.4	17	0.29	104	0.08	1.05	0.22	0.33	0.3	34.5	0.2	0.5	1.7
1899.18	80	7.47	0.11	31.6	86	1.17	187	0.25	3.58	0.44	1.46	0.8	88.1	1.4	0.5	7.2
1899.39	79	7.01	0.08	28.7	91	1.35	222	0.26	3.39	0.44	1.33	0.7	74.3	1.1	1.0	7.5
1899.60	98	6.90	0.05	29.6	72	1.43	255	0.28	4.47	0.48	1.91	0.8	87.4	1.6	2.0	9.4
1899.84	83	6.64	0.04	27.1	58	1.35	144	0.26	3.92	0.44	1.74	0.7	81.4	1.2	1.0	8.0
1900.04	55	8.93	0.05	24.3	44	1.07	203	0.19	2.61	0.38	1.20	0.5	61.5	0.8	0.5	5.4
1900.38	31	21.63	0.04	17.5	27	0.71	109	0.11	1.51	0.23	0.60	0.3	44.8	0.4	0.5	3.1
1900.66	57	12.18	0.06	24.8	53	1.04	187	0.18	2.40	0.37	1.01	0.5	64.8	0.7	0.5	5.3
1900.86	107	7.16	0.05	28.9	82	1.38	265	0.28	4.56	0.49	1.84	0.8	92.9	1.5	1.0	9.5
1901.10	69	9.16	0.05	26.1	58	1.01	221	0.20	3.15	0.42	1.37	0.6	74.4	1.0	0.5	7.4
1901.29	63	11.28	0.07	25.8	55	1.06	194	0.19	2.78	0.39	1.31	0.6	73.0	0.8	0.5	6.1
1901.51	91	9.00	0.05	26.4	58	1.33	221	0.25	3.66	0.45	1.62	0.6	80.6	1.1	1.0	7.2
1901.80	55	14.86	0.07	22.7	58	0.99	167	0.16	2.26	0.35	0.97	0.5	65.9	0.8	0.5	5.3
1902.05	65	15.71	0.07	27.4	61	1.31	193	0.20	3.08	0.37	1.27	0.5	67.9	0.8	1.0	6.8
1902.27	60	13.47	0.06	25.4	57	1.14	179	0.19	2.81	0.37	1.11	0.5	70.8	0.8	1.0	6.2
1902.45	65	11.69	0.06	25.1	64	1.14	190	0.20	3.00	0.41	1.38	0.6	72.1	0.9	1.0	7.0
1902.65	95	7.14	0.05	28.1	66	1.48	250	0.27	4.81	0.50	2.01	0.7	79.8	1.5	2.0	9.5
1902.91	56	9.96	0.05	24.9	50	1.14	192	0.20	2.72	0.44	1.22	0.6	76.1	0.8	0.5	5.6
1903.14	87	8.00	0.04	28.8	62	1.48	241	0.26	4.45	0.49	1.90	0.7	85.7	1.3	1.0	8.6
1903.41	90	7.18	0.06	32.2	72	1.57	260	0.28	4.50	0.52	1.88	0.8	91.7	1.4	1.0	9.8
1903.59	96	7.63	0.04	27.5	68	1.40	263	0.25	4.18	0.48	1.78	0.7	83.8	1.3	1.0	7.6
1903.89	69	9.05	0.05	27.5	75	1.31	220	0.22	3.34	0.44	1.52	0.6	73.1	1.0	0.5	7.0
1904.09	87	8.23	0.04	26.9	67	1.37	248	0.24	3.85	0.48	1.79	0.7	83.8	1.2	2.0	7.8
1904.33	87	7.98	0.05	28.4	73	1.46	268	0.24	4.04	0.50	1.76	0.8	87.0	1.3	1.0	9.0
1904.52	74	9.45	0.08	30.9	65	1.45	234	0.22	3.59	0.44	1.61	0.6	76.1	1.1	1.0	8.0
1904.79	85	8.16	0.05	28.5	70	1.47	248	0.26	4.19	0.45	1.68	0.7	86.7	1.4	2.0	7.9
1904.98	77	10.11	0.05	26.6	58	1.34	230	0.23	3.69	0.47	1.63	0.7	82.3	1.1	1.0	7.4
1905.21	84	8.60	0.06	27.7	71	1.50	266	0.26	4.19	0.50	1.83	0.8	87.0	1.4	1.0	8.1

Collingwood K-33

Sample Depth	S	Y	Ce	Pr	Nd	Sm	Eu	Gd	Tb	Dy	Ho	Er	Tm	Yb	Lu	Hf
m	%	PPM	PPM	PPM	PPM	PPM	PPM	PPM	PPM	PPM	PPM	PPM	PPM	PPM	PPM	PPM
1898.90	0.35	15.4	25.94	3.6	15.6	2.8	0.6	2.5	0.4	2.4	0.5	1.3	0.2	1.1	0.1	1.1
1899.18	2.51	21.8	57.51	8.0	31.8	5.7	1.1	4.4	0.7	4.1	0.7	2.3	0.3	1.9	0.3	2.7
1899.39	1.94	21.2	46.85	6.7	27.9	4.8	0.9	3.9	0.7	3.6	0.7	2.1	0.3	2.1	0.3	2.4
1899.60	1.10	15.4	55.71	6.9	25.6	5.1	1.0	3.4	0.5	3.4	0.6	1.8	0.4	1.9	0.2	2.7
1899.84	3.17	16.3	51.35	6.5	26.5	4.9	0.9	3.9	0.6	3.4	0.5	1.7	0.3	1.8	0.3	2.6
1900.04	0.93	15.5	42.83	5.8	23.6	4.1	0.9	3.9	0.5	3.0	0.5	1.6	0.2	1.6	0.2	1.9
1900.38	0.28	14.4	25.59	4.0	16.1	3.0	0.6	2.6	0.4	2.6	0.5	1.2	0.2	1.1	0.1	1.2
1900.66	1.56	17.9	41.62	5.8	23.3	4.5	1.0	3.8	1.1	3.2	0.7	1.7	0.2	1.6	0.2	1.9
1900.86	1.04	17.7	54.34	6.9	26.8	5.2	0.8	3.8	0.5	3.5	0.7	2.0	0.3	1.9	0.3	2.7
1901.10	1.90	18.9	50.31	6.3	26.2	4.5	0.9	3.6	0.6	3.4	0.6	1.8	0.2	1.7	0.2	2.3
1901.29	1.10	22.4	46.41	6.3	26.2	4.9	1.1	4.2	0.7	3.9	0.7	2.1	0.3	1.8	0.3	1.9
1901.51	0.85	16.4	48.33	6.3	23.3	4.3	0.8	3.7	0.5	3.3	0.6	1.8	0.3	1.6	0.3	2.2
1901.80	1.62	20.2	39.66	5.8	23.5	4.5	0.9	4.3	0.6	3.3	0.6	1.8	0.2	1.6	0.2	1.9
1902.05	0.82	21.2	42.11	6.0	23.1	4.5	1.1	3.9	0.7	3.5	0.6	1.9	0.3	1.9	0.3	2.0
1902.27	0.94	19.2	43.10	5.9	25.6	4.7	0.9	3.3	0.6	4.9	0.6	1.8	0.3	1.9	0.2	1.9
1902.45	1.33	18.8	43.85	6.3	25.0	4.7	0.9	3.5	0.5	3.9	0.6	1.8	0.3	1.6	0.2	2.0
1902.65	1.56	17.7	55.76	7.1	27.2	5.3	1.0	4.0	0.6	3.4	0.7	1.8	0.3	1.9	0.3	2.3
1902.91	0.90	19.1	46.76	5.9	24.3	4.3	0.9	4.3	0.6	3.5	0.7	1.8	0.3	1.7	0.3	2.0
1903.14	1.24	18.5	55.12	7.1	26.1	4.6	0.9	4.0	0.6	3.6	0.6	1.8	0.3	1.7	0.3	2.5
1903.41	1.29	21.4	62.49	8.1	30.4	5.5	1.1	4.3	0.6	4.1	0.8	2.3	0.3	2.0	0.3	2.6
1903.59	1.09	17.8	51.04	6.6	26.0	5.1	1.0	3.8	0.6	3.6	0.6	1.9	0.3	1.8	0.2	2.3
1903.89	1.52	19.9	49.24	6.8	26.9	5.7	1.1	4.6	0.6	3.7	0.7	1.7	0.2	1.6	0.3	2.3
1904.09	1.20	17.8	52.30	6.6	25.7	4.8	1.0	3.8	0.6	3.2	0.7	1.9	0.3	1.8	0.3	2.3
1904.33	1.24	18.7	53.60	6.9	27.6	4.8	1.0	3.8	0.5	3.6	0.6	1.8	0.3	1.9	0.3	2.5
1904.52	1.20	24.7	52.74	7.6	30.9	5.2	1.2	5.0	0.7	4.3	0.8	2.1	0.3	2.3	0.3	2.3
1904.79	1.26	19.0	50.98	6.5	26.0	4.9	0.9	4.0	0.5	3.5	0.7	2.2	0.3	1.7	0.3	2.4
1904.98	1.12	18.5	50.56	6.4	26.1	4.9	0.9	3.7	0.6	3.1	0.6	2.0	0.3	1.7	0.2	2.3
1905.21	1.15	20.8	55.44	7.4	29.3	5.3	1.0	4.2	0.6	3.6	0.7	2.2	0.3	2.0	0.3	2.4

Collingwood K-33

Sample Depth	Li	Rb	Ta	Nb	Cs	Ga	In	Re	Se	Te	Tl
m	PPM	PPM	PPM	PPM	PPM	PPM	PPM	PPM	PPM	PPM	PPM
1898.90	16.4	12.9	0.1	1.92	0.6	1.90	0.01	0.01	0.15	2.48	0.11
1899.18	23.0	65.0	0.5	6.43	2.8	7.43	0.02	0.06	1.60	1.36	0.51
1899.39	23.7	69.6	0.5	6.58	3.1	8.86	0.02	0.03	1.60	1.84	0.50
1899.60	26.5	88.7	0.6	6.85	4.7	10.39	0.02	0.01	0.15	1.45	0.47
1899.84	23.2	79.0	0.5	6.52	3.9	9.62	0.02	0.01	1.30	1.30	0.53
1900.04	20.5	48.9	0.4	4.86	2.3	6.43	0.01	0.03	0.50	0.99	0.33
1900.38	10.7	27.5	0.2	3.20	1.3	3.48	0.01	0.02	0.15	3.47	0.15
1900.66	17.8	44.9	0.3	4.90	2.3	5.90	0.01	0.05	1.20	2.17	0.44
1900.86	25.1	91.8	0.6	7.23	5.2	11.25	0.04	0.01	0.70	1.84	0.53
1901.10	18.9	66.9	0.4	5.29	3.1	7.53	0.02	0.02	1.50	1.39	0.42
1901.29	18.4	58.8	0.4	5.25	2.9	6.71	0.02	0.02	1.50	1.34	0.39
1901.51	22.1	77.6	0.4	6.86	3.8	9.10	0.02	0.01	0.30	1.50	0.40
1901.80	14.8	43.3	0.3	4.49	2.2	5.41	0.01	0.04	3.60	3.41	0.62
1902.05	16.8	58.2	0.4	5.17	3.0	7.10	0.01	0.01	0.60	2.39	0.33
1902.27	16.9	53.0	0.4	4.90	2.6	6.61	0.02	0.03	1.10	2.31	0.32
1902.45	17.9	61.5	0.4	5.24	2.9	7.22	0.01	0.01	1.10	1.83	0.36
1902.65	24.6	92.1	0.5	6.69	4.9	11.62	0.02	0.01	1.20	0.79	0.48
1902.91	17.1	57.4	0.4	5.37	2.6	6.31	0.01	0.02	0.90	2.29	0.35
1903.14	24.0	90.7	0.5	6.54	4.5	11.52	0.05	0.00	0.80	1.12	0.46
1903.41	25.9	94.1	0.6	7.68	4.6	11.02	0.03	0.01	1.30	1.68	0.50
1903.59	21.8	82.5	0.5	6.74	4.2	10.29	0.02	0.03	1.20	2.15	0.45
1903.89	19.3	65.3	0.4	5.64	3.1	8.21	0.03	0.02	1.20	1.33	0.42
1904.09	21.5	80.5	0.5	6.26	3.7	9.75	0.03	0.02	1.10	1.70	0.43
1904.33	20.4	89.0	0.5	6.90	4.2	11.01	0.03	0.01	1.30	1.16	0.47
1904.52	18.3	72.0	0.5	5.94	3.5	8.43	0.04	0.02	1.40	1.52	0.40
1904.79	21.6	84.0	0.5	6.85	4.0	9.82	0.03	0.01	0.60	1.30	0.48
1904.98	20.9	74.8	0.4	6.36	3.8	9.40	0.03	0.01	0.70	1.99	0.43
1905.21	22.4	86.1	0.6	7.35	4.3	10.41	0.03	0.01	1.10	1.79	0.46

Skybattle Bay M-11 (Upper)

Sample Depth	Mo	Cu	Pb	Zn	Ag	Ni	Co	Mn	Fe	As	U	Th	Sr	Cd	Sb	Bi
m	PPM	PPM	PPM	PPM	PPB	PPM	PPM	PPM	%	PPM	PPM	PPM	PPM	PPM	PPM	PPM
2520.20	4.91	38.53	9.49	88.9	184	64.3	8.20	184	1.83	10.5	4.9	8.9	478	0.47	2.07	0.16
2520.45	4.79	22.73	5.55	38.3	146	31.7	4.60	220	1.14	5.7	3.5	5.2	554	0.26	0.99	0.07
2520.66	21.68	50.06	9.43	62.1	517	66.2	9.20	176	1.98	13.7	9.1	7.3	440	1.29	1.93	0.19
2520.87	216.80	76.90	31.84	399.1	1461	452.5	43.00	147	5.00	63.9	18.7	7.7	231	12.69	11.54	0.87
2521.11	12.47	51.94	10.07	187.7	609	88.8	7.70	153	1.75	5.9	18.2	8.3	554	4.11	3.02	0.73
2521.32	11.73	52.15	10.60	95.6	400	85.4	9.70	177	2.06	9.1	9.9	9.2	429	1.15	3.12	0.40
2521.62	5.81	45.74	10.83	120.3	168	76.9	10.70	194	2.19	11.7	4.5	9.2	387	0.38	2.04	0.21
2521.85	3.58	47.40	8.92	133.6	191	67.4	7.30	175	1.72	8.1	5.9	8.4	499	0.42	1.68	0.13
2522.07	7.50	28.67	8.39	96.4	108	47.6	5.10	159	2.43	23.2	5.0	6.3	487	0.32	1.22	0.18
2522.28	4.72	62.74	9.10	113.0	444	98.7	9.10	161	1.72	4.8	5.9	8.5	441	0.47	1.78	0.18
2522.49	5.75	27.70	7.82	65.7	105	51.9	5.50	215	1.96	17.9	5.0	6.2	484	0.18	1.05	0.11
2522.72	4.68	62.22	10.15	132.4	388	89.7	8.20	162	1.75	6.2	7.0	8.4	449	0.53	1.67	0.12
2522.95	13.88	40.71	8.34	78.3	275	65.4	6.30	197	2.02	7.1	5.3	7.6	448	0.83	1.52	0.29
2523.15	6.02	43.97	9.31	144.2	398	71.2	8.50	191	1.65	6.3	6.5	7.7	400	1.79	1.51	0.15
2523.45	6.33	34.36	9.74	93.0	230	56.0	7.50	246	1.98	8.8	6.2	7.1	414	0.73	1.31	0.11
2523.65	3.64	39.00	9.64	74.4	198	63.6	8.00	199	1.69	7.2	4.2	8.8	341	0.39	1.29	0.13
2523.87	5.27	53.68	8.49	133.3	383	71.8	7.40	180	1.66	5.5	7.8	9.0	376	1.15	1.63	0.10
2524.13	6.87	59.51	8.89	151.3	507	86.4	9.70	159	1.66	6.8	11.5	8.6	382	2.32	1.96	0.07
2524.33	7.56	26.39	9.61	147.2	132	50.8	4.00	123	1.18	11.1	19.2	5.3	1083	1.09	1.11	0.06
2524.53	5.15	49.13	12.58	168.5	462	68.9	7.50	219	1.86	8.7	9.1	8.0	429	1.52	1.52	0.10
2524.71	5.18	34.65	9.75	79.7	177	57.1	8.40	307	2.25	11.7	3.8	7.8	329	0.44	1.36	0.07
2524.91	14.04	43.54	9.97	111.6	419	83.9	8.30	174	4.77	64.8	5.4	7.2	348	0.87	1.79	0.06
2525.11	6.14	56.40	8.62	153.9	450	93.6	9.10	188	1.79	4.7	5.8	8.8	401	1.87	1.38	0.06
2525.31	3.80	37.46	9.23	98.4	201	59.4	8.40	193	1.86	8.2	4.0	8.8	340	0.42	1.26	0.02
2525.51	4.01	47.39	8.21	132.9	303	72.8	9.00	190	1.77	5.6	4.4	8.2	343	0.60	1.31	0.07
2525.71	4.41	46.90	8.30	123.0	355	69.3	12.50	179	1.74	5.2	4.5	7.9	406	0.71	1.40	0.02
2525.86	3.73	36.84	8.76	92.4	146	66.0	8.30	207	1.75	6.7	3.9	8.0	398	0.33	1.29	0.07
2526.06	4.12	48.23	9.30	125.6	350	83.7	10.30	189	1.96	7.0	4.7	8.5	386	0.91	1.41	0.05
2526.26	4.30	36.94	9.65	121.5	170	66.5	8.00	181	2.12	11.6	6.9	8.0	434	0.39	1.34	0.04
2526.46	2.53	35.32	8.87	97.9	92	54.0	8.80	188	1.72	7.4	3.6	8.4	353	0.40	1.21	0.08
2526.66	9.72	53.75	9.87	158.4	702	96.7	10.50	196	1.95	7.1	6.5	8.5	380	3.88	1.43	0.08
2526.86	3.65	48.59	8.09	121.2	281	71.5	9.00	187	1.75	4.0	4.1	8.1	381	0.62	1.27	0.06
2527.06	4.82	30.45	9.13	80.9	221	53.5	8.20	192	1.79	6.8	3.4	8.0	318	0.53	1.15	0.04
2527.26	3.37	18.59	6.97	140.9	87	34.1	4.60	174	1.12	10.0	14.8	3.9	961	0.66	0.78	0.02
2527.44	5.96	29.51	14.33	95.8	105	44.2	9.20	262	1.89	8.2	3.5	8.4	255	0.49	1.14	0.02
2527.67	4.54	31.26	12.11	102.1	196	53.8	10.90	237	2.47	10.7	3.6	8.2	251	0.79	1.39	0.02
2527.88	3.41	43.14	9.18	114.1	211	71.5	9.80	197	2.00	4.8	4.6	8.8	344	0.58	1.50	0.05
2528.13	3.82	43.67	7.64	116.3	228	71.5	9.80	187	1.84	5.5	4.6	7.9	381	0.90	1.47	0.02
2528.33	4.94	49.00	8.49	138.9	405	78.8	10.30	200	1.97	6.3	4.5	8.0	378	1.05	1.62	0.04
2528.53	4.08	46.42	8.66	114.7	260	73.0	10.60	179	1.96	7.0	6.5	9.1	386	0.56	1.85	0.48
2528.72	3.18	42.68	10.43	129.0	217	68.5	10.60	184	1.94	6.2	4.8	9.3	331	0.51	1.91	0.30
2528.91	4.75	38.01	10.98	116.9	376	64.0	11.00	206	2.26	7.8	4.7	8.8	276	1.28	1.82	0.27
2529.11	6.50	34.96	9.82	137.7	255	59.2	7.70	238	1.61	7.4	4.4	7.1	329	2.41	1.37	0.17
2529.31	2.91	27.07	8.81	69.2	127	44.6	7.80	313	1.70	7.3	3.7	7.5	336	0.85	1.53	0.08
2529.51	12.01	83.55	11.49	157.8	1175	99.8	10.40	191	2.03	6.1	6.1	7.7	470	3.52	2.04	0.22
2529.71	3.77	30.45	9.05	139.2	186	62.8	4.70	182	1.26	4.2	18.1	6.4	806	0.85	1.40	0.12
2529.90	6.90	73.47	7.86	254.7	928	107.6	9.50	171	1.70	3.5	10.7	8.1	504	4.37	2.09	0.09
2530.09	6.46	42.08	13.80	133.3	301	75.9	9.80	189	2.15	8.7	8.2	8.1	479	1.58	1.84	0.11
2530.29	8.57	54.72	9.02	130.0	351	86.1	9.90	189	2.21	7.6	6.7	9.1	323	1.55	1.91	0.10
2530.49	9.13	65.43	9.68	133.0	715	105.2	9.50	183	2.15	7.3	7.3	9.6	321	2.28	2.14	0.09
2530.69	7.48	63.83	9.77	51.0	410	99.5	8.70	192	2.38	11.7	7.0	9.3	325	0.27	2.11	0.09

Skybattle Bay M-11 (Upper)

Sample Depth	V	Ca	P	La	Cr	Mg	Ba	Ti	Al	Na	K	W	Zr	Sn	Be	Sc
m	PPM	%	%	PPM	PPM	%	PPM	%	%	%	%	PPM	PPM	PPM	PPM	PPM
2520.20	96	11.02	0.34	28.8	124	1.25	277	0.25	5.01	0.65	1.84	0.9	79.8	1.7	2.0	9.5
2520.45	66	20.21	0.15	18.6	65	1.12	179	0.16	3.04	0.43	1.11	0.6	51.5	1.0	0.5	5.7
2520.66	160	13.92	0.30	29.9	85	1.32	218	0.21	4.26	0.61	1.62	0.6	70.6	1.4	2.0	8.1
2520.87	282	7.81	0.13	25.2	110	1.06	58	0.23	4.93	0.64	1.87	0.7	82.6	1.6	0.5	8.1
2521.11	289	14.17	2.86	51.4	186	1.07	253	0.21	4.68	0.61	1.76	0.7	64.1	1.4	2.0	11.0
2521.32	239	11.56	1.13	30.4	185	1.24	283	0.25	5.25	0.68	1.85	0.9	82.0	1.7	2.0	10.8
2521.62	113	11.07	0.61	32.9	158	1.23	283	0.25	4.99	0.59	1.94	0.8	75.1	1.8	2.0	10.5
2521.85	98	13.58	0.87	42.2	159	1.18	266	0.24	4.60	0.62	1.75	0.8	77.4	1.4	2.0	10.9
2522.07	63	15.35	1.47	42.5	104	0.88	208	0.17	3.45	0.49	1.29	0.6	57.7	1.1	1.0	6.8
2522.28	131	11.60	0.52	31.6	210	1.20	262	0.23	4.82	0.72	1.80	0.7	73.7	1.6	2.0	11.0
2522.49	61	19.36	1.21	27.1	116	0.99	221	0.14	2.86	0.45	1.12	0.5	57.0	0.9	0.5	6.8
2522.72	118	11.95	0.75	35.9	206	1.15	263	0.24	4.62	0.70	1.89	0.7	74.1	1.3	1.0	10.4
2522.95	147	14.34	0.62	24.4	146	1.34	254	0.21	4.35	0.70	1.61	0.7	86.0	1.3	1.0	8.1
2523.15	166	12.24	0.64	36.4	140	1.33	280	0.22	4.68	0.64	1.67	0.8	71.6	1.6	2.0	9.7
2523.45	101	12.96	1.07	41.6	108	1.63	243	0.20	4.22	0.56	1.52	0.6	62.9	1.4	2.0	7.9
2523.65	120	11.54	0.25	21.4	148	1.26	274	0.23	4.71	0.67	1.73	0.7	70.3	1.6	1.0	8.6
2523.87	155	11.17	0.55	35.9	179	1.27	291	0.24	4.84	0.70	1.85	0.9	76.1	1.5	1.0	10.6
2524.13	216	9.90	0.73	37.7	160	1.23	274	0.25	4.95	0.80	1.81	0.8	77.5	1.6	2.0	10.7
2524.33	64	24.40	>5.00	89.8	92	0.60	233	0.06	2.33	0.51	0.79	0.4	6.9	0.5	0.5	7.0
2524.53	121	12.27	0.95	42.3	143	1.47	246	0.22	4.62	0.64	1.61	0.7	69.3	1.3	1.0	9.2
2524.71	95	12.06	0.37	24.2	113	2.02	214	0.23	4.60	0.55	1.69	0.7	69.5	1.6	1.0	9.0
2524.91	108	11.36	0.93	27.5	132	1.17	71	0.20	4.02	0.56	1.48	0.7	58.8	1.3	0.5	7.5
2525.11	207	9.98	0.27	27.6	166	1.37	256	0.26	5.36	0.91	1.89	0.9	79.4	1.8	2.0	10.5
2525.31	101	10.86	0.34	31.1	120	1.19	278	0.22	4.57	0.71	1.75	0.8	72.1	1.4	1.0	8.3
2525.51	135	9.50	0.29	30.1	149	1.31	283	0.25	5.13	0.79	1.92	0.8	73.2	1.6	2.0	10.4
2525.71	143	10.33	0.36	30.5	154	1.18	275	0.23	4.76	0.69	1.77	0.9	101.0	1.7	1.0	9.5
2525.86	114	11.91	0.52	28.7	120	1.26	314	0.23	4.59	0.73	1.68	0.8	66.5	1.5	2.0	9.4
2526.06	161	10.81	0.31	30.4	150	1.31	278	0.26	5.25	0.77	1.95	0.9	76.6	1.6	2.0	9.9
2526.26	92	11.78	1.27	47.0	99	1.22	259	0.23	4.47	0.69	1.66	0.8	84.8	1.3	1.0	9.9
2526.46	110	10.51	0.25	29.9	108	1.21	285	0.25	4.66	0.75	1.69	0.8	70.7	1.6	1.0	8.5
2526.66	279	11.01	0.32	29.2	155	1.39	267	0.25	5.00	0.77	1.89	0.8	75.6	1.8	1.0	9.4
2526.86	154	11.20	0.21	30.9	155	1.38	288	0.25	5.14	0.78	1.80	0.9	72.9	1.7	2.0	10.4
2527.06	125	9.95	0.13	26.2	93	1.37	309	0.23	4.76	0.76	1.79	0.8	67.2	1.5	2.0	8.6
2527.26	35	24.38	>5.00	101.0	45	0.81	176	0.05	1.93	0.47	0.70	0.4	2.4	0.4	0.5	4.7
2527.44	105	11.00	0.25	28.8	91	1.79	337	0.23	4.89	0.62	1.86	0.8	62.2	1.5	1.0	8.0
2527.67	130	10.83	0.20	27.7	94	1.55	267	0.24	5.09	0.54	1.92	0.7	65.0	1.5	1.0	9.2
2527.88	156	10.03	0.27	32.1	148	1.43	294	0.26	5.64	0.70	2.08	0.8	72.2	1.6	1.0	11.4
2528.13	150	10.50	0.44	35.5	152	1.37	275	0.25	5.05	0.68	1.88	0.8	71.3	1.5	2.0	10.3
2528.33	193	10.19	0.25	29.6	161	1.46	259	0.25	5.44	0.71	1.94	0.9	76.0	1.7	2.0	10.9
2528.53	168	10.79	0.58	34.7	163	1.35	297	0.26	5.43	0.72	1.91	1.0	73.7	1.8	2.0	10.6
2528.72	146	9.47	0.39	33.4	145	1.34	305	0.28	5.59	0.72	1.99	1.0	97.6	1.8	2.0	9.8
2528.91	185	9.81	0.23	29.0	130	1.35	292	0.25	5.42	0.72	2.02	0.9	76.5	1.9	2.0	9.5
2529.11	142	12.94	0.14	24.9	82	1.49	237	0.20	4.23	0.64	1.52	0.7	59.1	1.3	1.0	7.2
2529.31	117	14.35	0.20	28.0	77	2.14	220	0.22	4.27	0.57	1.47	0.7	57.8	1.5	1.0	8.0
2529.51	251	14.13	0.15	22.8	159	1.35	220	0.26	5.01	0.76	1.71	0.8	71.2	1.7	1.0	9.1
2529.71	82	20.23	4.65	112.6	118	1.18	159	0.09	2.97	0.44	0.96	0.6	20.6	0.6	1.0	8.1
2529.90	322	13.91	0.80	46.8	224	1.19	238	0.24	4.82	0.72	1.61	0.8	72.8	1.4	2.0	11.1
2530.09	160	13.33	1.11	46.9	151	1.22	252	0.23	4.71	0.62	1.70	0.8	63.8	1.5	1.0	9.6
2530.29	178	10.71	0.43	37.5	189	1.40	281	0.25	5.44	0.67	1.81	0.9	73.8	1.6	2.0	11.4
2530.49	342	9.22	0.27	35.4	203	1.32	271	0.27	5.69	0.74	2.00	0.8	77.3	1.7	2.0	12.5
2530.69	195	9.90	0.48	30.8	173	1.50	251	0.27	5.82	0.79	1.92	0.9	81.8	1.9	2.0	11.4

Skybattle Bay M-11 (Upper)

Sample Depth	S	Y	Ce	Pr	Nd	Sm	Eu	Gd	Tb	Dy	Ho	Er	Tm	Yb	Lu	Hf
m	%	PPM	PPM	PPM	PPM	PPM	PPM	PPM	PPM	PPM	PPM	PPM	PPM	PPM	PPM	PPM
2520.20	1.23	34.6	48.80	6.7	27.0	5.2	1.1	4.5	0.7	4.8	1.0	2.9	0.4	2.7	0.4	2.5
2520.45	0.71	19.0	32.80	4.1	17.2	3.3	0.7	3.4	0.5	2.8	0.6	1.8	0.2	1.7	0.3	1.4
2520.66	1.58	36.3	50.91	7.3	29.9	5.9	1.2	5.1	0.9	5.4	1.1	3.0	0.4	2.4	0.3	1.7
2520.87	5.18	21.6	44.63	5.8	23.9	4.6	0.9	3.3	0.6	3.6	0.7	2.0	0.3	2.0	0.3	2.1
2521.11	1.33	105.7	75.35	11.8	47.5	9.3	2.2	10.7	1.7	11.3	2.5	7.5	1.0	5.9	0.9	1.7
2521.32	1.58	51.7	49.42	6.9	28.4	5.8	1.2	5.8	1.0	6.9	1.4	3.9	0.6	3.6	0.5	2.0
2521.62	1.76	43.1	52.11	7.4	29.4	5.3	1.2	5.3	0.9	5.7	1.1	3.3	0.5	3.3	0.5	2.1
2521.85	1.27	70.1	65.03	9.8	41.4	8.4	1.7	8.5	1.4	8.9	2.0	4.9	0.7	4.4	0.6	2.0
2522.07	2.31	72.8	65.39	9.5	40.8	7.1	1.8	8.3	1.4	9.0	2.0	5.5	0.8	4.1	0.6	1.7
2522.28	1.28	48.7	48.96	7.4	33.4	6.2	1.4	6.7	1.0	6.4	1.3	4.1	0.6	3.4	0.5	1.8
2522.49	1.79	50.7	36.75	6.5	27.8	6.1	1.2	5.8	0.9	6.5	1.4	3.9	0.6	3.4	0.5	1.4
2522.72	1.33	64.6	52.89	9.2	39.6	7.8	1.8	8.0	1.3	8.0	1.9	4.7	0.6	4.0	0.6	1.9
2522.95	1.59	34.9	38.89	5.5	22.4	4.0	1.0	4.5	0.6	4.3	1.0	2.6	0.4	2.7	0.4	1.7
2523.15	1.12	51.2	58.42	8.3	32.9	6.0	1.4	6.9	1.0	6.5	1.4	4.2	0.5	3.5	0.4	2.1
2523.45	1.51	62.1	70.27	10.1	40.3	7.6	1.7	8.3	1.2	8.0	1.7	5.0	0.6	3.7	0.5	1.7
2523.65	1.15	22.6	36.70	4.7	19.5	3.9	0.9	3.6	0.6	3.7	0.7	2.0	0.3	2.2	0.3	1.8
2523.87	1.13	54.8	58.04	8.9	36.2	7.3	1.6	7.9	1.2	7.5	1.4	3.8	0.6	3.7	0.5	2.1
2524.13	1.10	59.5	60.41	9.1	36.3	7.5	1.6	7.8	1.3	8.0	1.7	4.7	0.6	4.0	0.5	2.0
2524.33	1.06	161.5	104.80	17.1	68.5	12.2	3.5	16.1	2.4	17.8	3.7	11.4	1.4	8.4	1.2	0.2
2524.53	1.30	61.8	69.69	10.2	41.4	8.4	1.6	8.4	1.3	8.4	1.8	5.0	0.6	3.7	0.5	1.8
2524.71	1.66	26.3	42.13	5.5	21.2	3.9	0.8	3.7	0.6	3.9	0.8	2.4	0.3	2.3	0.3	1.8
2524.91	4.91	37.6	45.91	6.8	29.2	5.5	1.3	5.3	0.8	5.4	1.1	2.9	0.4	2.5	0.4	1.6
2525.11	1.10	29.3	45.01	6.7	26.1	5.1	1.1	5.1	0.7	4.5	0.9	2.5	0.4	2.8	0.4	2.1
2525.31	1.34	34.1	51.78	7.2	29.9	5.8	1.2	5.4	0.8	5.2	1.1	2.9	0.4	2.8	0.4	1.9
2525.51	1.13	33.5	48.41	7.1	27.9	5.0	1.2	4.9	0.7	4.3	1.0	3.2	0.5	2.8	0.4	2.0
2525.71	1.20	34.8	50.96	7.3	28.9	5.6	1.2	5.2	0.8	4.5	1.0	2.6	0.4	2.6	0.4	1.9
2525.86	1.20	34.2	45.82	6.6	26.3	4.7	1.0	4.8	0.7	4.7	0.9	2.8	0.4	2.9	0.4	1.7
2526.06	1.35	31.8	52.56	7.5	27.8	5.5	1.0	5.0	0.7	4.7	1.0	2.8	0.4	2.5	0.4	1.9
2526.26	1.60	68.0	76.98	10.9	43.5	7.9	2.0	7.7	1.3	8.7	1.8	4.8	0.7	4.2	0.6	1.8
2526.46	1.15	29.4	49.69	7.0	27.5	5.1	1.1	4.8	0.7	4.3	0.9	2.9	0.4	2.6	0.4	1.9
2526.66	1.32	31.0	46.94	6.7	26.2	4.3	1.0	4.7	0.7	4.4	0.9	2.9	0.4	2.7	0.4	1.9
2526.86	1.11	29.6	49.67	7.1	26.9	5.1	1.2	4.9	0.7	4.3	0.9	2.6	0.4	2.4	0.4	1.9
2527.06	1.15	21.1	45.84	6.2	25.3	4.8	0.9	4.5	0.5	3.4	0.7	2.0	0.3	2.2	0.3	1.8
2527.26	0.90	159.0	186.83	25.5	102.8	19.6	4.7	20.8	3.4	20.6	4.4	11.5	1.6	7.3	0.9	0.1
2527.44	1.13	22.6	49.69	6.4	25.5	4.4	0.9	4.5	0.7	3.9	0.8	2.1	0.3	2.2	0.3	1.9
2527.67	1.86	22.0	48.20	6.3	23.8	4.6	0.9	4.1	0.6	3.8	0.7	2.0	0.3	2.2	0.3	1.9
2527.88	1.22	30.1	54.35	7.5	29.7	5.6	1.2	5.1	0.8	4.6	0.9	2.8	0.4	2.5	0.4	1.9
2528.13	1.20	38.6	56.58	8.4	33.0	6.2	1.3	5.7	0.8	5.7	1.1	3.1	0.5	3.0	0.4	1.8
2528.33	1.31	30.9	46.06	6.5	25.5	4.6	1.0	4.3	0.6	4.0	0.9	2.4	0.4	2.5	0.4	1.8
2528.53	1.29	42.5	51.74	7.3	31.2	5.1	1.3	5.8	0.9	5.3	1.2	3.2	0.5	3.3	0.5	2.1
2528.72	1.19	33.4	52.63	7.3	28.5	5.8	1.2	5.3	0.8	5.1	1.0	2.9	0.4	2.9	0.5	2.1
2528.91	1.58	25.4	53.29	6.7	26.8	4.6	1.0	4.2	0.7	3.5	0.8	2.3	0.4	2.3	0.4	2.3
2529.11	1.03	19.5	43.72	5.9	22.2	3.9	0.8	3.5	0.6	3.2	0.6	2.1	0.3	1.8	0.3	1.5
2529.31	1.02	22.8	48.11	6.6	26.4	4.3	1.0	4.4	0.6	3.8	0.8	2.1	0.3	2.3	0.3	1.6
2529.51	1.55	23.4	39.51	5.6	21.8	3.7	0.9	3.5	0.6	3.4	0.8	2.1	0.3	2.3	0.3	1.9
2529.71	0.96	219.5	111.39	23.1	87.6	17.6	4.5	22.8	3.2	24.0	5.1	15.5	1.9	11.8	1.4	0.7
2529.90	1.16	73.0	65.77	11.3	45.9	9.2	2.0	9.7	1.5	9.6	1.9	5.4	0.8	4.2	0.6	1.8
2530.09	1.67	70.9	69.56	10.4	45.6	8.4	1.8	8.5	1.4	9.2	1.9	5.5	0.8	4.5	0.6	1.7
2530.29	1.58	41.7	52.73	8.2	33.7	6.1	1.3	6.3	0.9	6.2	1.2	3.5	0.5	3.4	0.4	2.0
2530.49	1.48	36.8	54.64	8.2	32.0	6.1	1.3	6.2	0.8	5.5	1.1	3.3	0.4	3.1	0.4	2.4
2530.69	1.63	35.9	48.05	7.8	29.3	5.8	1.2	5.2	0.8	5.3	1.1	3.2	0.5	3.1	0.4	2.07

Skybattle Bay M-11 (Upper)

Sample Depth	Li	Rb	Ta	Nb	Cs	Ga	In	Re	Se	Te	Tl
m	PPM	PPM	PPM	PPM	PPM	PPM	PPM	PPM	PPM	PPM	PPM
2520.20	24.4	114.5	0.5	7.06	6.4	12.82	0.03	0.03	2.90	2.83	0.84
2520.45	15.4	67.7	0.4	4.39	3.6	7.05	0.04	0.02	1.10	1.86	0.68
2520.66	21.1	91.1	0.4	5.92	5.0	10.39	0.02	0.10	3.20	3.31	3.25
2520.87	23.8	105.3	0.5	6.33	5.8	11.64	0.07	0.59	12.40	0.49	36.75
2521.11	22.3	99.2	0.4	5.39	5.6	11.47	0.03	0.07	10.50	1.44	1.21
2521.32	27.2	114.8	0.5	7.60	6.5	13.85	0.04	0.06	9.50	2.12	1.37
2521.62	25.2	111.4	0.5	7.70	6.1	12.82	0.05	0.02	8.00	2.30	0.91
2521.85	23.7	104.0	0.5	6.40	5.5	12.05	0.04	0.02	6.00	1.57	0.73
2522.07	16.2	72.1	0.3	4.46	3.6	7.40	0.03	0.03	4.20	1.82	0.77
2522.28	24.3	101.2	0.4	6.50	5.8	12.40	0.05	0.04	10.50	1.08	0.78
2522.49	13.9	60.9	0.3	4.44	3.2	6.86	0.03	0.02	3.80	2.45	0.70
2522.72	24.3	100.9	0.4	7.12	5.5	11.44	0.03	0.02	9.90	1.89	0.80
2522.95	24.0	89.9	0.4	6.39	5.0	10.71	0.05	0.12	7.10	2.64	0.60
2523.15	24.6	95.2	0.5	6.46	5.8	12.17	0.03	0.04	8.30	4.44	0.85
2523.45	22.5	91.5	0.4	5.65	4.7	10.09	0.04	0.02	5.20	3.22	0.70
2523.65	24.6	101.2	0.4	6.73	5.4	11.95	0.04	0.02	5.50	3.67	0.58
2523.87	24.2	107.0	0.5	7.23	5.8	12.25	0.05	0.03	9.00	2.38	0.88
2524.13	24.5	108.2	0.5	6.70	5.6	12.41	0.03	0.08	8.70	2.61	1.08
2524.33	12.5	49.2	0.1	1.44	2.4	5.42	0.02	0.04	4.20	1.30	1.25
2524.53	22.5	102.8	0.5	7.43	5.3	11.63	0.02	0.05	8.90	4.04	1.10
2524.71	20.9	101.9	0.4	6.32	5.5	12.44	0.03	0.02	5.10	2.17	0.58
2524.91	24.0	91.8	0.4	5.25	4.6	10.37	0.03	0.05	7.80	2.50	1.37
2525.11	26.4	114.0	0.5	7.61	5.8	14.52	0.03	0.05	10.20	1.43	1.00
2525.31	21.9	92.7	0.5	6.72	5.0	12.10	0.03	0.01	5.00	1.03	0.57
2525.51	25.5	104.9	0.5	6.97	5.7	13.13	0.05	0.03	7.30	2.16	0.62
2525.71	24.3	109.4	0.5	6.90	5.9	12.47	0.05	0.02	8.00	0.92	0.61
2525.86	23.8	107.2	0.4	6.68	5.3	11.75	0.04	0.02	5.90	2.53	0.57
2526.06	26.8	116.5	0.5	6.89	6.3	13.69	0.04	0.04	8.20	2.51	0.69
2526.26	24.3	95.9	0.5	6.21	5.2	11.39	0.04	0.02	4.30	1.91	0.79
2526.46	23.7	100.5	0.5	8.01	5.3	11.62	0.06	0.02	4.20	2.37	0.51
2526.66	28.4	109.9	0.5	6.98	5.7	13.67	0.04	0.08	10.00	3.01	1.29
2526.86	24.4	108.9	0.5	7.20	6.0	12.79	0.04	0.01	5.50	2.00	0.57
2527.06	23.1	101.0	0.5	6.31	5.3	11.66	0.04	0.01	3.60	1.74	0.70
2527.26	10.5	40.7	0.1	1.12	1.9	4.68	0.02	0.01	2.40	2.90	0.64
2527.44	27.3	103.5	0.5	6.97	5.5	11.81	0.04	0.02	3.40	3.22	0.56
2527.67	24.4	113.8	0.5	6.64	5.9	13.24	0.04	0.02	4.40	1.45	0.72
2527.88	29.5	128.8	0.5	7.78	6.9	14.17	0.07	0.02	6.20	1.60	0.66
2528.13	27.3	117.5	0.5	7.03	6.2	13.39	0.05	0.02	5.80	1.77	0.58
2528.33	28.4	120.3	0.5	7.29	6.5	14.66	0.05	0.04	8.30	2.05	0.63
2528.53	26.2	113.9	0.5	7.03	6.8	14.45	0.08	0.05	7.60	2.06	0.64
2528.72	30.0	125.0	0.5	7.34	7.0	14.31	0.04	0.02	5.60	1.70	0.64
2528.91	25.0	113.0	0.5	7.42	6.2	13.59	0.04	0.03	7.50	1.77	0.73
2529.11	22.2	92.3	0.4	5.58	4.9	10.21	0.05	0.06	4.60	3.24	1.23
2529.31	22.7	89.0	0.4	5.85	5.1	11.07	0.03	0.02	3.00	2.21	0.49
2529.51	23.3	108.3	0.5	6.86	6.2	13.13	0.04	0.11	13.00	3.47	1.30
2529.71	16.9	70.0	0.1	2.31	3.4	7.79	0.02	0.03	5.60	1.62	0.60
2529.90	24.6	106.2	0.4	6.69	5.8	13.03	0.02	0.12	14.10	1.54	0.97
2530.09	25.1	105.1	0.4	6.35	5.9	11.80	0.02	0.03	8.80	2.19	0.95
2530.29	27.0	112.8	0.5	7.92	6.7	13.30	0.04	0.06	8.20	1.76	0.97
2530.49	30.2	126.5	0.5	8.00	7.2	14.10	0.06	0.11	11.40	2.15	1.22
2530.69	29.2	125.9	0.5	8.27	7.2	15.20	0.06	0.06	9.00	2.09	1.17

Skybattle Bay M-11 (Lower)

Sample Depth	Mo	Cu	Pb	Zn	Ag	Ni	Co	Mn	Fe	As	U	Th	Sr	Cd	Sb	Bi
m	PPM	PPM	PPM	PPM	PPB	PPM	PPM	PPM	%	PPM	PPM	PPM	PPM	PPM	PPM	PPM
2530.96	3.36	4.66	5.01	15.5	122	9.8	1.2	145	0.85	9.6	8.2	4.3	442	0.16	0.38	0.02
2531.17	2.85	3.05	7.02	18.3	96	6.4	0.8	160	0.82	9.5	7.8	4.2	459	0.15	0.29	0.02
2531.37	2.56	11.83	12.78	43.7	81	27.6	9.3	376	2.54	15.7	1.7	8.1	199	0.16	0.46	0.11
2531.64	1.84	15.67	13.16	47.7	99	30.5	8.9	310	2.75	12.2	1.9	9.0	183	0.12	0.56	0.12
2531.86	1.98	15.23	14.10	51.8	119	33.1	10.8	305	2.91	16.3	1.9	9.4	182	0.13	0.56	0.09
2532.09	1.58	18.12	15.56	56.8	139	42.2	10.1	273	3.04	15.1	2.0	9.8	162	0.09	0.40	0.14
2532.31	0.98	14.17	13.57	61.9	94	29.0	9.3	277	2.75	10.0	1.9	9.9	176	0.16	0.48	0.09
2532.54	1.55	18.63	17.27	60.5	159	43.2	11.7	282	3.24	12.9	2.3	10.3	173	0.15	0.48	0.19
2532.82	0.82	15.94	14.26	79.8	108	34.1	10.9	229	3.27	12.3	2.1	9.9	155	0.21	0.39	0.10
2533.02	0.53	13.58	14.36	57.9	90	30.8	9.8	219	2.74	13.6	2.2	10.3	171	0.16	0.33	0.13
2533.22	0.41	15.85	14.68	59.9	92	30.1	8.5	243	2.64	9.8	1.9	9.4	165	0.09	0.37	0.11
2533.42	0.70	20.32	18.37	63.0	91	40.8	12.5	239	3.55	13.5	2.3	10.7	154	0.14	0.41	0.37
2533.70	0.35	13.26	14.03	53.3	72	30.2	10.5	219	2.70	16.4	2.0	10.5	167	0.11	0.31	0.10
2533.90	0.34	12.88	14.22	50.4	75	28.1	10.2	229	2.41	12.1	2.0	10.1	167	0.12	0.32	0.11
2534.10	0.44	15.09	14.59	58.5	112	30.5	8.8	208	2.59	12.9	2.0	10.1	150	0.12	0.33	0.09
2534.29	0.40	15.24	15.63	56.6	94	31.3	10.6	209	2.75	9.8	2.2	11.0	156	0.16	0.35	0.11
2534.56	0.43	14.39	12.89	55.1	90	29.1	9.4	212	2.54	11.0	2.1	10.0	155	0.14	0.31	0.10
2534.73	0.57	17.20	14.44	49.6	132	30.7	10.3	227	2.69	13.5	2.1	10.2	151	0.12	0.31	0.08
2534.95	0.46	14.93	14.24	48.6	127	32.2	10.7	206	2.57	13.8	2.2	10.2	155	0.14	0.34	0.08
2535.18	0.92	13.58	13.15	53.1	114	32.2	8.0	189	2.48	14.8	2.1	9.3	153	0.10	0.26	0.06
2535.38	0.50	12.25	12.96	42.1	112	27.5	7.9	153	2.52	17.1	2.3	10.0	138	0.08	0.30	0.06
2535.55	1.53	13.96	14.46	36.3	170	29.8	7.5	159	2.71	18.8	2.1	9.7	137	0.08	0.28	0.06
2535.81	0.62	18.41	15.87	50.0	122	36.8	9.1	171	3.02	14.6	2.5	11.1	129	0.07	0.32	0.11
2536.08	0.47	13.82	13.59	41.3	104	32.8	8.0	171	2.47	10.5	2.2	9.7	134	0.07	0.30	0.07
2536.28	0.41	18.17	16.73	49.1	131	33.0	8.6	181	2.98	14.8	2.4	12.1	149	0.21	0.49	0.44
2536.56	0.43	15.03	16.57	56.1	117	35.6	9.0	175	3.08	15.0	2.6	11.3	144	0.13	0.41	0.26
2536.72	0.45	17.25	16.68	53.0	145	37.3	10.9	173	3.24	15.3	2.6	12.5	134	0.10	0.42	0.24
2536.95	0.37	17.41	18.04	48.5	131	36.1	10.6	165	2.98	17.0	2.7	12.0	133	0.09	0.38	0.15
2537.15	0.27	13.09	13.71	57.7	98	27.7	10.0	173	2.68	12.7	2.2	11.5	131	0.12	0.33	0.13
2537.37	0.43	11.70	14.35	54.0	128	26.0	7.2	144	2.38	17.7	2.2	11.2	130	0.11	0.33	0.10

Skybattle Bay M-11 (Lower)

Sample Depth	V	Ca	P	La	Cr	Mg	Ba	Ti	Al	Na	K	W	Zr	Sn	Be	Sc
m	PPM	%	%	PPM	PPM	%	PPM	%	%	%	%	PPM	PPM	PPM	PPM	PPM
2530.96	42	14.34	1.00	35.7	36	0.41	153	0.06	0.98	0.19	0.36	0.2	1.1	0.2	0.5	2.2
2531.17	34	15.22	1.25	40.2	36	0.38	182	0.05	0.87	0.12	0.25	0.2	1.0	0.2	0.5	2.3
2531.37	83	11.41	0.16	24.8	61	4.01	258	0.32	4.94	0.53	1.67	0.8	67.8	1.6	2.0	8.7
2531.64	85	9.53	0.09	29.2	73	3.07	281	0.29	5.68	0.60	1.92	0.8	71.3	1.7	2.0	10.4
2531.86	84	9.07	0.09	29.7	70	2.77	278	0.29	5.58	0.57	1.97	0.9	73.3	1.7	2.0	10.4
2532.09	92	7.52	0.08	29.9	78	2.24	302	0.32	5.95	0.55	2.17	1.0	76.5	1.9	2.0	10.3
2532.31	86	8.20	0.08	30.7	71	2.07	284	0.29	5.74	0.58	1.95	1.0	73.9	1.8	2.0	9.8
2532.54	99	7.77	0.09	30.1	83	2.31	279	0.34	6.36	0.62	2.34	1.1	90.0	2.2	3.0	12.1
2532.82	93	6.21	0.09	31.4	67	1.48	259	0.30	6.16	0.56	2.21	0.9	80.0	1.9	2.0	10.5
2533.02	91	7.23	0.09	32.6	73	1.65	275	0.31	5.89	0.61	1.97	1.1	86.5	1.7	2.0	10.0
2533.22	85	7.57	0.07	30.0	72	1.70	267	0.31	5.76	0.57	2.09	0.9	75.7	1.8	2.0	10.6
2533.42	113	5.70	0.08	32.7	79	1.60	321	0.37	7.01	0.60	2.60	1.1	88.9	2.4	2.0	12.6
2533.70	90	7.48	0.08	32.1	70	1.65	275	0.34	5.70	0.59	1.96	0.8	88.8	1.7	2.0	10.2
2533.90	86	7.73	0.08	31.5	76	1.65	282	0.31	5.65	0.58	1.93	1.0	81.1	1.6	2.0	10.8
2534.10	84	7.20	0.08	29.3	78	1.50	271	0.28	5.31	0.55	1.81	0.8	77.5	1.6	1.0	9.4
2534.29	103	6.19	0.09	32.2	85	1.55	313	0.34	6.31	0.60	2.32	1.0	96.8	2.1	1.0	10.7
2534.56	93	6.63	0.08	32.8	78	1.56	285	0.32	5.94	0.58	2.17	0.9	84.7	1.8	3.0	10.1
2534.73	84	7.42	0.08	32.0	74	1.63	268	0.30	5.52	0.55	1.94	0.8	84.1	1.6	1.0	8.9
2534.95	87	6.73	0.09	31.3	82	1.52	294	0.31	5.51	0.57	2.00	0.9	85.4	1.8	1.0	9.3
2535.18	75	6.35	0.11	29.6	73	1.27	293	0.26	4.68	0.51	1.77	0.8	76.6	1.5	1.0	8.6
2535.38	90	5.15	0.13	31.4	82	1.21	253	0.30	5.09	0.54	1.83	0.8	93.7	1.3	2.0	9.1
2535.55	79	5.39	0.13	30.8	76	1.11	98	0.27	4.41	0.50	1.56	1.6	85.9	1.4	0.5	7.7
2535.81	113	4.38	0.11	34.3	94	1.33	161	0.37	6.24	0.60	2.22	1.1	102.1	2.0	2.0	11.4
2536.08	85	5.41	0.10	32.3	74	1.27	290	0.32	5.25	0.56	1.88	0.9	94.5	1.6	1.0	10.4
2536.28	101	5.06	0.10	34.8	95	1.44	382	0.36	6.31	0.57	2.32	1.0	96.6	1.9	2.0	11.1
2536.56	99	5.20	0.11	36.3	88	1.41	368	0.36	6.20	0.55	2.24	1.0	98.2	1.9	1.0	12.1
2536.72	105	4.49	0.10	38.6	90	1.38	333	0.40	6.48	0.54	2.36	1.1	102.5	2.0	2.0	13.1
2536.95	107	4.52	0.11	38.2	89	1.33	310	0.40	6.26	0.53	2.28	1.1	105.7	2.2	3.0	11.8
2537.15	91	5.24	0.09	31.1	72	1.39	292	0.32	5.93	0.55	2.18	0.9	94.8	1.7	2.0	10.7
2537.37	81	4.42	0.11	32.7	70	1.09	324	0.3	4.89	0.49	1.82	0.9	91.0	1.4	2.0	9.6

Skybattle Bay M-11 (Lower)

Sample Depth	S	Y	Ce	Pr	Nd	Sm	Eu	Gd	Tb	Dy	Ho	Er	Tm	Yb	Lu	Hf
m	%	PPM	PPM	PPM	PPM	PPM	PPM	PPM	PPM	PPM	PPM	PPM	PPM	PPM	PPM	PPM
2530.96	0.62	57.1	46.39	8.2	35.6	7.1	1.9	8.5	1.2	7.1	1.4	3.7	0.5	2.8	0.3	0.01
2531.17	0.61	64.3	47.83	9.0	40.5	8.1	2.2	9.4	1.4	8.3	1.6	4.2	0.6	3.0	0.5	0.04
2531.37	1.26	16.2	49.22	5.9	22.6	4.1	0.9	3.4	0.5	3.3	0.6	1.8	0.3	1.7	0.2	1.83
2531.64	1.42	16.6	56.09	6.6	25.2	4.6	0.9	3.2	0.5	3.0	0.6	2.3	0.3	1.7	0.2	2.03
2531.86	1.65	16.3	54.37	6.5	25.4	5.0	0.9	3.7	0.6	3.2	0.6	1.8	0.2	1.9	0.3	1.87
2532.09	1.79	17.0	57.95	7.1	26.6	5.1	1.2	3.9	0.6	3.2	0.6	1.7	0.2	2.0	0.3	2.34
2532.31	1.40	17.5	58.33	7.2	28.5	5.1	1.0	4.2	0.5	3.4	0.6	1.9	0.2	1.8	0.3	2.07
2532.54	1.93	18.4	61.56	7.8	29.3	5.2	1.0	4.0	0.6	3.4	0.7	1.9	0.3	1.9	0.3	2.48
2532.82	1.93	18.7	60.00	7.2	28.8	5.2	1.1	4.2	0.6	3.4	0.7	2.0	0.3	1.8	0.3	2.23
2533.02	1.37	19.4	64.24	7.4	30.2	5.7	1.1	4.4	0.6	3.7	0.7	1.8	0.3	2.0	0.4	2.31
2533.22	1.25	17.1	57.24	7.1	28.7	5.1	1.0	4.3	0.5	3.5	0.6	1.9	0.2	2.0	0.3	2.23
2533.42	1.97	19.9	61.37	7.6	29.3	5.1	1.1	4.2	0.7	3.8	0.7	1.9	0.3	2.0	0.3	2.56
2533.70	1.36	19.3	63.27	7.9	31.0	5.5	1.0	4.6	0.7	3.4	0.6	2.1	0.3	2.0	0.3	2.38
2533.90	1.00	17.9	76.10	7.8	29.2	5.3	1.0	4.1	0.6	3.4	0.7	1.8	0.3	2.1	0.3	2.38
2534.10	1.39	18.6	59.71	7.5	30.2	5.3	1.0	4.0	0.7	3.7	0.7	1.8	0.3	1.8	0.3	2.36
2534.29	1.26	21.3	68.58	8.2	33.1	5.6	1.0	4.2	0.7	3.5	0.7	1.8	0.3	1.8	0.3	2.51
2534.56	1.14	19.0	60.94	8.0	28.4	5.2	1.0	3.8	0.6	3.7	0.8	1.9	0.3	1.9	0.3	2.36
2534.73	1.45	18.6	65.34	7.8	31.2	5.1	1.1	3.6	0.6	3.6	0.7	2.2	0.3	2.1	0.3	2.38
2534.95	1.32	19.1	63.35	7.6	30.8	5.8	1.1	4.3	0.6	3.7	0.6	1.8	0.3	1.9	0.3	2.47
2535.18	1.47	20.7	57.31	6.9	29.6	5.1	1.1	4.3	0.7	3.5	0.7	1.8	0.3	1.8	0.3	2.36
2535.38	1.50	21.8	59.41	7.7	30.7	5.7	1.1	4.4	0.7	4.4	0.7	2.0	0.3	1.9	0.2	2.62
2535.55	1.91	22.6	60.16	7.1	31.3	5.1	1.2	4.5	0.6	3.2	0.8	1.9	0.3	1.8	0.3	2.42
2535.81	1.75	20.5	67.92	8.8	30.4	5.6	1.1	4.4	0.6	3.6	0.7	2.0	0.3	2.2	0.3	2.85
2536.08	1.41	21.1	59.71	8.2	29.3	6.2	1.2	4.0	0.6	3.6	0.6	2.0	0.3	2.0	0.3	2.72
2536.28	1.63	19.8	70.84	8.2	29.8	5.5	1.2	4.9	0.7	3.5	0.7	2.2	0.3	1.9	0.4	2.75
2536.56	1.76	20.4	66.47	8.0	27.7	5.4	1.1	4.7	0.7	3.8	0.6	2.1	0.3	2.1	0.3	3.07
2536.72	1.90	20.0	69.81	8.5	29.4	5.8	1.2	4.2	0.6	3.9	0.6	2.2	0.3	2.4	0.4	3.75
2536.95	1.66	20.4	70.58	8.2	30.6	5.8	1.1	5.6	0.7	4.1	0.7	2.3	0.3	2.3	0.3	3.39
2537.15	1.27	19.9	60.79	7.4	26.7	4.8	1.1	4.7	0.7	3.9	0.7	1.9	0.3	2.1	0.3	2.76
2537.37	1.32	21.3	62.00	7.2	27.9	5.5	1.3	4.6	0.6	3.7	0.7	2.3	0.3	1.9	0.3	2.43

Skybattle Bay M-11 (Lower)

Sample Depth	Li	Rb	Ta	Nb	Cs	Ga	In	Re	Se	Te	Tl
m	PPM	PPM	PPM	PPM	PPM	PPM	PPM	PPM	PPM	PPM	PPM
2530.96	9.9	20.2	0.05	1.27	1.1	2.52	0.01	0.03	1.00	2.61	0.72
2531.17	9.2	15.8	0.05	1.05	1.0	1.85	0.01	0.02	0.60	2.81	0.65
2531.37	26.9	106.8	0.50	7.28	5.5	11.62	0.05	0.01	0.70	2.84	0.58
2531.64	33.1	125.4	0.60	8.11	6.7	13.26	0.04	0.00	0.15	3.03	0.62
2531.86	30.7	115.4	0.50	7.76	6.5	13.71	0.04	0.00	0.40	1.49	0.63
2532.09	33.1	124.4	0.60	9.03	7.2	14.92	0.04	0.00	0.15	2.21	0.68
2532.31	30.6	116.7	0.60	7.88	6.7	13.67	0.06	0.00	0.15	1.49	0.54
2532.54	36.8	139.0	0.70	9.22	7.9	16.34	0.07	0.00	0.15	2.38	0.76
2532.82	34.3	124.4	0.60	8.53	7.0	14.72	0.04	0.00	0.70	0.76	0.59
2533.02	33.4	115.3	0.60	9.01	6.8	12.99	0.04	0.00	0.15	1.32	0.51
2533.22	32.7	119.2	0.60	8.66	6.4	13.85	0.04	0.00	0.40	0.72	0.49
2533.42	38.5	138.3	0.70	10.44	8.7	17.31	0.05	0.00	0.15	0.39	0.65
2533.70	32.4	110.1	0.60	8.79	6.6	14.12	0.03	0.00	0.40	0.92	0.49
2533.90	31.9	108.6	0.50	9.00	6.3	13.54	0.05	0.00	0.15	1.73	0.47
2534.10	29.9	106.1	0.50	7.79	5.9	11.80	0.04	0.00	0.15	1.16	0.49
2534.29	34.0	130.0	0.60	9.66	7.6	14.70	0.03	0.00	0.40	0.58	0.54
2534.56	33.4	121.0	0.60	8.92	6.9	14.47	0.02	0.00	0.15	1.07	0.53
2534.73	31.3	105.0	0.50	8.28	6.2	12.83	0.05	0.00	0.15	1.36	0.51
2534.95	30.6	109.4	0.60	8.20	6.3	12.71	0.02	0.00	0.15	0.96	0.53
2535.18	29.0	91.7	0.50	7.40	5.4	11.19	0.05	0.00	0.40	1.16	0.53
2535.38	28.5	104.3	0.50	7.71	5.8	11.47	0.03	0.00	0.40	0.40	0.56
2535.55	26.1	82.8	0.50	7.15	5.3	10.18	0.03	0.01	0.40	0.40	0.57
2535.81	37.7	127.8	0.70	9.60	8.4	15.22	0.05	0.00	0.50	0.35	0.66
2536.08	31.2	108.8	0.60	8.30	6.4	11.93	0.03	0.00	0.15	1.23	0.55
2536.28	36.3	133.1	0.70	9.16	7.8	15.46	0.11	0.00	0.50	0.50	0.67
2536.56	35.4	126.0	0.70	10.11	7.5	16.11	0.08	0.00	0.40	0.64	0.61
2536.72	41.4	134.7	0.70	9.99	8.7	16.53	0.06	0.00	0.60	0.40	0.68
2536.95	37.1	131.9	0.70	10.44	8.0	16.92	0.06	0.00	0.50	0.33	0.65
2537.15	32.1	112.5	0.60	8.85	6.5	14.38	0.03	0.00	0.30	0.20	0.52
2537.37	26.9	100.9	0.50	7.64	5.8	12.19	0.04	0.00	0.50	0.34	0.51

Pollux G-60

Sample Depth	Mo	Cu	Pb	Zn	Ag	Ni	Co	Mn	Fe	As	U	Th	Sr	Cd	Sb	Bi
m	PPM	PPM	PPM	PPM	PPB	PPM	PPM	PPM	%	PPM	PPM	PPM	PPM	PPM	PPM	PPM
1371.80	4.83	24.71	9.32	48.1	276	29.8	5.6	184	1.9	5.7	3.1	5.8	428	0.46	0.92	0.82
1372.07	3.47	28.09	10.12	51.7	317	34.0	6.8	188	1.9	3.7	3.7	7.1	529	0.29	0.80	0.39
1372.28	1.27	32.22	10.85	83.2	267	35.5	6.7	178	2.1	5.9	2.8	7.8	447	0.35	1.00	0.24
1372.50	0.93	40.61	8.41	67.8	287	47.5	8.5	153	2.0	3.0	3.3	8.5	391	0.20	0.85	0.21
1372.70	1.69	42.55	12.35	177.7	493	51.1	8.6	179	1.9	4.1	3.1	7.2	604	0.55	1.48	0.22
1372.90	1.22	37.13	7.94	77.7	352	40.1	8.5	192	2.3	4.9	2.9	7.3	491	0.28	1.03	1.33
1373.11	2.01	53.11	15.21	274.5	613	61.5	9.5	151	2.2	6.8	3.6	8.5	400	1.23	1.95	0.35
1373.32	3.14	60.26	13.06	96.5	1043	68.5	9.1	111	2.1	6.5	4.0	8.5	335	0.89	3.12	0.37
1373.53	3.32	52.40	14.65	122.8	956	77.9	10.6	110	1.9	8.0	4.1	8.6	390	1.13	3.19	3.21
1373.67	4.94	50.70	14.85	116.1	1624	65.2	10.8	90	2.0	6.9	3.3	7.8	240	3.30	4.23	0.68
1373.86	2.72	43.11	12.53	100.5	430	51.7	8.6	100	2.2	12.7	3.6	8.3	380	0.74	2.49	0.49
1374.07	2.04	38.57	12.05	84.4	347	50.4	9.8	112	2.2	8.8	2.3	7.8	258	0.46	1.90	0.26
1374.27	1.67	34.32	11.28	92.8	356	50.9	8.9	152	2.2	9.8	3.0	8.6	342	0.46	1.18	0.21
1374.51	2.57	22.24	9.96	66.1	464	25.2	6.4	167	2.0	5.8	3.2	7.6	370	0.49	0.86	0.14
1374.74	3.39	13.81	6.75	49.8	276	18.5	4.5	187	1.4	3.7	3.8	6.1	506	0.50	0.64	0.19
1375.02	4.05	15.47	8.27	54.9	286	22.7	6.1	163	1.6	3.8	6.7	6.8	525	0.43	0.71	0.06
1375.22	1.03	19.13	7.64	98.2	217	23.2	6.7	209	2.2	4.1	2.2	6.1	551	0.36	0.66	0.12
1375.45	1.08	38.02	9.57	78.1	295	32.9	8.1	185	2.1	3.0	2.6	7.1	467	0.23	0.87	0.11
1375.76	1.85	53.82	13.16	98.8	855	59.2	9.2	99	2.1	10.8	2.9	7.7	227	0.32	2.30	0.10
1375.86	1.79	47.91	12.71	115.9	523	60.5	9.1	94	2.2	10.1	3.0	7.5	300	0.29	1.51	0.11
1376.08	1.43	33.22	10.01	106.8	410	43.3	7.4	93	1.7	7.2	3.7	6.6	796	0.28	1.18	0.06
1376.31	1.32	38.81	12.82	78.1	365	47.5	8.8	96	1.9	9.2	2.7	8.3	279	0.17	1.23	0.15
1376.55	1.16	16.29	8.16	78.6	283	22.9	5.6	123	1.2	2.8	2.2	6.0	477	0.29	0.62	0.02
1376.75	0.79	21.02	8.93	47.4	345	22.2	5.1	140	1.5	4.0	3.4	7.2	366	0.20	0.77	0.07
1376.97	2.19	14.29	7.61	48.2	286	18.4	6.1	165	1.7	4.7	3.7	6.3	459	0.24	0.58	0.07
1377.50	2.36	10.23	4.13	31.9	208	11.8	3.1	252	2.0	4.4	2.3	3.7	452	0.21	0.35	0.05
1377.69	1.87	8.06	3.58	25.9	172	10.4	2.3	265	2.0	1.4	2.1	3.1	587	0.11	0.28	0.02
1377.97	1.22	16.53	6.13	36.5	295	22.3	5.1	258	2.5	5.1	2.6	4.1	724	0.14	0.58	0.13
1378.21	1.18	29.76	9.92	135.5	355	38.0	8.6	119	1.6	5.4	3.2	7.5	352	0.30	0.91	0.20
1378.48	1.33	37.40	11.12	98.9	407	48.3	8.8	104	1.7	6.4	3.1	7.8	294	0.23	1.05	0.22
1378.72	1.20	37.97	10.51	73.0	439	47.2	9.8	95	1.6	9.3	2.9	7.2	293	0.20	1.30	0.12
1378.95	1.41	42.37	10.97	107.9	478	49.6	8.5	93	1.6	7.8	2.5	7.7	262	0.26	1.23	0.17
1379.16	1.67	41.22	11.63	78.4	411	47.6	8.6	94	1.7	7.5	2.9	7.6	271	0.22	1.23	0.10
1379.37	1.72	40.38	12.31	111.8	482	57.5	9.4	97	1.8	8.4	2.8	7.7	281	0.21	1.29	0.13
1379.58	1.59	40.08	12.19	96.6	482	52.7	10.2	98	1.8	7.3	2.4	7.7	234	0.24	1.23	0.11
1379.78	1.61	34.73	11.41	82.6	453	43.7	8.8	109	1.5	6.2	2.7	7.7	298	0.26	1.08	0.13
1379.88	1.01	22.24	13.10	132.8	353	25.3	6.0	146	1.5	4.6	2.0	6.8	387	0.48	0.71	0.58
1380.18	1.06	21.47	8.08	87.3	336	25.9	6.5	174	1.7	7.3	2.0	6.4	409	0.31	0.79	0.42
1380.38	1.23	17.79	7.52	62.2	336	23.1	5.1	168	1.6	7.5	5.6	4.7	1084	0.28	0.87	0.33
1380.59	1.46	24.20	8.88	95.3	413	30.2	8.3	210	2.1	6.1	1.7	6.3	479	0.34	0.98	0.43
1380.70	2.37	17.96	8.53	47.2	347	21.1	5.0	136	1.4	3.0	2.4	7.0	349	0.29	0.87	0.54

Pollux G-60

Sample Depth	V	Ca	P	La	Cr	Mg	Ba	Ti	Al	Na	K	W	Zr	Sn	Be	Sc
m	PPM	%	%	PPM	PPM	%	PPM	%	%	%	%	PPM	PPM	PPM	PPM	PPM
1371.80	98	13.02	0.05	21.5	84	0.8	340	0.19	3.3	0.34	1.1	0.7	60.6	1.0	2.0	7.2
1372.07	117	11.51	0.57	31.3	88	1.0	380	0.21	3.8	0.37	1.4	0.8	72.7	1.0	1.0	8.2
1372.28	139	9.72	0.13	23.3	106	1.0	425	0.24	4.3	0.40	1.5	0.9	91.9	1.3	1.0	8.8
1372.50	164	7.98	0.13	28.9	146	1.0	488	0.28	5.1	0.44	1.9	1.0	86.2	1.6	1.0	10.1
1372.70	135	11.75	0.23	28.7	128	0.8	389	0.23	4.1	0.38	1.5	0.8	75.2	1.3	1.0	9.5
1372.90	150	10.82	0.15	28.2	128	0.9	392	0.23	4.4	0.37	1.5	0.9	74.7	1.3	1.0	9.7
1373.11	180	8.19	0.28	32.7	183	0.9	301	0.27	4.9	0.42	1.9	1.1	84.6	1.5	1.0	11.2
1373.32	245	6.82	0.14	30.6	214	0.8	465	0.28	4.9	0.42	1.8	0.9	86.0	1.3	2.0	11.1
1373.53	222	7.22	0.31	36.6	207	0.7	237	0.27	4.7	0.41	1.6	0.9	85.2	1.4	2.0	11.9
1373.67	312	4.71	0.05	25.3	171	0.8	294	0.32	5.5	0.45	1.9	1.0	89.3	1.6	2.0	11.4
1373.86	199	5.58	0.48	39.9	130	0.8	217	0.32	5.4	0.47	1.9	1.1	91.7	1.7	2.0	11.7
1374.07	179	5.04	0.08	25.2	123	0.8	287	0.32	5.2	0.47	1.8	1.1	88.4	1.4	2.0	11.2
1374.27	148	7.29	0.07	28.7	104	0.9	417	0.29	5.1	0.44	1.8	1.1	89.9	1.7	1.0	10.6
1374.51	107	9.87	0.05	27.7	72	1.1	333	0.23	3.8	0.42	1.3	0.8	81.9	1.0	2.0	8.0
1374.74	74	15.97	0.13	22.7	50	0.7	261	0.17	2.5	0.32	0.9	0.6	84.3	0.7	1.0	6.0
1375.02	66	12.12	0.58	27.0	52	0.8	287	0.16	2.4	0.35	0.8	0.5	83.3	0.7	1.0	6.0
1375.22	82	11.73	0.16	21.2	78	1.0	321	0.18	3.2	0.36	1.1	0.7	67.9	0.9	1.0	7.0
1375.45	100	10.13	0.15	25.2	99	1.1	333	0.22	4.0	0.37	1.3	0.7	70.7	1.0	1.0	8.8
1375.76	199	4.42	0.05	22.3	154	0.8	244	0.31	5.0	0.46	1.8	1.0	85.1	1.6	1.0	10.5
1375.86	185	5.09	0.21	29.1	150	0.8	218	0.31	5.1	0.44	1.8	1.1	91.5	1.6	1.0	11.8
1376.08	135	8.31	2.02	73.5	103	0.7	309	0.22	4.3	0.46	1.5	0.8	69.8	1.2	2.0	13.1
1376.31	153	4.78	0.07	23.5	107	0.8	287	0.32	4.9	0.50	1.8	1.0	90.8	1.7	1.0	10.9
1376.55	80	9.50	0.06	21.4	58	0.8	479	0.19	3.0	0.40	1.0	0.7	71.7	0.8	1.0	7.6
1376.75	105	8.78	0.05	26.9	74	1.1	377	0.24	3.9	0.42	1.3	0.8	83.1	1.1	1.0	8.2
1376.97	70	11.26	0.07	21.5	52	1.1	426	0.17	2.7	0.35	0.9	0.6	64.1	0.8	0.5	5.7
1377.50	51	19.32	0.07	14.0	40	1.9	379	0.11	1.8	0.22	0.5	0.4	43.6	0.5	0.5	4.4
1377.69	37	19.52	0.14	13.4	37	2.0	420	0.09	1.4	0.21	0.4	0.3	39.4	0.3	0.5	3.2
1377.97	73	14.36	0.57	27.1	60	2.1	499	0.14	2.3	0.28	0.7	0.5	48.6	0.6	0.5	5.2
1378.21	115	6.83	0.26	33.3	83	1.0	372	0.26	4.2	0.47	1.4	0.8	80.9	1.4	2.0	9.6
1378.48	147	5.37	0.14	30.5	105	0.9	390	0.30	4.8	0.46	1.7	1.0	80.8	1.5	2.0	10.9
1378.72	133	5.25	0.11	28.7	95	0.8	363	0.26	4.5	0.45	1.4	1.0	84.9	1.3	1.0	10.6
1378.95	143	4.86	0.07	27.6	100	0.8	410	0.28	4.8	0.45	1.6	1.0	82.6	1.4	1.0	11.4
1379.16	149	4.93	0.11	27.6	103	0.8	388	0.30	4.9	0.44	1.6	1.0	81.7	1.5	1.0	11.2
1379.37	148	4.91	0.13	29.3	119	0.8	313	0.30	4.9	0.46	1.7	0.9	86.1	1.4	1.0	10.9
1379.58	147	4.71	0.05	25.8	109	0.9	328	0.31	4.8	0.46	1.7	0.9	84.3	1.6	1.0	10.2
1379.78	123	6.10	0.04	25.9	113	0.9	378	0.27	4.3	0.46	1.5	0.9	87.2	1.3	2.0	9.0
1379.88	98	8.93	0.05	22.5	89	1.1	392	0.21	3.5	0.40	1.2	0.7	65.9	1.2	1.0	7.2
1380.18	93	9.94	0.05	20.5	84	1.3	380	0.19	3.3	0.37	1.1	0.6	65.1	1.1	0.5	6.8
1380.38	74	16.03	2.53	80.9	61	1.2	451	0.16	2.7	0.34	0.9	0.5	58.5	0.9	1.0	7.9
1380.59	90	11.36	0.06	20.1	83	1.5	418	0.19	3.1	0.33	1.0	0.7	64.7	0.9	1.0	7.3
1380.70	88	8.45	0.08	22.6	78	1.1	459	0.19	3.3	0.42	1.1	0.6	81.2	1.0	0.5	7.3

Pollux G-60

Sample Depth	S	Y	Ce	Pr	Nd	Sm	Eu	Gd	Tb	Dy	Ho	Er	Tm	Yb	Lu	Hf
m	%	PPM	PPM	PPM	PPM	PPM	PPM	PPM	PPM	PPM	PPM	PPM	PPM	PPM	PPM	PPM
1371.80	0.8	18.7	35.9	5.2	19.8	3.3	0.7	2.9	0.5	2.9	0.6	1.5	0.2	1.7	0.3	1.75
1372.07	0.8	40.3	52.8	8.1	29.8	6.4	1.3	6.2	1.0	6.5	1.2	3.1	0.5	3.2	0.4	1.98
1372.28	0.9	18.7	39.1	5.3	19.8	3.5	0.6	3.3	0.5	3.1	0.6	1.7	0.3	2.2	0.4	2.36
1372.50	0.8	23.9	45.2	6.3	23.3	4.5	0.8	4.2	0.6	3.8	0.8	2.2	0.4	2.6	0.3	2.59
1372.70	0.9	36.1	45.4	7.2	27.1	4.7	1.1	5.4	0.8	5.1	1.1	2.9	0.4	3.0	0.4	2.12
1372.90	1.0	27.9	43.6	6.5	26.0	4.8	0.9	5.0	0.7	4.8	0.9	2.3	0.4	2.7	0.4	2.04
1373.11	1.2	38.0	51.6	8.7	33.8	6.6	1.2	6.5	0.9	5.6	1.0	3.1	0.5	3.2	0.5	2.36
1373.32	1.3	28.1	47.7	7.7	26.2	5.2	0.9	4.4	0.6	4.4	0.8	2.2	0.4	2.7	0.4	2.53
1373.53	1.2	43.9	55.4	8.8	31.0	5.9	1.4	6.5	0.9	6.0	1.1	3.3	0.5	3.6	0.5	2.19
1373.67	1.2	15.0	40.3	5.5	18.8	3.3	0.6	3.0	0.4	2.6	0.5	1.7	0.3	2.1	0.3	2.67
1373.86	1.5	54.2	64.1	11.0	41.3	8.1	1.9	8.4	1.3	8.2	1.7	4.5	0.6	3.8	0.6	2.58
1374.07	1.3	15.1	36.8	5.0	18.0	2.9	0.6	2.6	0.4	2.5	0.5	1.5	0.3	2.2	0.3	2.39
1374.27	1.0	19.5	46.1	6.4	23.0	4.0	0.8	3.4	0.5	3.2	0.6	1.8	0.3	2.1	0.3	2.60
1374.51	0.6	30.5	46.9	6.8	25.2	4.5	0.8	4.1	0.5	3.1	0.6	2.0	0.3	2.1	0.3	2.45
1374.74	0.4	24.6	37.1	5.5	21.5	3.7	0.7	3.9	0.6	3.7	0.7	2.1	0.3	2.3	0.3	2.24
1375.02	0.6	40.0	45.4	7.2	28.0	5.5	1.1	6.1	0.9	5.5	1.1	3.4	0.5	3.1	0.4	2.41
1375.22	0.9	22.7	35.1	5.6	22.0	3.9	0.9	3.8	0.6	3.6	0.7	1.9	0.3	2.2	0.3	1.86
1375.45	0.8	24.0	39.5	6.1	22.3	4.6	0.7	4.2	0.6	3.8	0.7	2.3	0.4	2.4	0.4	2.09
1375.76	1.5	11.4	36.7	4.8	16.9	2.9	0.4	2.2	0.3	1.9	0.4	1.3	0.2	1.9	0.3	2.42
1375.86	1.5	24.5	44.1	6.7	24.6	4.5	0.9	3.9	0.7	4.5	0.8	2.3	0.4	2.7	0.4	2.43
1376.08	1.2	169.2	103.4	17.9	72.0	13.6	4.1	17.0	2.8	21.1	4.1	12.2	1.6	9.5	1.3	1.71
1376.31	1.2	14.6	40.7	5.6	20.0	3.1	0.7	2.7	0.4	2.4	0.5	1.6	0.3	2.1	0.3	2.75
1376.55	0.5	18.1	34.3	5.4	18.8	3.4	0.6	2.7	0.5	3.0	0.5	1.6	0.3	2.1	0.3	2.02
1376.75	0.5	17.1	43.6	6.7	22.8	4.1	0.7	3.5	0.5	3.0	0.6	1.8	0.3	2.1	0.3	2.51
1376.97	0.6	19.0	36.3	5.6	21.0	3.8	0.7	3.8	0.5	3.0	0.6	1.8	0.3	1.8	0.3	1.99
1377.50	0.3	13.1	21.1	3.2	11.3	2.3	0.4	2.1	0.3	2.0	0.4	1.3	0.2	1.3	0.2	1.12
1377.69	0.2	16.5	21.4	3.4	12.7	2.8	0.6	3.2	0.4	2.9	0.5	1.6	0.2	1.4	0.2	1.06
1377.97	0.6	40.0	48.8	8.1	37.6	7.3	1.5	7.6	1.1	6.5	1.2	3.0	0.4	2.4	0.3	1.38
1378.21	0.8	34.0	56.0	9.2	38.8	7.3	1.4	7.3	1.1	6.3	1.1	3.0	0.4	2.6	0.4	2.35
1378.48	1.0	24.6	51.2	8.2	33.6	5.8	1.1	4.7	0.7	4.7	0.8	2.3	0.3	2.6	0.4	2.46
1378.72	1.0	22.6	46.2	7.0	28.1	5.1	1.0	3.9	0.6	3.6	0.7	2.1	0.3	2.1	0.4	2.31
1378.95	1.1	15.1	40.5	5.4	19.4	3.3	0.6	2.6	0.4	2.6	0.5	1.7	0.2	2.0	0.3	2.45
1379.16	1.1	20.6	43.0	6.3	25.3	4.6	0.8	4.0	0.5	3.2	0.6	1.9	0.3	2.2	0.3	2.59
1379.37	1.2	23.7	46.5	7.3	27.8	5.2	1.0	4.8	0.6	4.2	0.7	2.3	0.3	2.3	0.4	2.44
1379.58	1.1	12.8	39.0	5.4	18.3	3.1	0.5	2.5	0.4	2.2	0.4	1.4	0.2	1.8	0.3	2.39
1379.78	0.8	14.5	40.9	5.5	18.9	3.3	0.6	2.8	0.4	2.4	0.4	1.6	0.3	2.2	0.3	2.46
1379.88	0.5	13.6	35.8	4.2	16.9	2.3	0.5	1.9	0.4	2.1	0.5	1.5	0.3	1.6	0.3	1.91
1380.18	0.5	12.3	32.5	4.4	15.8	2.7	0.6	2.3	0.4	2.0	0.4	1.6	0.3	1.6	0.2	2.03
1380.38	0.5	192.4	148.6	26.1	121.5	25.2	6.7	31.2	5.1	32.0	6.0	15.3	1.6	7.8	1.0	1.37
1380.59	0.6	14.0	29.7	3.9	13.9	2.4	0.4	2.1	0.3	2.1	0.4	1.4	0.3	1.6	0.3	2.20
1380.70	0.5	18.1	39.0	5.0	20.9	3.3	0.7	3.2	0.5	2.8	0.6	1.8	0.3	1.6	0.3	1.98

Pollux G-60

Sample Depth	Li	Rb	Ta	Nb	Cs	Ga	In	Re	Se	Te	Tl
m	PPM	PPM	PPM	PPM	PPM	PPM	PPM	PPM	PPM	PPM	PPM
1371.80	13.6	58.0	0.4	5.11	3.8	8.10	0.12	0.01	3.2	2.03	0.41
1372.07	14.9	70.4	0.4	5.54	4.3	9.35	0.05	0.02	4.4	2.62	0.41
1372.28	16.5	78.5	0.4	6.45	5.1	10.32	0.04	0.01	5.6	2.59	0.41
1372.50	21.8	97.7	0.5	7.71	6.6	12.79	0.03	0.01	6.2	1.31	0.45
1372.70	17.1	79.3	0.5	6.46	5.2	10.65	0.05	0.02	10.0	1.78	0.39
1372.90	19.5	85.1	0.4	6.36	5.5	10.08	0.03	0.02	7.4	1.19	0.37
1373.11	20.5	94.1	0.5	7.30	6.4	11.69	0.05	0.02	12.7	1.25	0.49
1373.32	22.1	94.0	0.5	7.41	6.2	11.58	0.02	0.02	18.1	0.80	0.48
1373.53	20.6	88.0	0.4	7.23	6.1	11.17	0.04	0.04	18.4	0.83	0.49
1373.67	22.6	87.8	0.6	8.47	7.0	12.53	0.05	0.04	20.7	0.19	0.62
1373.86	22.3	98.2	0.6	8.58	7.2	12.79	0.04	0.01	10.1	0.48	0.68
1374.07	23.3	85.8	0.6	8.71	6.5	12.99	0.04	0.02	7.9	0.58	0.55
1374.27	20.4	97.2	0.5	8.39	6.2	12.37	0.06	0.02	4.7	1.25	0.51
1374.51	16.1	73.8	0.5	6.13	4.4	9.54	0.03	0.02	4.3	2.40	0.46
1374.74	11.9	44.5	0.3	4.48	2.8	6.02	0.01	0.01	2.8	1.81	0.38
1375.02	12.6	44.0	0.3	4.33	2.5	5.80	0.03	0.02	3.3	1.20	0.31
1375.22	13.9	58.3	0.4	4.77	3.2	7.27	0.02	0.01	3.3	2.43	0.39
1375.45	17.3	70.1	0.4	5.88	4.2	9.58	0.04	0.00	4.7	1.21	0.45
1375.76	23.2	89.8	0.6	8.23	6.1	12.61	0.03	0.04	13.7	0.84	0.65
1375.86	21.9	93.6	0.6	8.59	6.4	12.76	0.04	0.02	10.7	0.30	0.61
1376.08	20.5	83.5	0.4	5.45	5.1	10.44	0.03	0.03	9.0	0.88	0.47
1376.31	24.7	85.4	0.6	8.92	6.1	13.10	0.04	0.02	7.4	0.52	0.60
1376.55	18.5	50.4	0.3	4.90	3.0	6.40	0.04	0.02	3.3	1.66	0.28
1376.75	18.5	72.3	0.4	6.40	4.1	8.92	0.03	0.00	2.7	1.30	0.39
1376.97	15.5	44.7	0.3	4.14	2.6	6.19	0.02	0.02	2.2	3.24	0.28
1377.50	9.6	33.0	0.2	3.07	1.7	4.28	0.01	0.00	1.5	3.16	0.17
1377.69	8.9	25.3	0.2	2.65	1.3	3.31	0.02	0.01	1.0	4.48	0.12
1377.97	14.7	41.5	0.3	3.92	2.4	5.60	0.02	0.01	3.3	2.92	0.25
1378.21	22.4	76.1	0.5	6.77	4.7	10.57	0.05	0.01	4.1	1.38	0.40
1378.48	23.1	93.2	0.5	7.91	5.9	11.66	0.05	0.02	6.1	0.42	0.51
1378.72	23.6	82.8	0.5	7.30	5.4	10.72	0.02	0.02	6.3	0.90	0.48
1378.95	21.5	91.7	0.5	7.36	5.7	11.61	0.03	0.02	7.0	0.97	0.51
1379.16	24.4	82.9	0.5	7.77	5.9	11.77	0.04	0.02	6.1	0.62	0.55
1379.37	23.8	90.1	0.5	7.90	6.2	13.04	0.04	0.02	7.0	1.03	0.58
1379.58	23.4	87.3	0.5	8.34	5.9	12.31	0.04	0.02	5.7	0.35	0.53
1379.78	21.0	88.9	0.5	7.63	5.3	11.31	0.05	0.02	5.4	1.17	0.43
1379.88	19.5	60.1	0.4	5.19	4.1	8.45	0.04	0.01	2.8	1.57	0.37
1380.18	19.6	63.6	0.3	5.26	3.7	7.87	0.01	0.01	3.7	0.84	0.34
1380.38	13.8	47.3	0.3	3.91	2.9	6.66	0.01	0.01	2.9	3.60	0.29
1380.59	17.3	57.1	0.4	4.96	3.6	7.98	0.02	0.01	2.7	3.04	0.34
1380.70	19.7	53.9	0.4	5.18	3.5	7.30	0.01	0.01	3.3	1.58	0.32

*Yellow highlighted values indicate element concentration is below the lower detection limit of analysis; value presented is half of the minimum detection limit.

Method Detection Limit for ICP-MS

Analyte	Unit	MDL
Mo	PPM	0.05
Cu	PPM	0.02
Pb	PPM	0.02
Zn	PPM	0.2
Ag	PPB	20
Ni	PPM	0.1
Co	PPM	0.2
Mn	PPM	2
Fe	%	0.02
As	PPM	0.2
U	PPM	0.1
Th	PPM	0.1
Sr	PPM	1
Cd	PPM	0.02
Sb	PPM	0.02
Bi	PPM	0.04
V	PPM	1
Ca	%	0.02
P	%	0.001
La	PPM	0.1
Cr	PPM	1
Mg	%	0.02
Ba	PPM	1
Ti	%	0.001
Al	%	0.02
Na	%	0.002
K	%	0.02
W	PPM	0.1
Zr	PPM	0.2
Sn	PPM	0.1
Be	PPM	1
Sc	PPM	0.1
S	%	0.04
Y	PPM	0.1
Ce	PPM	0.02
Pr	PPM	0.1
Nd	PPM	0.1
Sm	PPM	0.1
Eu	PPM	0.1
Gd	PPM	0.1
Tb	PPM	0.1
Dy	PPM	0.1
Ho	PPM	0.1
Er	PPM	0.1
Tm	PPM	0.1
Yb	PPM	0.1
Lu	PPM	0.1
Hf	PPM	0.02
Li	PPM	0.1
Rb	PPM	0.1
Ta	PPM	0.1
Nb	PPM	0.04
Cs	PPM	0.1
Ga	PPM	0.02
In	PPM	0.01
Re	PPM	0.002
Se	PPM	0.3
Te	PPM	0.05
Tl	PPM	0.05

APPENDIX E: POROSITY CALCULATIONS AND DATA

The following formulas were used to calculate porosity for samples:

Bulk density from immersion in n-hexane:

$$\rho_b = \frac{W_a}{W_a - W_l}(\rho_l - \rho_a) + \rho_a$$

ρ_b = Bulk density of sample

W_a = Weight of sample in air

W_l = Weight of sample in n-hexane

ρ_l = Density of n-hexane (0.666 g/cm^3)

ρ_a = Density of air (0.0012 g/cm^3)

Grain density from He-pycnometry:

$$V_g = \frac{[V_1(p_f - p_1) + V_2(p_f - p_2)]}{p_f - p_1}$$

$$\rho_g = \frac{W_a}{V_g}$$

V_g = Sample grain volume

V_1 = Chamber 1 volume

V_2 = Chamber 2 volume

p_f = Final equilibrium pressure

p_1 = Initial pressure of chamber 1

p_2 = Initial pressure of chamber 2

ρ_g = Grain density

Collingwood K-33

Sample Depth	Bulk Density	Grain Density	Porosity
m	g/cm^3	g/cm^3	%
1899.39	2.55	2.69	5.26
1900.66	2.58	2.70	4.44
1901.29	2.54	2.75	7.71
1902.27	2.60	2.68	2.91
1902.91	2.58	2.66	3.22
1904.52	2.56	2.67	4.14

Skybattle Bay M-11 (Upper)

Sample Depth	Bulk Density	Grain Density	Porosity
m	g/cm^3	g/cm^3	%
2520.45	2.53	2.70	5.91
2520.87	2.53	2.66	4.63
2521.85	2.51	2.59	2.86
2522.07	2.56	2.75	6.92
2523.65	2.52	2.65	4.68
2524.13	2.48	2.55	2.79
2524.33	2.55	2.86	10.88
2526.26	2.56	2.63	2.66
2527.26	2.59	2.74	5.57
2528.33	2.48	2.56	3.12
2529.90	2.47	2.54	2.74
2530.69	2.49	2.52	1.66

Pollux G-60

Sample Depth	Bulk Density	Grain Density	Porosity
m	g/cm^3	g/cm^3	%
1371.80	2.60	2.62	1.01
1372.50	2.55	2.60	2.02
1372.70	2.53	2.60	2.54
1373.53	2.51	2.57	2.54
1374.27	2.54	2.61	2.79
1375.02	2.63	2.71	2.69
1375.76	2.51	2.59	3.13
1377.50	2.65	2.73	3.21
1378.48	2.54	2.63	3.62
1379.78	2.54	2.64	3.62

Skybattle Bay M-11 (Lower)

Sample Depth	Bulk Density	Grain Density	Porosity
m	g/cm^3	g/cm^3	%
2530.96	2.62	2.69	2.43
2531.37	2.61	2.75	5.27
2532.09	2.60	2.69	3.30
2535.81	2.57	2.67	3.81
2536.95	2.57	2.62	2.02

APPENDIX F: LOW PRESSURE NITROGEN GAS ADSORPTION ISOTHERM DATA

Skybattle Bay M-11

Sample Depth (m)	2520.45		2520.87		2521.85		2522.07	
	Relative Pressure	Quantity Adsorbed	Relative Pressure	Quantity Adsorbed	Relative Pressure	Quantity Adsorbed	Relative Pressure	Quantity Adsorbed
	p/p°	cm^3/g (STP)	p/p°	cm^3/g (STP)	p/p°	cm^3/g (STP)	p/p°	cm^3/g (STP)
	0.010	0.100	0.010	0.078	0.010	0.179	0.010	0.266
	0.044	0.141	0.044	0.104	0.044	0.227	0.044	0.338
	0.074	0.162	0.074	0.116	0.074	0.255	0.072	0.374
	0.112	0.184	0.112	0.131	0.112	0.295	0.111	0.415
	0.137	0.198	0.138	0.140	0.138	0.320	0.137	0.441
	0.169	0.213	0.169	0.150	0.169	0.347	0.168	0.470
	0.201	0.228	0.201	0.161	0.201	0.377	0.200	0.500
	0.232	0.243	0.233	0.172	0.233	0.407	0.232	0.531
	0.265	0.259	0.264	0.183	0.264	0.443	0.264	0.563
	0.296	0.275	0.297	0.194	0.297	0.474	0.295	0.594
	0.329	0.291	0.330	0.206	0.329	0.509	0.327	0.629
	0.360	0.307	0.360	0.217	0.361	0.546	0.360	0.665
	0.392	0.325	0.392	0.230	0.392	0.582	0.392	0.700
	0.424	0.342	0.424	0.242	0.424	0.618	0.424	0.737
	0.456	0.363	0.455	0.258	0.455	0.658	0.456	0.776
	0.487	0.382	0.487	0.272	0.488	0.703	0.486	0.813
	0.519	0.404	0.519	0.288	0.519	0.744	0.519	0.855
	0.551	0.425	0.551	0.302	0.551	0.787	0.551	0.895
	0.582	0.447	0.583	0.318	0.583	0.833	0.583	0.939
	0.615	0.471	0.615	0.335	0.615	0.877	0.615	0.986
	0.646	0.498	0.646	0.354	0.646	0.927	0.647	1.037
	0.679	0.529	0.679	0.376	0.678	0.979	0.678	1.095
	0.710	0.564	0.710	0.401	0.710	1.042	0.710	1.161
	0.742	0.605	0.742	0.430	0.741	1.111	0.741	1.234
	0.774	0.653	0.774	0.465	0.773	1.190	0.773	1.326
	0.805	0.710	0.806	0.507	0.805	1.282	0.805	1.431
	0.836	0.783	0.837	0.561	0.836	1.394	0.835	1.557
	0.869	0.882	0.868	0.629	0.868	1.532	0.868	1.737
	0.900	1.021	0.900	0.722	0.900	1.712	0.899	1.969
	0.931	1.247	0.932	0.872	0.932	1.968	0.931	2.323
	0.961	1.669	0.963	1.135	0.962	2.384	0.960	2.900
	0.992	3.031	0.994	2.018	0.994	3.608	0.993	4.493
	0.964	2.182	0.966	1.454	0.966	2.930	0.966	3.658
	0.930	1.702	0.926	1.130	0.932	2.573	0.926	3.070
	0.901	1.463	0.899	1.005	0.899	2.354	0.902	2.844
	0.871	1.294	0.868	0.901	0.869	2.208	0.870	2.635
	0.839	1.157	0.835	0.819	0.837	2.087	0.831	2.449
	0.806	1.049	0.803	0.754	0.801	1.975	0.806	2.351
	0.771	0.955	0.772	0.706	0.769	1.890	0.773	2.242
	0.737	0.882	0.740	0.662	0.740	1.826	0.741	2.149
	0.709	0.830	0.708	0.625	0.709	1.764	0.711	2.073
	0.678	0.778	0.677	0.592	0.678	1.705	0.677	1.991
	0.643	0.727	0.645	0.561	0.643	1.643	0.645	1.916
	0.613	0.685	0.613	0.531	0.609	1.583	0.614	1.844
	0.582	0.645	0.580	0.502	0.579	1.531	0.584	1.779
	0.550	0.608	0.547	0.477	0.550	1.484	0.552	1.711
	0.517	0.574	0.517	0.456	0.518	1.437	0.519	1.641
	0.485	0.514	0.487	0.420	0.487	1.343	0.490	1.485
	0.453	0.399	0.455	0.320	0.457	1.010	0.455	0.927
	0.422	0.373	0.423	0.287	0.422	0.883	0.425	0.837
	0.388	0.353	0.390	0.269	0.390	0.810	0.393	0.789
	0.358	0.336	0.358	0.255	0.358	0.751	0.360	0.749
	0.326	0.320	0.326	0.243	0.325	0.705	0.329	0.715
	0.294	0.304	0.295	0.231	0.294	0.667	0.297	0.681
	0.262	0.290	0.262	0.220	0.262	0.633	0.265	0.649
	0.230	0.276	0.231	0.210	0.231	0.601	0.233	0.619
	0.199	0.262	0.199	0.200	0.200	0.573	0.201	0.590
	0.167	0.249	0.167	0.191	0.167	0.544	0.169	0.563
	0.135	0.236	0.135	0.184	0.136	0.520	0.137	0.536
	0.104	0.221	0.104	0.174	0.104	0.492	0.105	0.507

Skybattle Bay M-11

Sample Depth (m)	2523.65		2524.13		2524.33		2526.26	
	Relative Pressure	Quantity Adsorbed	Relative Pressure	Quantity Adsorbed	Relative Pressure	Quantity Adsorbed	Relative Pressure	Quantity Adsorbed
	p/p°	cm³/g (STP)	p/p°	cm³/g (STP)	p/p°	cm³/g (STP)	p/p°	cm³/g (STP)
	0.010	0.591	0.010	0.285	0.010	0.376	0.010	0.104
	0.044	0.724	0.044	0.348	0.044	0.570	0.044	0.140
	0.072	0.795	0.073	0.384	0.073	0.662	0.074	0.158
	0.111	0.875	0.112	0.438	0.112	0.758	0.112	0.181
	0.136	0.924	0.136	0.473	0.137	0.815	0.138	0.196
	0.167	0.982	0.167	0.510	0.169	0.879	0.170	0.213
	0.199	1.043	0.199	0.555	0.201	0.942	0.201	0.231
	0.239	1.123	0.231	0.598	0.233	1.004	0.233	0.250
	0.261	1.167	0.263	0.643	0.265	1.065	0.265	0.272
	0.302	1.247	0.297	0.688	0.297	1.125	0.298	0.292
	0.334	1.316	0.328	0.733	0.329	1.186	0.330	0.311
	0.360	1.368	0.358	0.774	0.360	1.246	0.361	0.332
	0.391	1.434	0.390	0.821	0.393	1.311	0.392	0.353
	0.423	1.500	0.421	0.870	0.424	1.377	0.424	0.376
	0.455	1.574	0.453	0.921	0.456	1.452	0.456	0.400
	0.486	1.639	0.486	0.974	0.488	1.528	0.487	0.426
	0.519	1.710	0.517	1.030	0.520	1.610	0.520	0.454
	0.550	1.779	0.548	1.080	0.551	1.688	0.551	0.479
	0.581	1.850	0.579	1.133	0.583	1.776	0.583	0.507
	0.613	1.928	0.614	1.190	0.614	1.864	0.615	0.534
	0.646	2.015	0.644	1.247	0.646	1.967	0.647	0.564
	0.677	2.106	0.676	1.309	0.678	2.085	0.679	0.602
	0.708	2.203	0.707	1.378	0.709	2.216	0.710	0.641
	0.741	2.320	0.739	1.459	0.741	2.376	0.742	0.688
	0.772	2.450	0.770	1.549	0.773	2.568	0.774	0.744
	0.804	2.601	0.771	1.566	0.805	2.812	0.805	0.811
	0.834	2.780	0.806	1.675	0.837	3.120	0.837	0.893
	0.869	3.013	0.834	1.796	0.867	3.534	0.869	1.001
	0.900	3.294	0.869	1.954	0.898	4.169	0.901	1.143
	0.931	3.687	0.900	2.135	0.930	5.267	0.932	1.361
	0.961	4.263	0.932	2.391	0.962	7.708	0.963	1.769
	0.993	5.704	0.963	2.766	0.993	15.010	0.993	2.986
	0.966	4.966	0.993	3.582	0.966	11.717	0.966	2.226
	0.928	4.493	0.966	3.105	0.931	8.862	0.934	1.789
	0.902	4.280	0.934	2.848	0.902	7.054	0.902	1.521
	0.863	4.044	0.901	2.666	0.868	5.630	0.868	1.336
	0.837	3.930	0.869	2.532	0.834	4.654	0.837	1.211
	0.806	3.815	0.837	2.420	0.800	3.993	0.804	1.108
	0.774	3.714	0.805	2.323	0.775	3.613	0.773	1.030
	0.742	3.627	0.773	2.238	0.737	3.169	0.739	0.957
	0.710	3.547	0.742	2.167	0.710	2.932	0.709	0.903
	0.678	3.471	0.710	2.100	0.680	2.701	0.678	0.852
	0.647	3.400	0.678	2.035	0.648	2.493	0.646	0.803
	0.615	3.329	0.646	1.973	0.616	2.315	0.614	0.755
	0.582	3.258	0.614	1.907	0.584	2.157	0.582	0.712
	0.551	3.189	0.583	1.845	0.552	2.018	0.550	0.673
	0.519	3.123	0.551	1.789	0.519	1.892	0.518	0.636
	0.489	2.930	0.518	1.736	0.486	1.759	0.487	0.590
	0.458	2.095	0.487	1.635	0.455	1.508	0.456	0.470
	0.418	1.785	0.456	1.314	0.422	1.415	0.422	0.420
	0.389	1.680	0.424	1.156	0.391	1.350	0.391	0.389
	0.359	1.595	0.392	1.052	0.359	1.285	0.359	0.365
	0.327	1.516	0.360	0.967	0.327	1.225	0.327	0.344
	0.296	1.446	0.328	0.901	0.295	1.165	0.295	0.324
	0.263	1.379	0.296	0.841	0.264	1.107	0.262	0.307
	0.232	1.317	0.263	0.794	0.232	1.051	0.231	0.292
	0.200	1.258	0.230	0.750	0.200	0.996	0.199	0.277
	0.168	1.200	0.199	0.712	0.167	0.937	0.168	0.264
	0.136	1.143	0.168	0.679	0.136	0.881	0.136	0.254
	0.105	1.082	0.136	0.653	0.104	0.816	0.104	0.240
			0.104	0.620				

Skybattle Bay M-11

Sample Depth (m)	2527.26		2528.33		2529.90		2530.96	
	Relative Pressure	Quantity Adsorbed	Relative Pressure	Quantity Adsorbed	Relative Pressure	Quantity Adsorbed	Relative Pressure	Quantity Adsorbed
	p/p°	cm³/g (STP)	p/p°	cm³/g (STP)	p/p°	cm³/g (STP)	p/p°	cm³/g (STP)
	0.010	0.044	0.010	0.115	0.010	0.094	0.010	0.165
	0.044	0.079	0.044	0.156	0.044	0.124	0.044	0.201
	0.073	0.095	0.074	0.176	0.074	0.141	0.074	0.222
	0.111	0.114	0.112	0.201	0.112	0.163	0.112	0.247
	0.138	0.125	0.137	0.218	0.138	0.177	0.138	0.266
	0.169	0.136	0.169	0.236	0.170	0.194	0.169	0.286
	0.201	0.149	0.201	0.257	0.201	0.214	0.201	0.311
	0.233	0.160	0.233	0.277	0.233	0.234	0.233	0.334
	0.265	0.171	0.265	0.297	0.266	0.255	0.265	0.358
	0.297	0.181	0.297	0.316	0.297	0.274	0.297	0.383
	0.330	0.193	0.330	0.336	0.330	0.295	0.330	0.408
	0.361	0.202	0.360	0.353	0.361	0.307	0.361	0.429
	0.393	0.212	0.392	0.374	0.392	0.324	0.392	0.455
	0.424	0.223	0.424	0.396	0.424	0.343	0.424	0.481
	0.456	0.236	0.456	0.422	0.455	0.366	0.456	0.515
	0.487	0.247	0.488	0.447	0.487	0.391	0.488	0.549
	0.520	0.260	0.519	0.474	0.519	0.419	0.520	0.583
	0.549	0.272	0.551	0.496	0.551	0.442	0.550	0.609
	0.583	0.285	0.583	0.522	0.583	0.462	0.583	0.642
	0.615	0.298	0.615	0.545	0.615	0.485	0.614	0.672
	0.647	0.312	0.646	0.572	0.646	0.511	0.646	0.711
	0.679	0.327	0.678	0.604	0.678	0.538	0.678	0.755
	0.710	0.346	0.710	0.639	0.710	0.570	0.710	0.808
	0.742	0.369	0.741	0.679	0.742	0.609	0.742	0.871
	0.774	0.396	0.773	0.729	0.773	0.655	0.773	0.948
	0.805	0.428	0.805	0.789	0.805	0.709	0.806	1.046
	0.837	0.472	0.836	0.861	0.837	0.780	0.836	1.174
	0.869	0.531	0.869	0.959	0.869	0.869	0.868	1.355
	0.901	0.619	0.900	1.091	0.900	0.986	0.899	1.612
	0.932	0.764	0.931	1.294	0.932	1.167	0.931	2.005
	0.962	1.064	0.963	1.653	0.963	1.500	0.964	2.434
	0.994	2.611	0.995	2.780	0.993	2.451	0.994	3.011
	0.966	1.441	0.965	1.979	0.966	1.787	0.965	2.617
	0.926	1.017	0.933	1.611	0.934	1.451	0.931	2.450
	0.900	0.876	0.901	1.388	0.899	1.238	0.899	2.249
	0.869	0.756	0.868	1.227	0.864	1.097	0.867	1.967
	0.833	0.661	0.834	1.102	0.835	1.001	0.831	1.684
	0.803	0.599	0.799	0.998	0.801	0.918	0.800	1.480
	0.769	0.543	0.769	0.923	0.772	0.859	0.772	1.341
	0.737	0.499	0.736	0.854	0.738	0.807	0.741	1.216
	0.707	0.466	0.708	0.807	0.702	0.751	0.704	1.097
	0.671	0.431	0.671	0.750	0.671	0.707	0.677	1.027
	0.643	0.405	0.644	0.709	0.639	0.658	0.645	0.954
	0.611	0.377	0.608	0.657	0.607	0.614	0.614	0.885
	0.580	0.352	0.580	0.619	0.577	0.574	0.582	0.818
	0.548	0.330	0.546	0.579	0.544	0.538	0.547	0.759
	0.516	0.310	0.516	0.547	0.514	0.512	0.518	0.718
	0.484	0.281	0.484	0.495	0.482	0.460	0.485	0.652
	0.453	0.240	0.452	0.411	0.451	0.376	0.453	0.535
	0.421	0.225	0.420	0.375	0.419	0.347	0.421	0.489
	0.391	0.215	0.390	0.354	0.389	0.326	0.390	0.463
	0.360	0.204	0.358	0.334	0.356	0.307	0.358	0.436
	0.328	0.195	0.326	0.317	0.325	0.289	0.327	0.412
	0.296	0.185	0.293	0.299	0.293	0.273	0.295	0.386
	0.263	0.174	0.263	0.284	0.261	0.258	0.263	0.362
	0.232	0.165	0.231	0.270	0.230	0.243	0.231	0.342
	0.199	0.155	0.199	0.258	0.198	0.233	0.199	0.324
	0.167	0.146	0.167	0.246	0.167	0.224	0.167	0.306
	0.137	0.137	0.136	0.238	0.135	0.219	0.136	0.293
	0.105	0.126	0.104	0.225	0.104	0.206	0.104	0.275

Skybattle Bay M-11

Sample Depth (m)	2532.09		2535.81	
	Relative Pressure	Quantity Adsorbed	Relative Pressure	Quantity Adsorbed
	p/p°	cm³/g (STP)	p/p°	cm³/g (STP)
	0.010	1.195	0.010	0.544
	0.042	1.445	0.044	0.665
	0.078	1.607	0.072	0.730
	0.111	1.735	0.111	0.806
	0.135	1.829	0.137	0.859
	0.174	1.969	0.169	0.918
	0.199	2.055	0.201	0.982
	0.235	2.193	0.233	1.046
	0.262	2.286	0.264	1.112
	0.293	2.396	0.296	1.177
	0.327	2.516	0.329	1.249
	0.359	2.633	0.360	1.322
	0.392	2.751	0.392	1.389
	0.421	2.856	0.424	1.467
	0.453	2.970	0.456	1.548
	0.484	3.083	0.487	1.610
	0.516	3.194	0.519	1.684
	0.550	3.317	0.551	1.756
	0.581	3.428	0.581	1.839
	0.614	3.555	0.614	1.923
	0.643	3.669	0.646	2.010
	0.676	3.814	0.678	2.106
	0.708	3.968	0.709	2.211
	0.828	4.742	0.742	2.339
	0.836	4.824	0.773	2.488
	0.869	5.166	0.805	2.661
	0.899	5.586	0.836	2.872
	0.930	6.212	0.869	3.162
	0.963	7.288	0.900	3.533
	0.993	9.299	0.932	4.101
	0.966	8.266	0.962	5.037
	0.929	7.588	0.995	7.578
	0.895	7.190	0.965	6.289
	0.871	6.974	0.931	5.643
	0.831	6.698	0.902	5.292
	0.807	6.550	0.869	4.996
	0.767	6.346	0.832	4.734
	0.742	6.227	0.802	4.550
	0.712	6.093	0.772	4.392
	0.704	6.059	0.739	4.243
	0.679	5.953	0.706	4.093
	0.648	5.826	0.675	3.961
	0.609	5.662	0.645	3.829
	0.583	5.555	0.613	3.693
	0.553	5.432	0.581	3.554
	0.514	5.268	0.551	3.426
	0.486	4.724	0.520	3.300
	0.450	3.420	0.484	2.681
	0.426	3.178	0.458	1.892
	0.394	3.011	0.426	1.632
	0.360	2.875	0.393	1.505
	0.329	2.766	0.361	1.413
	0.297	2.655	0.329	1.340
	0.265	2.546	0.297	1.270
	0.234	2.442	0.265	1.206
	0.202	2.338	0.233	1.143
	0.170	2.236	0.200	1.083
	0.138	2.133	0.169	1.029
	0.107	2.024	0.137	0.978
			0.106	0.925

APPENDIX G: COPYRIGHT PERMISSIONS

ELSEVIER LICENSE
TERMS AND CONDITIONS

Aug 06, 2015

This is an Agreement between Danielle Kondla ("You") and Elsevier ("Elsevier"). It consists of your order details, the terms and conditions provided by Elsevier, and the payment terms and conditions.

All payments must be made in full to CCC. For payment instructions, please see information listed at the bottom of this form.

Supplier	Elsevier Limited The Boulevard,Langford Lane Kidlington,Oxford,OX5 1GB,UK
Registered Company Number	1982084
Customer name	Danielle Kondla
Customer address	315 Ascot Circle SW Calgary, AB T3H 0X2
License number	3663850039246
License date	Jul 07, 2015
Licensed content publisher	Elsevier
Licensed content publication	International Journal of Coal Geology
Licensed content title	Depositional environment and hydrocarbon potential of the Middle Triassic strata of the Sverdrup Basin, Canada
Licensed content author	Danielle Kondla,Hamed Sanei,Ashton Embry,Omid H. Ardakani,Christopher R. Clarkson
Licensed content date	1 August 2015
Licensed content volume number	147
Licensed content issue number	n/a
Number of pages	14
Start Page	71
End Page	84
Type of Use	reuse in a thesis/dissertation
Portion	full article
Format	electronic
Are you the author of this Elsevier article?	Yes
Will you be translating?	No
Title of your thesis/dissertation	Unconventional Hydrocarbon Potential of a Middle Triassic Source Rock in the West-Central Sverdrup Basin, Canadian Arctic Archipelago
Expected completion date	Aug 2015
Estimated size (number of pages)	154
Elsevier VAT number	GB 494 6272 12
Price	0.00 CAD
VAT/Local Sales Tax	0.00 CAD / 0.00 GBP
Total	**0.00 CAD**
Terms and Conditions	

INTRODUCTION

1. The publisher for this copyrighted material is Elsevier. By clicking "accept" in connection with completing this licensing transaction, you agree that the following terms and conditions apply to this transaction (along with the Billing and Payment terms and conditions established by Copyright Clearance Center, Inc. ("CCC"), at the time that you opened your Rightslink account and that are available at

any time at http://myaccount.copyright.com).

GENERAL TERMS

2. Elsevier hereby grants you permission to reproduce the aforementioned material subject to the terms and conditions indicated.
3. Acknowledgement: If any part of the material to be used (for example, figures) has appeared in our publication with credit or acknowledgement to another source, permission must also be sought from that source. If such permission is not obtained then that material may not be included in your publication/copies. Suitable acknowledgement to the source must be made, either as a footnote or in a reference list at the end of your publication, as follows:
"Reprinted from Publication title, Vol /edition number, Author(s), Title of article / title of chapter, Pages No., Copyright (Year), with permission from Elsevier [OR APPLICABLE SOCIETY COPYRIGHT OWNER]." Also Lancet special credit - "Reprinted from The Lancet, Vol. number, Author(s), Title of article, Pages No., Copyright (Year), with permission from Elsevier."
4. Reproduction of this material is confined to the purpose and/or media for which permission is hereby given.
5. Altering/Modifying Material: Not Permitted. However figures and illustrations may be altered/adapted minimally to serve your work. Any other abbreviations, additions, deletions and/or any other alterations shall be made only with prior written authorization of Elsevier Ltd. (Please contact Elsevier at permissions@elsevier.com)
6. If the permission fee for the requested use of our material is waived in this instance, please be advised that your future requests for Elsevier materials may attract a fee.
7. Reservation of Rights: Publisher reserves all rights not specifically granted in the combination of (i) the license details provided by you and accepted in the course of this licensing transaction, (ii) these terms and conditions and (iii) CCC's Billing and Payment terms and conditions.
8. License Contingent Upon Payment: While you may exercise the rights licensed immediately upon issuance of the license at the end of the licensing process for the transaction, provided that you have disclosed complete and accurate details of your proposed use, no license is finally effective unless and until full payment is received from you (either by publisher or by CCC) as provided in CCC's Billing and Payment terms and conditions. If full payment is not received on a timely basis, then any license preliminarily granted shall be deemed automatically revoked and shall be void as if never granted. Further, in the event that you breach any of these terms and conditions or any of CCC's Billing and Payment terms and conditions, the license is automatically revoked and shall be void as if never granted. Use of materials as described in a revoked license, as well as any use of the materials beyond the scope of an unrevoked license, may constitute copyright infringement and publisher reserves the right to take any and all action to protect its copyright in the materials.
9. Warranties: Publisher makes no representations or warranties with respect to the licensed material.
10. Indemnity: You hereby indemnify and agree to hold harmless publisher and CCC, and their respective officers, directors, employees and agents, from and against any and all claims arising out of your use of the licensed material other than as specifically authorized pursuant to this license.
11. No Transfer of License: This license is personal to you and may not be sublicensed, assigned, or transferred by you to any other person without publisher's written permission.
12. No Amendment Except in Writing: This license may not be amended except in a writing signed by both parties (or, in the case of publisher, by CCC on publisher's behalf).
13. Objection to Contrary Terms: Publisher hereby objects to any terms contained in any purchase order, acknowledgment, check endorsement or other writing prepared by you, which terms are inconsistent with these terms and conditions or CCC's Billing and Payment terms and conditions. These terms and conditions, together with CCC's Billing and Payment terms and conditions (which are incorporated herein), comprise the entire agreement between you and publisher (and CCC) concerning this licensing transaction. In the event of any conflict between your obligations established by these terms and conditions and those established by CCC's Billing and Payment terms and conditions, these terms and conditions shall control.
14. Revocation: Elsevier or Copyright Clearance Center may deny the permissions described in this License at their sole discretion, for any reason or no reason, with a full refund payable to you. Notice of such denial will be made using the contact information provided by you. Failure to receive such notice will not alter or invalidate the denial. In no event will Elsevier or Copyright Clearance Center be responsible or liable for any costs, expenses or damage incurred by you as a result of a denial of your permission request, other than a refund of the amount(s) paid by you to Elsevier and/or Copyright Clearance Center for denied permissions.

LIMITED LICENSE

The following terms and conditions apply only to specific license types:
15. **Translation**: This permission is granted for non-exclusive world **English** rights only unless your license was granted for translation rights. If you licensed translation rights you may only translate this content into the languages you requested. A professional translator must perform all translations and reproduce the content word for word preserving the integrity of the article. If this license is to re-use 1 or 2 figures then permission is granted for non-exclusive world rights in all languages.
16. **Posting licensed content on any Website**: The following terms and conditions apply as follows: Licensing material from an Elsevier journal: All content posted to the web site must maintain the copyright information line on the bottom of each image; A hyper-text must be included to the Homepage of the journal from which you are licensing at http://www.sciencedirect.com/science/journal/xxxxx or the Elsevier homepage for books at http://www.elsevier.com; Central Storage: This license does not include permission for a scanned version of the material to be stored in a central repository such as that provided by Heron/XanEdu.
Licensing material from an Elsevier book: A hyper-text link must be included to the Elsevier homepage at http://www.elsevier.com . All content posted to the web site must maintain the copyright information line on the bottom of each image.

Posting licensed content on Electronic reserve: In addition to the above the following clauses are applicable: The web site must be password-protected and made available only to bona fide students registered on a relevant course. This permission is granted for 1 year only. You may obtain a new license for future website posting.
17. **For journal authors:** the following clauses are applicable in addition to the above:
Preprints:
A preprint is an author's own write-up of research results and analysis, it has not been peer-reviewed, nor has it had any other value added to it by a publisher (such as formatting, copyright, technical enhancement etc.).
Authors can share their preprints anywhere at any time. Preprints should not be added to or enhanced in any way in order to appear more like, or to substitute for, the final versions of articles however authors can update their preprints on arXiv or RePEc with their Accepted Author Manuscript (see below).
If accepted for publication, we encourage authors to link from the preprint to their formal publication via its DOI. Millions of researchers have access to the formal publications on ScienceDirect, and so links will help users to find, access, cite and use the best available version. Please note that Cell Press, The Lancet and some society-owned have different preprint policies. Information on these policies is available on the journal homepage.
Accepted Author Manuscripts: An accepted author manuscript is the manuscript of an article that has been accepted for publication and which typically includes author-incorporated changes suggested during submission, peer review and editor-author communications.
Authors can share their accepted author manuscript:

- immediately
  - via their non-commercial person homepage or blog
  - by updating a preprint in arXiv or RePEc with the accepted manuscript
  - via their research institute or institutional repository for internal institutional uses or as part of an invitation-only research collaboration work-group
  - directly by providing copies to their students or to research collaborators for their personal use
  - for private scholarly sharing as part of an invitation-only work group on commercial sites with which Elsevier has an agreement
- after the embargo period
  - via non-commercial hosting platforms such as their institutional repository
  - via commercial sites with which Elsevier has an agreement

In all cases accepted manuscripts should:

- link to the formal publication via its DOI
- bear a CC-BY-NC-ND license - this is easy to do
- if aggregated with other manuscripts, for example in a repository or other site, be shared in alignment with our hosting policy not be added to or enhanced in any way to appear more like, or to substitute for, the published journal article.

Published journal article (JPA): A published journal article (PJA) is the definitive final record of published research that appears or will appear in the journal and embodies all value-adding publishing activities including peer review co-ordination, copy-editing, formatting, (if relevant) pagination and online enrichment.
Policies for sharing publishing journal articles differ for subscription and gold open access articles:
Subscription Articles: If you are an author, please share a link to your article rather than the full-text. Millions of researchers have access to the formal publications on ScienceDirect, and so links will help your users to find, access, cite, and use the best available version.
Theses and dissertations which contain embedded PJAs as part of the formal submission can be posted publicly by the awarding institution with DOI links back to the formal publications on ScienceDirect.
If you are affiliated with a library that subscribes to ScienceDirect you have additional private sharing rights for others' research accessed under that agreement. This includes use for classroom teaching and internal training at the institution (including use in course packs and courseware programs), and inclusion of the article for grant funding purposes.
Gold Open Access Articles: May be shared according to the author-selected end-user license and should contain a CrossMark logo, the end user license, and a DOI link to the formal publication on ScienceDirect.
Please refer to Elsevier's posting policy for further information.
18. **For book authors** the following clauses are applicable in addition to the above: Authors are permitted to place a brief summary of their work online only. You are not allowed to download and post the published electronic version of your chapter, nor may you scan the printed edition to create an electronic version. **Posting to a repository:** Authors are permitted to post a summary of their chapter only in their institution's repository.
19. **Thesis/Dissertation**: If your license is for use in a thesis/dissertation your thesis may be submitted to your institution in either print or electronic form. Should your thesis be published commercially, please reapply for permission. These requirements include permission for the Library and Archives of Canada to supply single copies, on demand, of the complete thesis and include permission for Proquest/UMI to supply single copies, on demand, of the complete thesis. Should your thesis be published commercially, please reapply for permission. Theses and dissertations which contain embedded PJAs as part of the formal submission can be posted

publicly by the awarding institution with DOI links back to the formal publications on ScienceDirect.

I, the undersigned, hereby grant permission for the material co-authored by me in this thesis (Unconventional Hydrocarbon Potential of a Middle Triassic Source Rock in the West-Central Sverdrup Basin, Canadian Arctic Archipelago) with Danielle Michelle Kondla, to be used online by 'The Vault'- University of Calgary and Libraries and Archives Canada.

Previously published co-authored material included in this thesis is reprinted from International Journal of Coal Geology, vol. 147-148, D. Kondla, H. Sanei, A. Embry, O.H. Ardakani, C.R.Clarkson, Depositional environment and hydrocarbon potential of the Middle Triassic strata of the Sverdrup Basin, Canada, p. 71-84, Copyright 2015, with permission from Elsevier.

Danielle Kondla has also signed a Theses Non-Exclusive License with Library and Archives Canada.

Name of Co-author	Signature of Co-author	Date
Dr. Hamed Sanei		
Dr. Ashton Embry		
Dr. Omid Haeri Ardakani		
Dr. Christopher R. Clarkson		
Dr. Xibo Wang		
Dr. Chunqing Jiang		